DEPARTMENT OF BIOMATERIALS AND MEDICAL DEVICE ENGINEERING
FACULTY OF BIOMEDICAL ENGINEERING

DOCTORAL DISSERTATION

Development of the Silanization Process for Spherical Aluminosilicates Dedicated as Filler for Polymers used in Medical Devices

mgr inż. Agnieszka Antończyk

SUPERVISOR
dr hab. inż. Witold Walke, prof. PŚ

ASSISTANT SUPERVISOR
dr inż. Magdalena Antonowicz

ZABRZE 2024

I would like to express my sincere thanks to all the people,
who believed in this topic and supported me
during my work on the doctoral dissertation.

Special thanks go to the supervisors,
dr hab. inż. Witolda Walke, prof. PŚ,
dr hab. inż. Damiana Nakoniecznego,
dr inż. Magdaleny Antonowicz.

TABLE OF CONTENTS

I. INTRODUCTION

Currently used materials for bone cement fillers, such as aluminum oxide or zirconium oxide, despite their good mechanical properties, are not always able to provide a good bond to the matrix. The lack of a good bond affects the deterioration of functional properties, but mainly leads to the occurrence of cracks in this type of composite materials. Proposing an alternative ceramic in the form of spherical aluminosilicates can provide an effective solution to this problem. Thanks to its spherical shape and low apparent density in the range of 1g/cm^3, it makes it an ultralight filler with properties similar to fillers currently used in composites. The use of this type of ceramic requires the selection of an appropriate fraction of it and the development of a silanization process to ensure proper adhesion properties by creating appropriate functional groups on its surface. Determining the properly prepared surface of spherical aluminosilicates also requires conducting many tests with varying process parameters and proposing selected test methods for evaluation, based on which the optimal option will be selected. Subsequently, the proposed spherical aluminosilicate variant will be introduced as a filler for commercially used bone cement - Poly(methyl methacrylate). Improving the physicochemical properties of PMMA through the use of a filler in the form of spherical aluminosilicate may improve the safety of bone cement when implants are fixed with it in bone surgery and will also improve its performance as a material used for bone restorations.

The dissertation aimed to develop a silanization process for spherical aluminosilicates to obtain amine, carboxyl and nitrogen functional groups that improve their adhesion with the matrix compared to those currently used (Al_2O_3 and ZrO_2) in bone cements.

The results obtained can provide a basis for further studies *in vitro* and *in vivo* and conduct further research in the surface modification of spherical aluminosilicates. They may also contribute to developing other types of composite biomaterials for use on medical devices.

II. LITERATURE REVIEW

1. Problems of skeletal disorders in statistical terms

Studies have shown that there are 12,000 fractures of the neck of the femur per year in Poland, with as many as 4 million men and 5 million women potentially at risk of osteoporosis. The most common fractures involve the vertebrae of the spine, the bones of the hand (radius), and the bones of the femoral neck. As is well known, our bones build up during growth and then stabilize until the age of 30. During adolescence, as much as 40% of bone mass grows. However, in people over 40-50 years of age, physiological bone mass loss begins, the rate of which in healthy adults is estimated at about 1% per year. In postmenopausal women and those predisposed to osteoporosis, this rate can be much higher and exceed 3 - 5% per year [1-4].

Osteoporosis is a bone disease, affecting the entire human skeleton. In the course of this disease, there is a decrease in the density of the bones and a disruption in the cohesion of their tissues, resulting in a much higher susceptibility to fractures, which can occur even with small loads. Bones become brittle and fracture easily. It is called the silent thief of bones because it does not give any pain for a very long time and often the first symptom is a fracture. The estimated number of people with osteoporosis in Poland in 2022, based on epidemiological indicators, is 2.1 million, of which 1.7 million are women [1-4].

Comparing the estimated number of patients with the value of registered prevalence, it was estimated that the degree of underestimation of the number of osteoporosis patients in 2022 was 75%. This corresponds to a figure of 1.62 million undiagnosed people, of whom 470,000 were over the age of 80 [1-4].

In 2022, 146 thousand fractures were reported, most commonly attributed to osteoporosis. The value of reimbursement of services for this reason amounted to PLN 795 million, 65% of which is allocated to services for fractures of the proximal end of the femur (BKKU) (35.4 thousand fractures in 2022). Only 6-7% of patients are treated pharmacologically. After the first fracture, the risk of another fracture increases 2-10-fold. The most common fractures are of the spine, radius bone (Colles' fracture), BKKU [1-7]. Fig. 1 presents age-specific and sex-specific incidences of radiographic vertebral, hip and distal forearm fractures, while Fig. 2 shows X-ray images of various bone defect fillings.

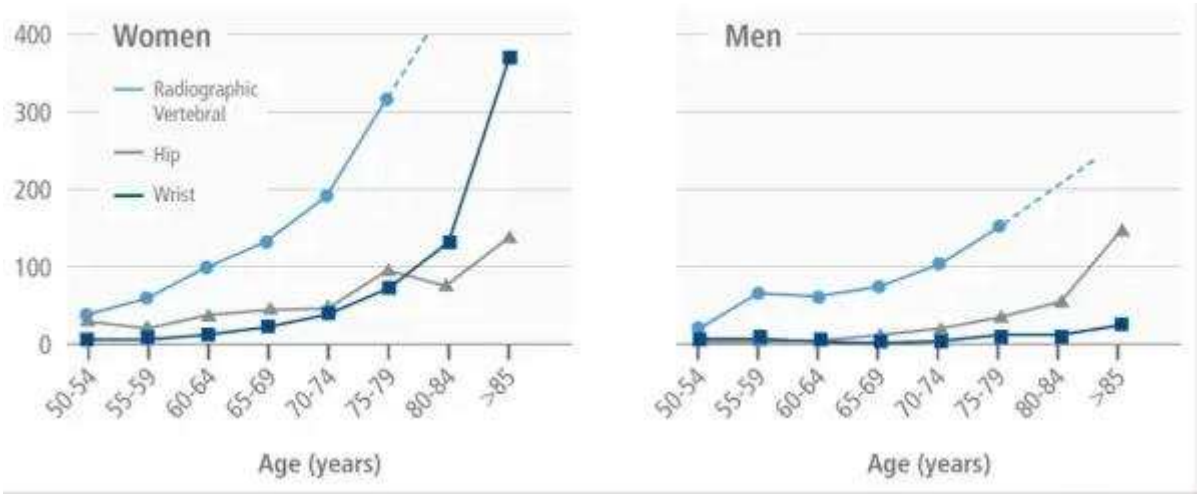

Fig. 1. Age-specific and sex-specific incidence of radiographic vertebral, hip and distal forearm fractures [4]

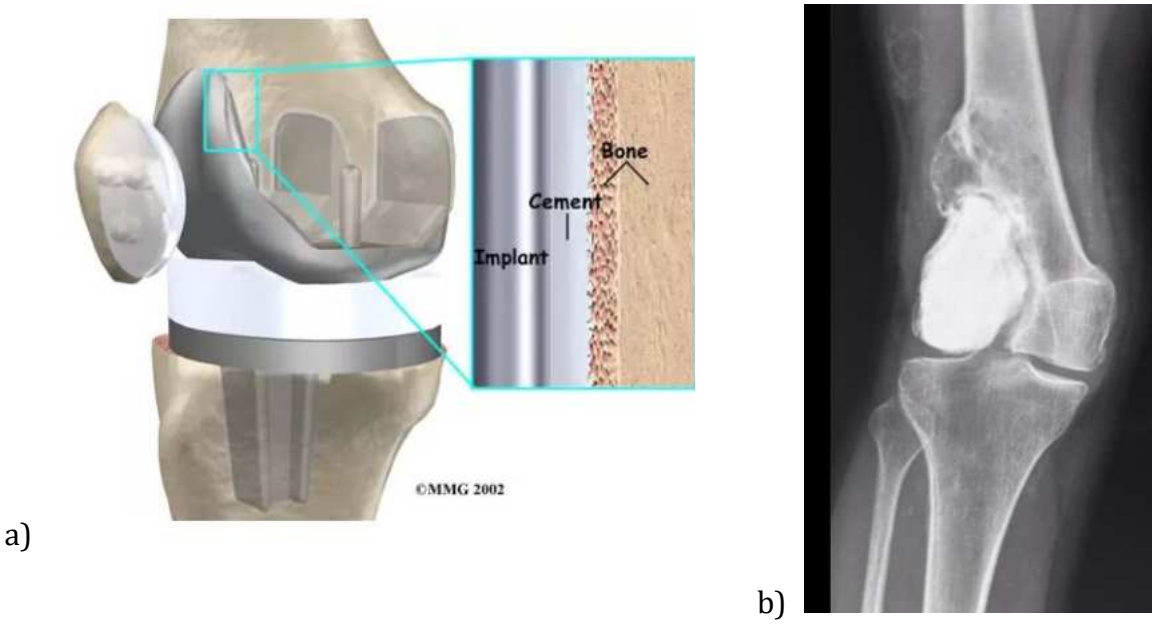

a) b)

Fig. 2. a) Cement-fixed knee endoprosthesis [7],
b) Case of recurrent bone tumor post excision and bone cementing [8]

Spinal fractures are the most common in osteoporosis. Per 1,000 people, 1.45 women and 0.73 men suffer compression fractures each year. After the age of 50, these fractures occur in one in four women, and after the age of 85 in one in two. Very surprisingly, about 70% of fractures are asymptomatic. This may be a consequence of prolonged stresses on the vertebrae causing microfractures that do not give rise to pain as in the case of sudden vertebral collapse, where the consequence is sharp piercing pain. Fractures can occur during routine daily activities, when getting out of bed, sneezing, or tripping over an obstacle. Only 25% of fractures occur as a result of a fall [9-13].

Spinal injuries, i.e. vertebral fractures, are treated with vertebroplasty. This is a minimally invasive procedure dedicated to people suffering from chronic pain in the spine, mainly in compression fractures of the vertebrae. The procedure involves the precise injection of bone cement into the area of the fractured or broken bone - Fig. 3. The main aspect of such a procedure is to mechanically reinforce the vertebral body and prevent further bone degradation and maintain proper sagittal balance of the spine (Fig. 4) [9-13].

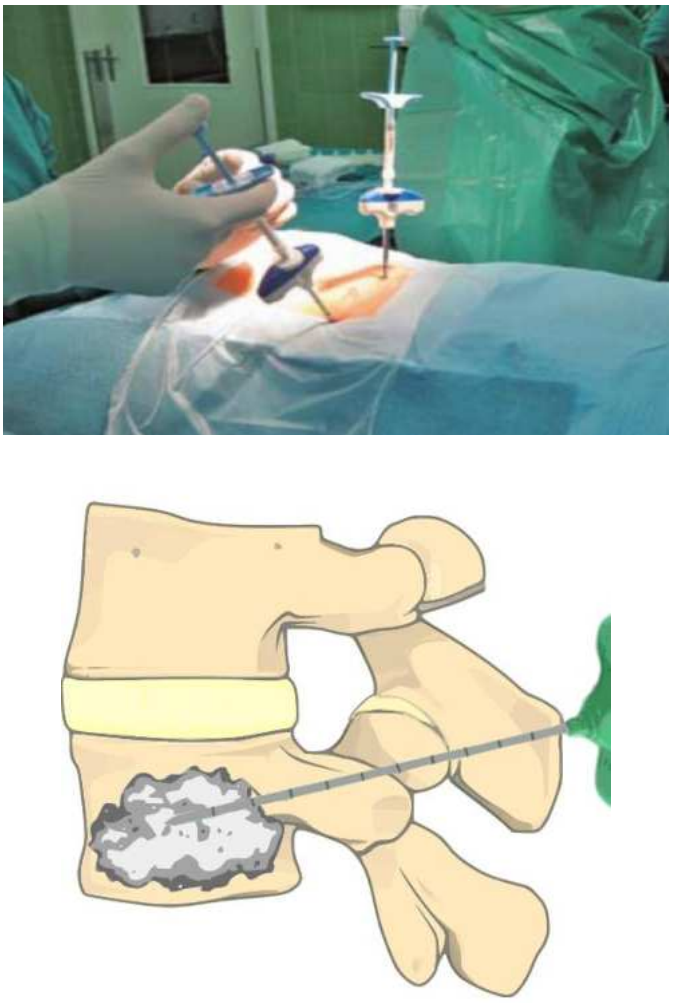

Fig. 3. Vertebroplasty procedure (top), and the process of injecting bone cement into the vertebra (bottom) [11,12]

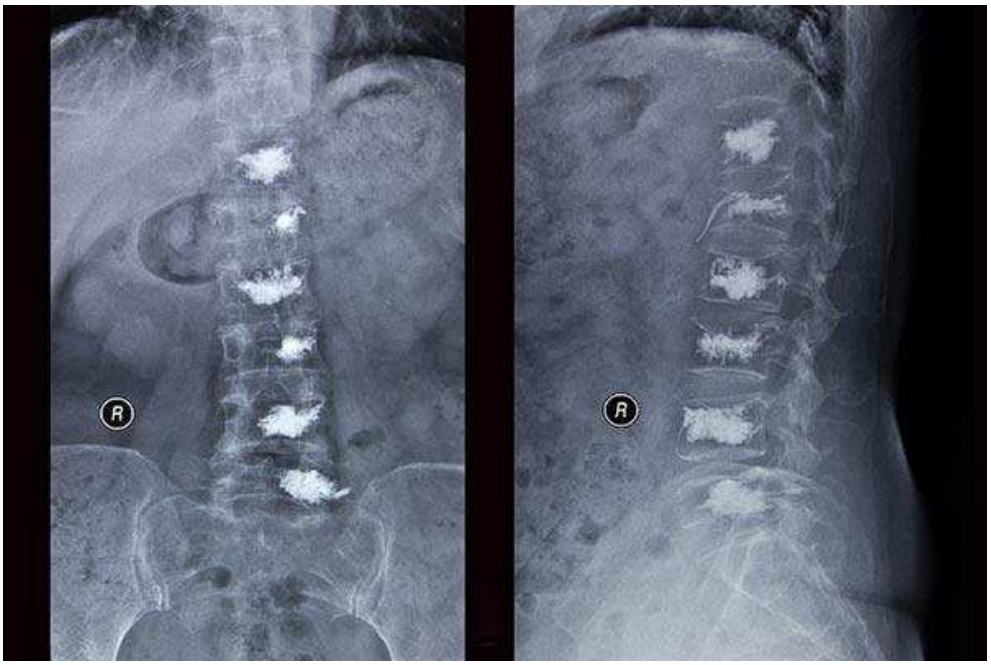

Fig. 4. X-ray of the spine after vertebroplasty surgery [13]

Osteoporosis is not the only problem of recent times. Newer statistics show that a large number of cases also involve problems with partial or complete missing teeth. Contrary to appearances, missing teeth are not a natural consequence of the ageing process. Nearly 90% of the population neglects gum and periodontal disease, which can contribute to tooth loss in later life. Nearly 70% of people aged 35-45 have lost more than one tooth, and a quarter of people aged 65-75 have no teeth at all Tab. 1. Such a dental condition can cause deterioration of physical as well as mental health. According to the report "9 Million Reasons - Denture Users in Poland", one in 2 Poles aged 40 or more wears a denture, and a significant number of patients need more serious medical intervention to regain not only a beautiful smile but also full functionality of the chewing apparatus (Fig. 5) [14-19].

Tab. 1. The proportion of denture wearers by age group and type of denture (Base edentate/dentate, n=2504) [15]

Age group	No upper or lower denture		Complete upper and lower dentures		Complete upper and partial lower dentures		Complete upper denture only		All other combinations of complete and partial dentures		Total
	n	%	n	%	n	%	n	%	n	%	n
50–64 years	838	68.8	42	3.5	10	0.8	41	3.4	287	23.6	1,218
65–74 years	392	42.8	98	10.7	51	5.6	67	7.3	308	33.6	916
75 years and over	100	27.0	88	23.8	24	6.5	41	11.1	117	31.6	370
Total	1,330	53.1	228	9.1	85	3.4	149	5.9	712	28.4	2504

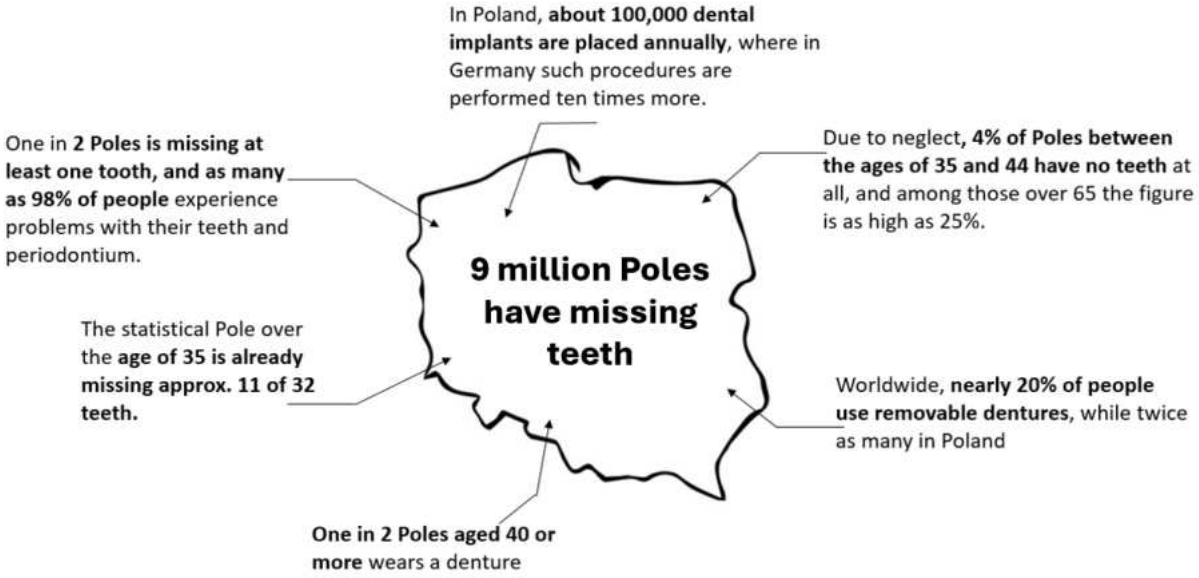

Fig. 5. Statistics of missing teeth in Poland

To restore the aesthetic appearance of teeth, we use removable or fixed prosthetic restorations. Dental solutions, or prosthetics, are adjusted accordingly after consultation with a dentist. Fixed prosthetic restorations can include overlay restorations, crowns, bridges and veneers, among others. The prosthetic solutions presented can be a part with a previously implanted implant or a crown and root post. For such solutions, bone cements are used for their permanent placement in the bone or tooth - Fig. 6.

Fig. 6. Placement of an overlay restoration on a tooth using bone cement [20]

2. The application of bone cements in the treatment of bone and stomatognathic defects

In accordance with the current trend towards achieving superior aesthetics, durability, and biocompatibility, increasingly innovative solutions are being developed in the realm of ceramic materials used in prosthodontics. These modern materials are distinguished by their excellent strength, bright color, and translucency, allowing them to seamlessly blend with the patient's natural dentition. However, alongside the growing popularity of these materials, challenges have emerged, particularly in the bonding between the core (or substructure), and the veneered surface. This issue often results in delamination or even complete detachment of the veneered layer, which compromises the overall integrity of the prosthetic restoration. To mitigate such failures, it is essential to enhance the bonding between these layers through both chemical and mechanical means. Modern dentistry already employs various techniques to improve this adhesion. Special bonding agents are utilized to increase the material's adhesion to the tooth or bone substrate, thereby improving the durability of the restoration. Recent research has focused extensively on zirconium oxide as one of the most promising materials in contemporary prosthodontics. While zirconium oxide offers several advantages, a critical analysis of the literature reveals some shortcomings, particularly in its bonding capacity [21, 60].

The most significant drawback of zirconium oxide is its insufficient bonding between the core and the veneered surface in fired prosthetic restorations (commonly referred to as ceramic restorations on a metal substructure). This issue is primarily due to the inherent instability of zirconium oxide's structure, which can lead to micro-gaps,

cracks, and even spalling, necessitating repairs to the prosthetic restoration. To address this, ongoing research is investigating various surface modification techniques to enhance adhesion between these layers. One promising approach involves the silanization process, which aims to increase surface area and improve bonding efficiency [21,35,60].

In addition to challenges related to ceramic materials, concerns have also been raised regarding the mechanical properties of currently used bone cement. The cement often exhibits suboptimal mechanical characteristics, potentially compromising the long-term stability of the bone-implant interface. According to established standards and regulations, the minimum mechanical requirements for bone cement include a compressive strength of approximately 70 MPa, a bending strength of ≥ 50 MPa, and a Young's modulus of ≥ 1800 MPa. When bone cement lacks these critical properties, it can wear down prematurely, leading to implant loosening or insufficient fracture stabilization [21].

Moreover, the high polymerization temperature of matrix-based bone cements, such as poly(methyl methacrylate) (PMMA), presents another significant challenge. While PMMA-based cements offer satisfactory cohesion time, their high polymerization temperatures can induce thermal necrosis in the surrounding bone tissue. This issue is particularly prevalent in the fixation of endoprostheses, where the bone cement layer is often thicker around the implant shaft than elsewhere. Consequently, optimizing the mechanical properties and reducing the thermal impact of bone cement is essential for enhancing the success and longevity of implant-based restorations. Ongoing research and development in this area aim to overcome these limitations and improve the overall performance of both ceramic materials and bone cement in prosthodontics [19,22].

2.1 Properties of bone cement

Bone cement is a chemical compound that is used to fix an implant in the bone, fill a defect in the bone and stabilize it in case of complex fractures. It is a self-polymerizing mass that is formed by mixing two components - a powder (i.e., polymer) with a liquid (i.e., monomer). The powder is usually in the form of regular spheres or less regular particles of micrometer diameter. In addition, there is a special initiator of the polymerization process, while the liquid component contains an inhibitor. Mixing these components causes a radical polymerization reaction, resulting in a structure of mutually entangled chains [21].

Bone cement is a porous material, which in itself allows bone tissue to osteointegrate with it. This process involves the penetration of bone cells into the pores of the material and their proliferation. It is generally accepted that 200-400 μm is considered the optimal pore size for the proper occurrence of the tissue reaction. The full process of biomechanical osteointegration is relatively lengthy, but results in a permanent structural and functional connection between the bone tissue and the implant [22-28]. To increase the bioactivity of bone cement in terms of improving the ability of bone tissue to form a bio-bond, the literature has found the use of modifications involving the targeted introduction of the following additives such as CeraVital (bioactive ceramic), hydroxyapatite, bio-glass [21]. Currently, the market offers acrylic bone cements, such as: C-ment 1-3, CMW1-3, Endurance. Osteobond, Palacos R, Simplex P, Versabond , Mendec Spine acrylic resin and Kyphx HV-R [21-28].

Bone cement used in bone surgery should have the following properties [21-28]:

- biocompatibility,
- bioactivity,
- relatively fast setting time (about 15 min after mixing powder and liquid),
- duration of plastic state, depending on the destination, not more than 5 min ,
- ability to properly transfer static and dynamic loads,
- high coefficient of friction,
- properties similar to bone (e.g., elasticity),
- high fatigue strength,
- resistance to cracking,
- resistance to abrasive processes,
- wear resistance,
- high vibration damping coefficient.

Biomaterials such as bone cement are expected to be biocompatible, meaning that they should not cause negative reactions in the body, such as inflammation, allergic or immunological reactions. The biocompatibility of bone cement depends on its chemical composition and surface characteristics, such as roughness and wettability [22-28].

Modern biomaterials should also exhibit bioactive characteristics, which, in the context of bone cement, refers to two aspects: antimicrobial action and support of osteointegration. If bone cement does not have the right properties, it can wear out too

quickly, leading to implant loosening or insufficient fracture stabilization. In more serious cases, implant rupture or serious infection can occur [22-28].

Other problems associated with the use of bone cement include too high a temperature during polymerization, which can cause thermal damage to the surrounding bone tissue (necrosis) and extravasation. On the other hand, elevated temperature around the implant can promote antibiotic therapy and help eliminate biofilm on the implant. In addition, polymerization shrinkage can lead to improper anchorage of the implant, which can cause further postoperative complications [22-33].

According to recommendations from standards and regulations, the minimum mechanical requirements of bone cement are shown in the Tab. 2 - Tab. 4. For cement intended for filling bone defects, the compressive strength should be min. R_c =30 MPa, for applications in the spongy bone part. However, for the attachment of endoprostheses, cement should have a compressive strength a minimum R_c =70 MPa. Flexural strength ≥ 50 MPa, Young's modulus E ≥ 1800 MPa [22].

Tab. 2 Compressive properties of bone cements derived from a compression test according to ISO 5833 [30]

Type of Cement	Compression Tests at 24 Hours after Hand Mixing, According to ISO5833		
	Failure Stress [MPa]	Failure Strain [%]	Modulus of Elasticity [MPa]
CEMEX RX	101.8	7.1	2608
CMW 3	101.7	7.1	2518
CMW 1 Genta	96.5	7.0	2147
SULFIX-6	96.3	6.9	2461
CMW 3 Genta	95.9	6.9	2177
Palacos R Genta	80.7	6.2	1993
Boneloc	80.0	6.5	2177

Tab. 3. Tensile properties of bone cements derived from a tensile test at 28 days after mixing. Specimens made according to ISO 53455, specimens stored in air at room temperature, crosshead speed 25 mm/min [30]

Properties	Bone cement	Dental cements	Bone (compact tissue)
Bending strength R_g(MPa)	> 50	60-112	160-180
Bending modulus of elasticity E_g(MPa)	> 1800	3000-8300	17000-19000
Compressive strength R_c(MPa)	> 70	145-351	130-220

Tab. 4. Example values of basic properties of selected PMMA bone cement [29]

	Bone cement (PMMA)				
Property	OSTEOBONG	CEMEX Isoplastic	PALACOS R.	PALACOS R+G	Bone Cement (The CMW Endurance)
Tensile strength [MPa]	40,49	———	———	———	———
Compressive strength [MPa]	105,33	85,15	104,56	85,9	———
Flexural strength [MPa]	———	45,95	69,74	46,3/56,3	———
Hardness [MPa]	———	2478	19,76	———	———
Module E [GPa]	———	———	2,81	1,8/2,2	———
Hydration degree [%]	———	———	———	2,69	———
Maximum polimerization temperaturę [°C]	———	———	———	———	64
Contact angle [°]	———	———	———	———	75,47

It should also be noted that the integrity of the bone-cement complex is a key aspect of its application, as the success of implantation depends on the integrity of this connection. It has been found that the border of this anastomosis is the most susceptible to local damage - which can later lead to its weakening, resulting in various pathologies [22-33].

The following types of bone cement can be distinguished [22-27]:

- polymeric,
- calcium phosphate,
- hydrogel,
- composite,
- bioactive acrylate

Examples of types of dental cements are [22]:

- glass-ionomeric cements,
- silicone cements,
- silicon-phosphate cements,
- amalgams,

2.2 Bone cement application method

The first step in the bone cement application procedure is to combine the filler with the bonding fluid. Bone cement application involves injecting the powder and liquid mixture prepared in this way into the target site. The injected homogeneous mass with low viscosity hardens over time. Depending on whether the cement is to perform a fixing or supplementary function, different requirements are placed on its mechanical properties (Fig. 7).

Fig. 7. Vacuum applicator for bone cement injection [29]

Bone cement, as a polymer composite, most commonly based on PMMA (polymethyl methacrylate), contains chemical additives that serve specific functions in the polymerization process or modify its properties. Hand-mixed cement tends to stick to gloves, while cement applied with an injector (under pressure) has very low viscosity, which is advantageous for its fixation in bone. However, this low viscosity poses risks, such as monomer leakage into the bloodstream and the occurrence of embolism. When using injector-applied cement, the rate of viscosity change over time and the temperature are critical factors [22]. There are three types of cement used:

- Low viscosity,
- Medium viscosity,
- High viscosity.

Low-viscosity and high-viscosity cements differ not only in their mixing and working times but also in the properties that affect their effectiveness in medicine, especially in the context of cement-based alloplasty. High-viscosity cements, due to their shorter mixing phase and longer working time, can provide better denture seating, which is important for implant stability and durability [21-28].

It is worth noting that the success of acrylic cement procedures largely depends on the mechanical interlocking of the cement with the bone. Although there is no direct integration of bone tissue with cement, the resulting boundary layer in the form of a connective tissue membrane is crucial because it can carry significant loads [21-28].

For the permanent attachment of implants, the precise filling of the space between the prosthesis and bone tissue and the effective penetration of the cement into the spongy substance are crucial. The physical properties of the cement, its preparation technique and the method of implantation are important for optimal results. Changes in ambient temperature, which affect the polymerization time of the cement, require the surgeon to plan precisely and act at the right moment [21-28].

2.3 Materials used for bone cements

One of the most popular types of bone cement is the so-called acrylate cement, with a base composed of polymethyl methacrylate (PMMA). This material has good mechanical properties (Young's modulus of 1800-2200 MPa, compressive strength of 75-105 MPa, and flexural strength of 60-75 MPa), but it has lower fracture resistance compared to bone. Due to its properties, such as its cohesion time (around a few minutes), this does not affect the cement's applicability. However, attention must be paid to polymerization shrinkage, which can lead to implant loosening, and the elevated temperature generated during the polymerization process. Additionally, it has been shown that hardened cement may contain remnants of unreacted monomer, which can cause allergic reactions. Other drawbacks include poor adhesion to bone surfaces and inorganic materials, rapid resorption, and permeability to radiation [21-33].

In addition to PMMA, the powder in acrylate cements also contains other additives essential for initiating the polymerization process. These additives may include copolymers of MMA with other polymers, such as styrene and methyl acrylate. One of the primary additives is benzoyl peroxide (approximately 0.75% to a maximum of 2.3% by powder weight), which acts as the polymerization initiator. The typical weight ratio of powder to liquid is 2:1. An important aspect to consider during the mixing and application of the cement is the environmental conditions. A temperature change (e.g., lowering it) can prevent the initiation of the polymerization process. Another factor is high humidity, which can affect the properties of the powder and ultimately the bone cement [21-33].

To improve the properties of acrylate cements, numerous modifications are introduced by manufacturers. The main modification is the addition of drugs, including antibiotics like gentamicin, to reduce post-operative infectious complications when an implant is inserted [24-27].

The main modifications with ceramic additives are presented in articles [30-33]. The main path of modification of bone cements is the addition of ceramic materials, their modification and combination with nanometric materials, in particular nano silver, which is designed to resist biofilm formation [25] or orgone products, e.g. collagen, hydroxyapatite, which are designed to increase osteointegration [33]. To improve osteoinductive properties (including the addition of bio-glass), which induce an extracellular and intracellular response of bone tissue [22,25]. The use of various modifiers, i.e., ceramics, allows to an increase mechanical property, the use of, for example, vitreous charcoal can reduce the polymerization temperature [21-23]. Other modifiers can be various types of drugs especially antibiotics in the publication [34] presented results show a faster improvement after the use of bone cement with antibiotic as an additional element in the therapy, although there was no difference in the blood supply to the ankle in the average time horizon of treatment. However, as the clinical picture shows, the combination therapy allows faster control of ulcer infection and accelerates wound healing.

Tab. 5. Basic mechanical properties of surgical cements without and with ceramic addition [21]

Material	Rm (MPa)	Rg (MPa)	Rc (MPa)	Er (MPa)	Eg (MPa)	Ec (MPa)	Rgs (MPa)	Rcs (MPa)	Ers (MPa)	Egs (MPa)	Ecs (MPa)
CMWI	20.0	52.7	85.3	3559.0	3474.7	2082.0	-	-	-	-	-
CMWI + Al_2O_3 (10-20 μm; 4g-9% wt.)	-	54.5	88.9	-	3554.5	2194.7	-	-	-	-	-
CMWI + Al_2O_3 (10-20 μm; 6g-13% wt.)	-	56.2	88.3	-	3886.8	1948.5	-	-	-	-	-
Palacos R with Gentamycin	-	68.4	70.5	-	3092.5	1379.0	-	-	-	-	-
Palacos R with Gentamycin + Al_2O_3 (10-20 μm; 6g-13% wt.)	-	55.3	76.6	-	3552.3	2107.0	-	-	-	-	-
Palacos R + E2 (Al_2O_3; 10-20 μm; 6g-13% wt.)	-	51.0	79.6	-	3504.0	2556.0	-	-	-	-	-
Simplex P	32.0	58.2	93.6	2759.0	3172.0	1961.2	-	-	-	-	-
Simplex P + Al_2O_3 (10-20 μm; 2g-4.8% wt.)	-	68.6	84.2	-	3334.2	1987.2	-	-	-	-	-
Simplex P + Al_2O_3 (10-20 μm; 6g-13% wt.)		55.4	86.3	-	3287.0	2067.0	-	-	-	-	-
Simplex P + Al_2O_3 (10-20 μm; 4g-9% wt.)	26.0	53.5	83.1	3242.0	3398.3	1862.2	-	-	-	-	-
Palacos R	-	70.4	74.9	2740.7	2093.0	1094.0	61.7	62.2	2772.2	1920.2	1202.0
Palacos R + Al_2O_3 (0.3 μm; 2g-4.8% wt.)	-	69.2	72.0	2932.2	2307.7	2307.7	1007.2	64.4	81.5	2962.5	1066.3

3. The application of ceramic fillers in bone cements

Ceramic materials are known for their chemical stability and inertness to external environments, which contributes to their outstanding biological performance. They exhibit resistance to aggressive conditions, including oxidation, and remain inert to long-term exposure to sulfur compounds and alkaline salts present in the atmosphere. Additionally, ceramics are well tolerated by surrounding tissues, with numerous studies demonstrating the absence of adverse effects such as toxicity, allergenicity, mutagenicity, and carcinogenicity. With excellent mechanical properties and high biocompatibility,

these materials can be utilized in a wide variety of medical devices and implantology. The main materials used are aluminum oxide and zirconium oxide [36-44].

- **Aluminum oxide – Al_2O_3**

Aluminum oxide (Al_2O_3) is one of the most popular ceramic materials, also known as alumina or alumina ceramics. It is an inorganic, odorless chemical compound that occurs as a white or colorless crystalline substance. Alumina is an electrical insulator with relatively high thermal conductivity and does not dissolve in water. It is characterized by a very high hardness, reaching 9 on the Mohs scale, making it often used for abrasion-resistant components in the energy and cement industries. High-pure alumina is used in the pharmaceutical, cosmetic and food industries.

Alumina material has gained popularity due to its favorable price/performance ratio. It makes it possible to produce large components for hydraulic and pneumatic conveying with a hard coating, as well as widespread use in kitchen and bathroom valves.

Depending on the content of pure alumina, which ranges from 92% to 99.9%, components with different properties are obtained. In addition, aluminum oxide can be reinforced with zirconium oxide, which increases its resistance to heat shock and cracking [45]. The basic properties of alumina were shown on Tab. 6.

Due to its properties, i.e. high chemical resistance, the αAl_2O_3 variety otherwise known as alumina or sapphire is the most common choice as an implantable material. On the other hand, the presence of the γAl_2O_3 phase allows the formation of porous structures used as a coating in implant materials [42-45].

Tab. 6. Basic properties of alumina [45]

Property	Entity	Value
Compressive strength	MPa	1500
Bending strength	MPa	300
Young's modulus	GPa	350
Thermal expansion coefficient	K -1*10-6	8
Heat shock resistance	ΔTºC	140
Thermal conductivity coefficient	W/m*K	19-30
Max. working temperature	°C	1650

Currently, the clinical applications of Al_2O_3 bioceramics are primarily found in bone reconstructive surgery, particularly in orthopedics, dentistry, and otorhinolaryngology. These applications predominantly utilize high-purity and high-density aluminum oxide. One of the most mechanically demanding implantable structures made partially or entirely from aluminum oxide is the hip endoprosthesis. These implants typically feature a metal stem, often coated with Al_2O_3, along with a ceramic head and acetabulum crafted from dense aluminum oxide with a smooth surface. Such designs are now manufactured by reputable companies and are used in clinics across Europe, America, and Japan [46].

In knee joint reconstructive surgery, aluminum oxide is utilized in conjunction with polyethylene components, yielding promising results compared to metal-polyethylene endoprostheses, although the outcomes are still not fully satisfactory. Similarly, cementless elbow endoprostheses incorporating aluminum oxide components have consistently failed to deliver unequivocally positive results, despite initial clinical trials dating back to the early 1980s. The applications of Al_2O_3 bioceramics focus on dense aluminum oxide sintered with a smooth surface, as porous ceramics possess inferior mechanical properties, rendering them unsuitable for mechanically demanding implantable structures [46].

The proposal to use Al_2O_3 (aluminum oxide) powder as an alternative material for bone grafts is attracting interest, and in vivo results are promising. However, to date, no clinical trials have been conducted in this area. Historically, the first dental implants made of polycrystalline alumina were introduced by Sandhaus in Switzerland in 1965. Over the past decade or so, numerous modifications have been made regarding both the shape of ceramic dental endoprostheses, the quality of the alumina used, and the surgical technique and instruments used during implantation of artificial dental roots [46].

An example of clinical success in this area can be seen in the results of 347 FRIALIT Tübingen implants at a West German clinic between 1982 and 1985, which were successful in 92.5% of cases. Kawahara [46] proposed the use of Al_2O_3 monocrystal coated with porous aluminum oxide to combine high mechanical strength with strong anchorage of the implant in the tissues [46].

- **Zirconium oxide (IV) – ZrO_2**

Zirconia ceramics include zirconium oxide. In the natural environment, zirconium dioxide is found under the name baddeleyite, as a crystalline solid. Pure zirconium is a

transition metal that readily combines with carbon, nitrogen and oxygen, leading to the formation of zirconium oxide on its surface. Jons Jacob Berzelius was the first to obtain the valid form of zirconium oxide in 1824 and the pure metal. Zirconium (IV) oxide belongs to the group of ceramic materials. A polymorphic powder with a white color. Zirconium oxide crystals form grains of 0.2 - 0.5 μm in size. It is characterized by polymorphism in three allotropic varieties unilinear, tetragonal and regular. At room temperature, zirconium assumes a single-stranded form, then above 1170°C it transforms to a tetragonal form. Above 2370°C, zirconium dioxide assumes the regular form[48 –56].

We can also distinguish such grades as iridium oxide, magnesium oxide and calcium oxide. Zirconium dioxide is a high-performance ceramic material used mainly for small parts with high bending and fracture toughness (*Tab. 7)* [48-56].

Tab. 7. Physical properties of zirconium(IV) oxide [53-54]

Physical property	Symbol	Value for ZrO_2	Entity
Melting point	T	2715	°C
Boiling point	T	4300	°C
Density	ρ	5.68	g/
Thermal conductivity coefficient	λ	2.5-3.0	W/m·K
Linear expansion coefficient	α	10.5·	1/K
Porosity	-	<0.1	%

Zirconium oxide has good biocompatibility. Previous studies confirm the absence of mutagenic or irritating effects of prostheses made using ZrO_2. Due to its chemical resistance also under acidic conditions, this material does not exhibit by-products that could irritate or cause inflammation of living tissues. The disadvantage of zirconium oxide is the so-called low-temperature degradation, which consists of an uncontrolled phase transformation (from tetragonal to mono-diagonal) which generates stresses and ultimately leads to microcracks. This defect can be caused by impurities present in the material, incorrectly carried out heat treatment processes or mechanical [48, 50, 51].

The clinically proven biocompatibility of zirconium oxide (ZrO_2) has contributed to its widespread use in dentistry. ZrO_2 is used, among other things, in the manufacture of orthodontic brackets and crown and root inlays and is also used for the manufacture of substructures for partial and complete crowns. Zirconia bridges are also a popular choice

for replacing missing teeth in both anterior and lateral sections, as well as for reconstructing the entire dental arch. In the medical field, zirconium oxide is also used for hip head prostheses, modifications of bone implants, construction of implant abutments and many other applications [49, 57, 58].

Current improvement research is directed toward the use of a new type of filler in polymer composites based on spherical aluminosilicates. This material shows similar mechanical and physicochemical properties to the group of ceramic materials currently used in composite materials. Due to their unique physical properties, i.e. low density, spherical shape, they represent a promising ultralight filler alternative to those used so far. The current interests of researchers are focused on exploiting their properties for applications in biomaterials engineering. Among other things, such work is presented in a review on cenospheres, where an outline of a proposal for a new material used in biomedical engineering was presented [59]. Another proposal of the author is to make a composite based on spherical aluminosilicates [60].

4. Characteristics of spherical aluminosilicates as filler for polymeric composite materials.

Spherical aluminosilicates are also called microspheres or cenospheres. It is a material extracted in dust furnaces during the combustion of hard coal. It is found in the ash, or more precisely, it is extracted after immersion in bodies of water called lagoons. Due to their characteristic structure, microspheres belong to the group of modern materials that significantly improve the properties of the final product [59 - 61].

4.1 Formation of spherical aluminosilicates

The central place as well as the beginning of the process of aluminosilicate formation is the combustion of coal or lignite in power plants or thermal power plants. In the dust furnace, we can find, among other things, large amounts of dust, ash and slag. As the temperature increases during combustion, the highly dispersed mineral substance melts [61]. Materials, i.e. aluminosilicates, clay minerals, minerals with high SiO_2 content transform T=1200°C. Those mineral particles that form glassy phases or eutectic mixtures assume a spherical shape. Gases that were released during combustion form a cavity inside the spherical form. Due to the prevailing high temperature in the combustion chamber, the outgoing waste gases and ashes are activated, i.e. a rapid cooling process to consolidate the spherical form. Microspheres in the gas and ash storm are deposited on

special filters (e.g. electrostatic precipitators), where they are then precipitated and transported pneumatically to retention tanks. This is one of the simplest and cheapest ways to obtain cenospheres, since this process uses the phenomenon of sedimentation under the influence of gravitational forces. This provides an opportunity to separate the ash and slag fractions, which sink to the bottom, from the microspheres, which, thanks to their density of $\rho < 1$ g/cm^3, float to the surface. The collected material is then cleaned in drip chambers by rinsing with filtered water. The final stage is drying in gravity dryers and segregation due to the value of bulk weight. After thorough cleaning and drying (moisture value <1%), spherical aluminosilicates are tightly packed [59-61].

However, attention should be paid, to the initial process, i.e. coal combustion. This is a key condition for the formation and quantity of microspheres in ash. Studies show that during the combustion of hard coal we get siliceous ash, while in the case of lignite we have to deal with a significant amount of calcium oxides, which prevents the formation of microspheres [61]. After an in-depth analysis of studies at a Russian power plant on the number of microspheres, it was shown that their content in ash can vary between 0.07%-3.35%. This is a small proportion of the total process, as the average microspheres obtained is about 1%. To obtain the best quality and quantity, the prerequisite must be the combustion of hard coal and the use of liquid slagging techniques. Due to the increasing use of microspheres, they are extracted all over the world, including the US, Russia, Kazakhstan and India [59-61].

4.2 Properties of microspheres

A microsphere is a light-colored grain in a spherical shape filled with gas. It consists of two parts: the shell, which is the solid part, and the gas, which fills its interior. The outer part, or shell, consists of aluminosilicate grains of amorphous structure. The structure of the phase composition of the cenosphere is shown in
Fig. 8 [64].

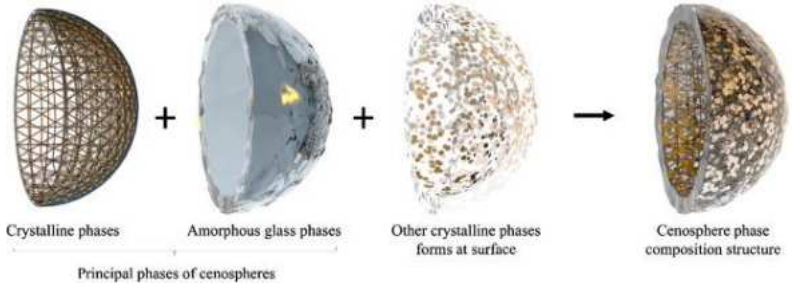

Fig. 8. Schematic phase composition structure of a cenosphere [64]

Crystalline inclusions may appear. The crust consists mainly of a dominant vitreous phase and a crystalline phase. The vitreous phase consists of oxides of silicon and aluminum and, to a lesser extent, iron and calcium. The crystalline phase consists of quartz and mullite, and in lesser content, we can find hematite and magnetite. Of course, other compounds can occur, while their content is trace amounts. The microspheres contain trace amounts of heavy metals, including Cu, Ni, Pb, Zn, Cr. The chemical composition of microspheres is presented in *Tab. 8* [59-61].

Tab. 8. The potential composition of spherical aluminosilicates

Name	SiO_2	Al_2O_3	Fe_2O_3	K_2O, Na_2O, TiO_2, SO_3, P_2O_3, CaO, MgO
Quantity [%]	50-65	19-42	0.7-6.5	< 1%

When cenospheres are dried, gypsum, portlandite and brucite can transform in a more stable form such as carbonates, namely calcite, dolomite and probably magnesite by absorbing carbon dioxide from the air [64].

The interior of the microsphere is mainly filled with CO_2 and N_2. In smaller amounts, we can distinguish CO, O_2 and H_2O. The grain size of microspheres is in the range of 0.125 - 0.500 mm (93%). The largest fraction by volume is 0.250 - 0.300 mm. In contrast, fractions above 0.500 mm (6%) and less than 1% are dusty, i.e. the finest fractions [59-64]. After chemical composition, the phase-mineral composition is a key factor that makes cenospheres a distinctive material. It is generally accepted that cenospheres are composed of an amorphous outer shell and a crystalline internal structure. According to the ternary diagram, based on the presence of iron and its associated crystalline compounds, cenospheres can be categorized into magnetic and nonmagnetic types (see Fig. 9). For instance, cenospheres from the Sialic group are magnetic, owing to the presence of SiO_2, whereas those from the ferrcalcsialic group are nonmagnetic. It can be inferred that a reduction in silicon content within the mineral constituents leads to a decrease in ash content in cenospheres with smooth shells. The average phase composition ranges between minimum and maximum percentage values [63].

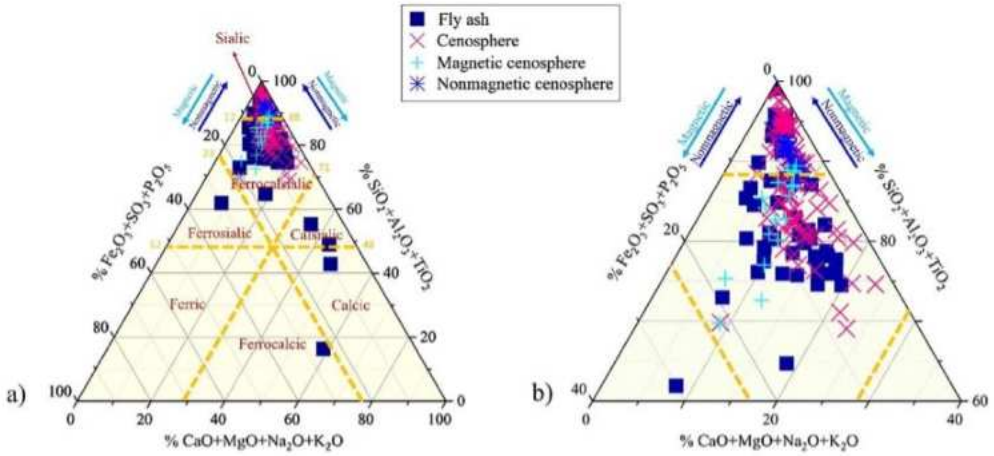

Fig. 9. The ternary diagram of chemical composition of selected fly ashes and cenospheres prepared by Ranjbar and Kenzel [59-64]: a) full diagram, b) magnification of the cenospheres forming area – sialic and ferrcalcsialic groups

Due to their unique structure, spherical aluminosilicates are increasingly used in the construction industry. A key property of spherical aluminosilicates is that they have no harmful effects on living organisms, allowing them to be considered as a material for use in human products. Thanks to their compact outer wall, they have low porosity, which gives them low absorbency. In addition, they exhibit significant compressive and crushing strength. Microspheres are a ceramic group material which gives them significant resistance to chemical agents and resistance to temperature amplitude. Their spherical structure and gas filling allow microspheres to participate in other materials as an ultralight filler. Their bulk density is only 0.45 g/cm^3. In addition, thanks to their low thermal conductivity coefficient, they have thermal insulation properties. Microspheres also exhibit vibration damping capabilities [59-64].

4.3 Application of microspheres

Microspheres, thanks to their unique properties, are increasingly used in industry in general, including construction, mining, automotive, ceramics and plastics. Currently in the building materials industry they play the role of fillers, improving the parameters, i.e. thermal insulation and fire resistance of products such as insulating screeds, cement thermal insulation of ceilings, insulating semi-finished products or plasters with increased thermal and acoustic insulation. Cementitious composites, insulating dusts and lightweight concretes perform an important function of fireproofing as barriers that prevent the passage of fire. The use of microspheres as a filler in composites offers the

possibility of increasing the durability of the composite at reduced temperatures, and a decrease in apparent density due to reduced absorption [59-64].

Such a solution makes it possible to use concrete in a wider temperature range, for example. By replacing the filler with microspheres from typical fillers, i.e. chalk or various types of fibers, it makes it possible to achieve lower density, higher stability and stiffness, and surface smoothness in composites. The addition of microspheres to sealing compounds or putties makes it possible to reduce the use of synthetic rubber, further protecting the mass from cracking. In foams, aluminosilicates allow for dimensional retention and shape stability [59-64]. In other industries, microspheres can be part of automobile structural components such as bodywork, anti-corrosion coatings, and also be part of power cable insulation. A promising research direction for microspheres is to use them as protection against radioactive waste. Aspiring directions for aluminosilicates are the space industry, medical industry and in the production of detonators. The main advantage of using aluminosilicates in industry is the reduction of production costs, over and above that we gain additional improvement in the properties of the selected product [59-64].

4.4 Composite based on spherical aluminosilicates

Currently, there are two requirements for ceramic-filled composites. They are to show the absence of toxicity to tissues and the human body, as well as the absence of metabolic products that can lodge in the structure of the polymer. However, the overriding task is to take advantage of the mechanical properties afforded by the use of ceramic materials. This can be directed at transferring the resulting stresses to the implant, until fusion with the bone. The use of microspheres as a filler, will produce a composite material with unique properties. Doped polymer composites are currently used in components that constitute implants, e.g. nails and screws that fix damaged bone struts during fractures. They can also be used as an initial scaffold for bone, where the matrix will begin to degrade after some time. It is inevitable to produce components, small implants or other solutions for medicine using 3D printing, where polymer matrix composite is the best candidate here based on this technology [59-64].

The modifications associated with the use of spherical aluminosilicates primarily involve the initial modification of the material and then the manufacture of a composite, mainly on a polymer basis. This procedure is aimed at verifying as well as demonstrating

the properties that a composite using aluminosilicates can have. One example of such a publication is the use of an aluminosilicate filler, PA-12_CS, compared to pure PA-12, had overall better mechanical properties and was more resistant to SBF at elevated temperatures and soaking times. These results showed that the material has potential for use in biomedical applications. [59-64]. The use of aluminum-silicate cenospheres in the production of syntactic foams holds significant promise due to their potential applications in creating alloys with various programmable porosities, such as aluminum, magnesium, and titanium alloys [62–69]. This is especially relevant for magnesium-based degradable alloys and titanium implant alloys, which can serve as bone scaffolds and implant screws. These materials enable bone tissue to grow through the implant, supporting both the healing process and integration with the bone [59-64]. In other studies, attempts have been made to produce a composite based on the High-density polyethylene (HDPE) is used as the matrix material, and fly ash cenospheres are used as the filler [65-69].

5. Methods to improve the adhesion of ceramic materials with a matrix of polymeric materials

Current work on increasing filler adhesion in polymer matrix focuses primarily on the use of modifiers in the form of silanes in the silanization process. The use of these chemicals, according to the authors of the work [69, 70], improves the rupture force in composites, which translates into increased mechanical and chemical bonds between the filler and matrix in composite materials. According to the authors of the works ... the most favorable solution for improving adhesion is the silanization process. The advantage of this process is the possibility of modifying the surface of ceramic materials in which there is an increased risk of delamination between filler and matrix, by producing chemical compounds to eliminate this phenomenon.

Silanes can enhance the properties of composites by linking inorganic materials with polymeric ones through physical or chemical interactions. To successfully bond polymer matrices with organic or inorganic materials, the silane molecule must possess bifunctional groups capable of reacting with both phases, forming a bridge between them. The general chemical structure of silane coupling agents enables this interaction, facilitating stronger adhesion and improved compatibility between the components[71-77]:

$$R(4n-1)\text{-}Si\text{-}(R'X)n \ (n = 1,2),$$

Where[71]:

R - denotes the alkoxy group,

X - stands for organofunctional group,

R' - denotes an alkyl bridge connecting a silicon atom and an organofunctional group.

Most known silanes are trialkoxysilanes, and their organofunctional groups play a key role in determining their interaction with polymer matrices based on compatibility and reactivity. A non-reactive alkyl group in the silane can enhance compatibility with non-polar matrices due to their similar polarity, whereas reactive organofunctional groups can covalently bond or be compatible with polymer matrices. Common organofunctional groups in silanes include amine, mercaptan, glycidoxy, vinyl, and methacryloxy groups, each offering different bonding or interaction capabilities with specific polymers [71-78].

Silanes are adhesion promoters in many systems. They are used as surface modifiers to enhance adhesion or as films on their surface to improve the properties of materials, such as hydrophobicity, corrosion resistance, UV resistance or mechanical properties [71].

5.1 Organosilicon compounds

Self-organizing properties of organosilicon compounds are among the most popular silanizers currently used in surface functionalization (Fig. 10). They were first observed in 1980 by Sagiv on layers formed from n-octadecyltrichlorosilane (OTS) [71].

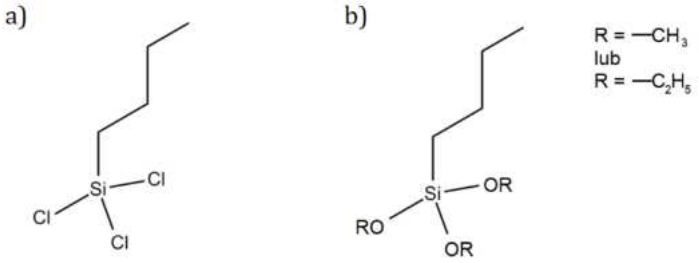

Fig. 10. The most common organosilicon compounds that spontaneously organize are on hydroxylated surfaces [71-78]: a) trichlorosilane and b) trialkoxysilane (the names of the compounds are abbreviated, derived from the form of the front group of molecules, lengths of the alkyl chains are random)

These compounds play a unique role because, like organic compounds or monolayers, they form strong bonds with substrates. In both cases, van der Waals interactions between alkyl chains promote the self-organization of molecules [71-78]. The key difference from sulfur-organic compounds lies in the structure of the active head group, which, in this case, consists of three functional groups attached to a silicon atom. For trichlorosilanes and trialkoxysilanes, the head groups are $-SiCl_3$ and $-Si(OR)_3$, respectively, where R represents an alkyl group, typically a methyl ($-CH_3$) or ethyl ($-C_2H_5$) group. These functional groups enable covalent bonding with surfaces that have free hydroxyl groups during the silanization process, ensuring a strong and durable attachment [71].

The exact description of the silanization process depends on the conditions under which the reaction occurs. However, the general mechanism of silanization in solution can be presented as a three-step process (Fig. 11).

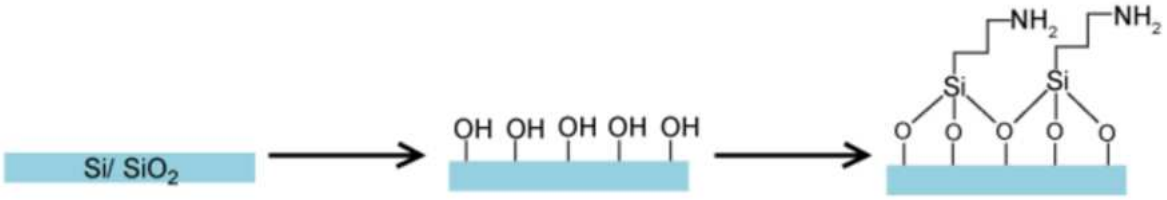

Fig. 11. Silanization process diagram [78]

In the initial stage of silanization, trialkoxysilane (or trichlorosilane) undergoes hydrolysis, facilitated by water adsorbed on the substrate surface or present in the solution. This reaction produces trisilanols in solution, which initially bind loosely to the substrate through hydrogen bonds. In the subsequent step, the trisilanol condenses on the surface via a reaction between its silanol groups (Si–OH) and the hydroxyl groups on the substrate. Alternatively, trichlorosilanes can directly condense on the substrate without water, producing HCl as a byproduct. Wasserman's study [71-77], which found no chlorine in the monolayer formed from trichlorosilane, suggests that all three silanol groups of the molecule may bond to the substrate, forming a structured layer as depicted in Figure 12.

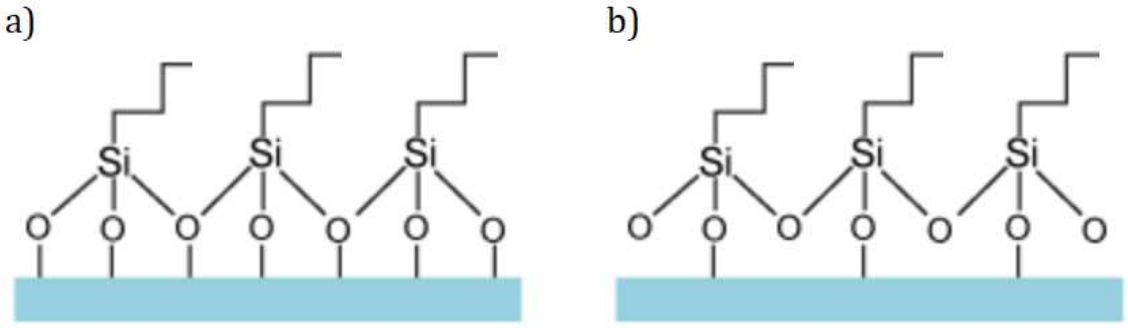

Fig. 12. Diagram of the silane monolayer structure formed by [78]: a) bonding of all silanol groups with surface hydroxyl groups, b) bonding of one silanol group with the substrate, while the remaining two bond with groups of neighboring molecules

However, the density of free hydroxyl groups on the substrate surface is often too low ($\sim 10^{15}$ groups per cm^2, or about 1 hydroxyl group per 20 $Å^2$) for the silanization reaction to proceed reliably. Numerous studies support the idea that only one silanol group binds directly to the substrate, while the remaining two form Si-O-Si siloxane bonds with neighboring molecules. This intermolecular bonding process, known as cross-linking, results in a stronger attachment of the silane monolayer to the substrate. Evidence for this can be seen in layers formed from monoalkoxy- or monochlorosilane compounds, which lack reactive side groups and tend to form less stable structures. Additionally, some research suggests that trisilanols can undergo initial spatial crosslinking in solution, forming oligomers that later react with surface hydroxyl groups. The structural model shown in Figure 13b aligns with both the cross-linking mechanism and the formation of silane monolayers described in these studies [71-79].

However, the presented mechanisms for the formation of silane monolayers are not entirely correct. As early as 1980, Sągiv [71] pointed out that the length of Si-O-Si bridges is too small (< 3.2 Å) to provide adequate space for alkyl chains, whose cross-sectional diameter is 4.6 Å (Fig. 13a).

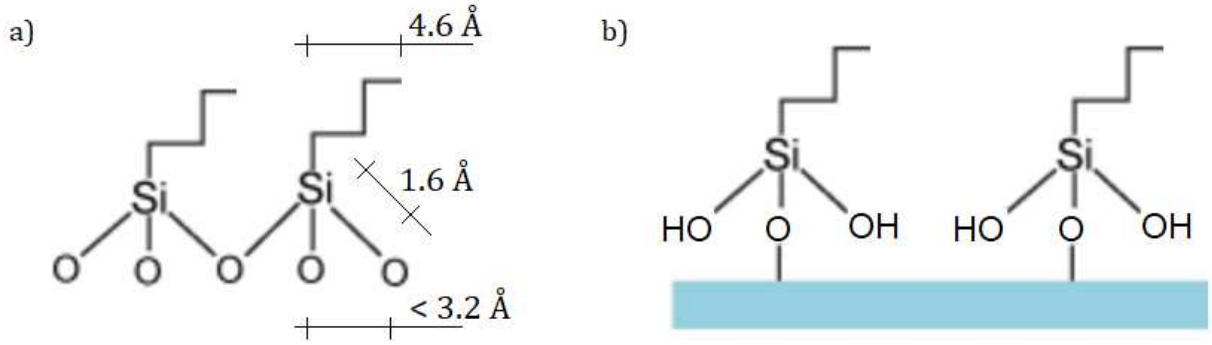

Fig. 13. (a) Schematic of the connection between cross-linked silanol molecules with distances indicating steric repulsion of the alkyl chains, (b) Schematic of the structure of the silane monolayer formed by binding one of the three hydrolyzed silanol groups to the substrate. The unbound silanol groups do not disrupt the ordering of the dense monolayer [71-78]

A detailed structural analysis of silane layers has revealed that extensive crosslinking between silane molecules can cause distortions within the front functional groups, preventing the formation of a densely packed and ordered monolayer. However, it has also been found that the silanol groups themselves are small enough not to interfere with monolayer formation when the two side groups undergo hydrolysis, converting into –OH groups that remain unreactive with other atoms. Infrared spectroscopy data support this, showing an increase in Si-OH bonds as silane coverage on the substrate grows, indicating that these hydrolyzed side groups may stay unbound. In summary, silanol groups can form hydrogen bonds with water molecules present on the substrate, bond with the silanol groups of neighboring molecules, or interact with the surface hydroxyl groups of the substrate [71].

Despite findings that silane monolayers are molecularly flat and exhibit a thickness consistent with the length of their alkyl chains, no evidence of long-range ordering within these silane layers has been observed. Proper substrate preparation is critical for achieving high-quality monolayers in all organosilicon compounds. The manufacturing and storage conditions of the substrates significantly influence their physical and chemical properties. For instance, contaminated oxidized silicon surfaces may contain siloxane bonds (Si-O-Si) instead of free silanol groups (Si-OH), which are essential for effective bonding. Ensuring the presence of hydroxyl groups requires thorough purification and activation of the substrate [71-78].

The reproducibility of forming organosilicon monolayers remains challenging because the quality of the layers is highly sensitive to the manufacturing conditions. A

major issue in creating monolayers from trialkoxysilane compounds is controlling the water content in the solution. Since trialkoxysilanes have low reactivity due to the nature of their –OR functional groups, water is necessary for the hydrolysis process. Insufficient water hinders hydrolysis, resulting in an incomplete monolayer. Conversely, excessive water leads to over-polymerization of the molecules in the solution, which disrupts the formation of a uniform monomolecular layer. Trichlorosilane compounds, on the other hand, can be deposited under anhydrous conditions due to their higher reactivity, reducing the risk of excessive polymerization and improving the monolayer formation [71-78].

Among trialkoxysilanes, 3-aminopropyltriethoxysilane (APTES) and 3-aminopropyltrimethoxysilane (APTMS) are popular and frequently used compounds (Fig. 14). However, obtaining a good quality monolayer of these compounds is a troublesome issue. As short-chain alkyl compounds, they show less tendency to self-organize than longer-chain compounds In addition, the presence of an amine functional group can adversely affect the homogeneity of surface coverage due to the formation of hydrogen bonds between the amine groups of the silane molecules and the silanol groups of the substrate Another problem is the aforementioned polymerization of silane molecules, occurring under conditions of high-water concentration in solution [71-82].

a)

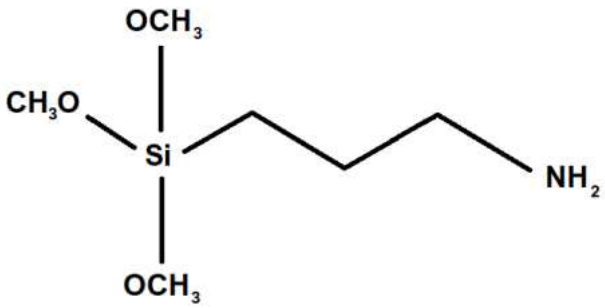

b)

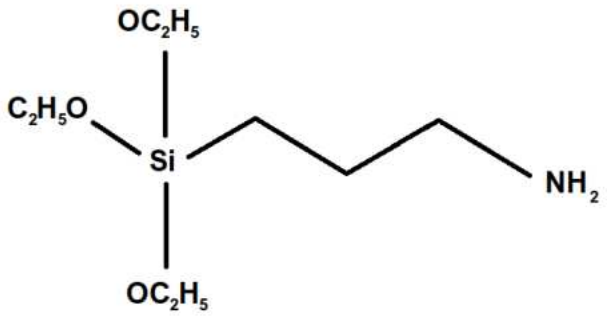

Fig. 14. Schematic of the structure of the compound: a) 3-aminopropyltrimethoxysilane (APTMS) and b) 3-aminopropyltriethoxysilane (APTES) [71-82]

Proposed technologies for producing monolayers are not entirely consistent. For example, Petri et al. obtained flat, stable and uniform surfaces by immersing freshly cleaned silicon substrates in a toluene solution containing 1% (m/m) APTMS for 4 min at 60°C [71-82]. Howarter et al. claimed that solutions with a low concentration of APTES (1%) produce good-quality films only when the settling time of the molecules is limited to 1 h [71-82]. However, they did not observe a significant dependence of monolayer quality on solution temperature. Han et al. used a 5% solution of APTES in ethanol at room temperature, in which they stored substrates for a period of several hours [71-82]. On the other hand, Heid et al. found that aminosilane compounds form disordered multilayers [71-83]. Discrepancies regarding how monolayers are produced, and their quality also exist for other silane compounds. Silberzan et al. [83] claimed that a sufficient time for the formation of a monolayer from an OTS compound is 3 min, while Wasserman et al. [48] believed that a time of at least 24 h is required, and Banga et al. [71-82] - 90 min. The polymerization of silane molecules and the non-schematic mechanism of their anchoring on the surface is the main source of problems with the reproducibility of the produced layers. A small difference in water content and in the concentration of surface Si-OH groups causes significant differences in the quality of the resulting monolayers. In addition, the lack of mobility of silane molecules on the adsorbed surface also affects the lower ordering of organosilane compounds than thiol compounds on gold. This is because the bond formed between the silane molecules and the surface hydroxyl groups is irreversible. This means that - in contrast to organosulfur compounds - the silane molecule bound to the substrate cannot move on the surface. Nevertheless, the permanent strong bonding of organosilane molecules to the substrate guarantees

exceptional mechanical and thermal stability of the monolayers [71-83]. This makes silanes ideally suited materials for surface modification and functionalization. However, they do not represent suitable systems for fundamental research as model systems. It is worth noting here that despite the problems and challenges associated with the judging of APTES and APTMS compounds, they are widely used as active layers for further immobilization of molecules [71-83].

5.2 3-aminopropyltriethoxysilane (APTES)

One of the aminoalkoxysilanes used for surface modification is 3-aminopropyltriethoxysilane (APTES), which contains a polar and chemically active aminopropyl group and three readily hydrolyzable alkoxy groups (Fig. 14). These groups can react with hydroxyl groups on the surface of the material and generate the reactive silyl alcohol silanol, in the presence of water (aqueous solution) or air [71-83].

APTES is used in silanization, the functionalization of surfaces with aminoalkoxysilane molecules. It can self-organize on the surface of oxides. This ability is used, for example, to regulate surface properties. In addition, it is used as a coupling agent for organic groupings or nanoparticles to the oxide surface. It can also be used to covalently attach inorganic modifiers such as graphene oxide, SiO_2, TiO_2, MgO or ZnO, or silver nanowires to organic materials [71-83].

5.3 Tetraethoxysilane TEOS

Tetraethoxysilane (TEOS; tetraethyl silicate), with the chemical formula $Si(OC_2H_5)_4$ an organic chemical compound belonging to the alkoxysilane group (Fig. 15). It can be considered an orthoester of silicic acid and ethanol. TEOS is produced through the reaction of tetrachlorosilane ($SiCl_4$) with ethanol, which results in the replacement of chlorine atoms by ethoxy groups. TEOS plays a crucial role in various chemical processes, particularly in the sol-gel reaction, a versatile method used for creating solid materials from small molecules. During the sol-gel process, TEOS reacts with water in a hydrolysis reaction, which leads to the formation of silanol groups (Si–OH). These silanols subsequently undergo condensation reactions, producing orthosilicic acid, $Si(OH)_4$. This reaction is typically followed by further polymerization, forming silica-based materials.

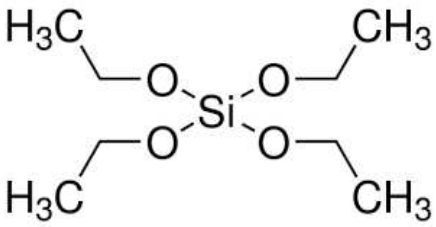

Fig. 15. Example diagram of the structure of tetraetoksysilane (TEOS)[83-84]

The resulting silanols undergo condensation to ≡Si-O-Si≡ siloxanes (where Si≡ denotes a silicon atom with any 3 substituents, it does not denote a triple bond). This reaction can proceed with the release of an ethanol or water molecule [85 - 89].

$$\equiv Si{-}OEt + HO{-}Si\equiv \rightleftarrows \equiv Si{-}O{-}Si\equiv + EtOH$$

$$\equiv Si{-}OH + HO{-}Si\equiv \rightleftarrows \equiv Si{-}O{-}Si\equiv + H_2O$$

TEOS processes are usually carried out in an alcohol-water solution, where alcohol is also involved in the reactions, causing a shift in equilibrium toward the substrates. The final product is silica, and often takes the form of large macromolecules. These products are of equal spherical shape and of the same size during the Stöber process, and the diameter of such particles ranges from 5nm to 2μm [84-93].

6. Summary of the literature review

Despite limitations concerning mechanical properties and the issue of high temperatures during polymerization, bone cements continue to be widely used in medical applications. However, with the advancement of technology and the increasing demands placed on polymer-based composites, various modifications related to the type, form, and percentage content of fillers within the composite matrix are being implemented. Currently utilized modifications based on alumina and zirconia, although they improve mechanical properties, do not eliminate the phenomenon of micro-crack or crack formation at the interface with the filler. This issue is partially mitigated by employing adhesive agents that enhance adhesion to bone or implants. One such solution involves the modification of the filler—in this case, the ceramic—by increasing surface area and introducing functional groups such as amine, carboxyl, and nitrogen groups, which enhances the chemical bonding between the filler and the matrix. Such an approach can reduce or eliminate the formation of cracks in the composite. Another solution could be to change the filler in the composite. Based on literature reports [59, 60], a spherical

aluminosilicate may serve as an alternative to the currently used alumina and zirconia. This type of ceramic possesses properties comparable to those of existing ceramic materials; however, due to its unique chemical structure and form, it can be classified as an ultra-lightweight filler for composites [60, 62, 68]. For the effective application of this type of ceramic, a dedicated modification process must be developed to ensure appropriate surface development. This will provide better adhesion of chemical compounds that directly influence the reduction of micro-crack occurrences or delamination during the use of composite materials, including bone cement. Furthermore, the selection of the appropriate fraction and type of silane will affect the formation of functional groups on the surface of the spherical aluminosilicate, improving the chemical bond between the filler and the polymer matrix [60, 66, 68].

In summary, the unresolved issues regarding the application of spherical aluminosilicates include:

- the formation of functional groups on the surface that enhance mechanical and chemical bonding,
- the selection of silanization process parameters that facilitate the creation of functional groups for different fractions of spherical aluminosilicates, with a comparison to results obtained for alumina and zirconia,
- the selection of the appropriate fraction and type of silane that allows for the creation of bone cement incorporating spherical aluminosilicates with consistent service properties,
- the development of a polymer composite fabrication process based on spherical aluminosilicates with modified surfaces, ensuring uniform distribution of the filler within the matrix, considering the physical characteristics of the filler (ultra-lightweight filler),
- the maintenance or reduction of polymerization temperature in the case of application in commercial bone cements,
- a lack of literature reports regarding the toxic effects on tissues and information concerning residual metabolic products lingering within the polymer structure.

III. RESEARCH

1. Aim and thesis of the work

Recent work on composite materials based on ceramic fillings has focused on issues related to adhesion between matrix and filling to avoid micro-cracking, fracture or delamination. An additional problem that occurs in the selection of ceramic materials used as fillers is to ensure that the mechanical as well as physicochemical property requirements are appropriate for the final form of composite biomaterials, such as bone cement inserted into the osseous or stomatognathic system. One solution to the aforementioned problems may be the use of an alternative filler ceramic material in the form of spherical aluminosilicate. However, the use of this type of ceramic is primarily related to the development of a process of surface modification, so that the proposed filler material fully combines with the matrix and does not cause a reduction in the functional properties of bone cement. Therefore, the purpose of the dissertation is:

Development of a silanization process for spherical aluminosilicates to obtain amine, carboxyl and nitrogen functional groups that improve their adhesion with the matrix compared to those currently used (Al_2O_3 and ZrO_2) in bone cement.

The issues pursued in the development of a filler surface in the form of spherical aluminosilicate used in bone cement in both skeletal and stomatognathic reconstruction are in the area of issues in the discipline of biomedical engineering. The selected fraction and modification of spherical aluminosilicate will be used as a filler for a poly(methyl methacrylate) matrix composite to produce bone cement and to compare it with those currently used in medicine. Hence, based on a review of the literature and the experience of other authors of the study, the following research thesis was adopted as part of the study:

The development of a silanization process for spherical aluminosilicates will enable their permanent chemical and physical bonding to the polymer matrix in composite materials, and thus provide an alternative solution to currently used fillers for bone cements dedicated to biomedical engineering applications.

Verification of the adopted thesis will require the realization of an adequate scope of research that will allow full characterization of the proposed variants of spherical aluminosilicates with different fractions as well as surface morphology. The proposed

research plan, the block diagram of which is shown in Fig. 16 will allow to describe and characterize the chemical and physical processes occurring on the surface of modified powders (aluminosilicates with fractions C_{90}, C_{150}, C_{212}), and further enable evaluation the mechanical and physicochemical properties of the composite material based on poly(methyl methacrylate) matrix spherical aluminosilicates used as bone cement in reconstructive surgery.

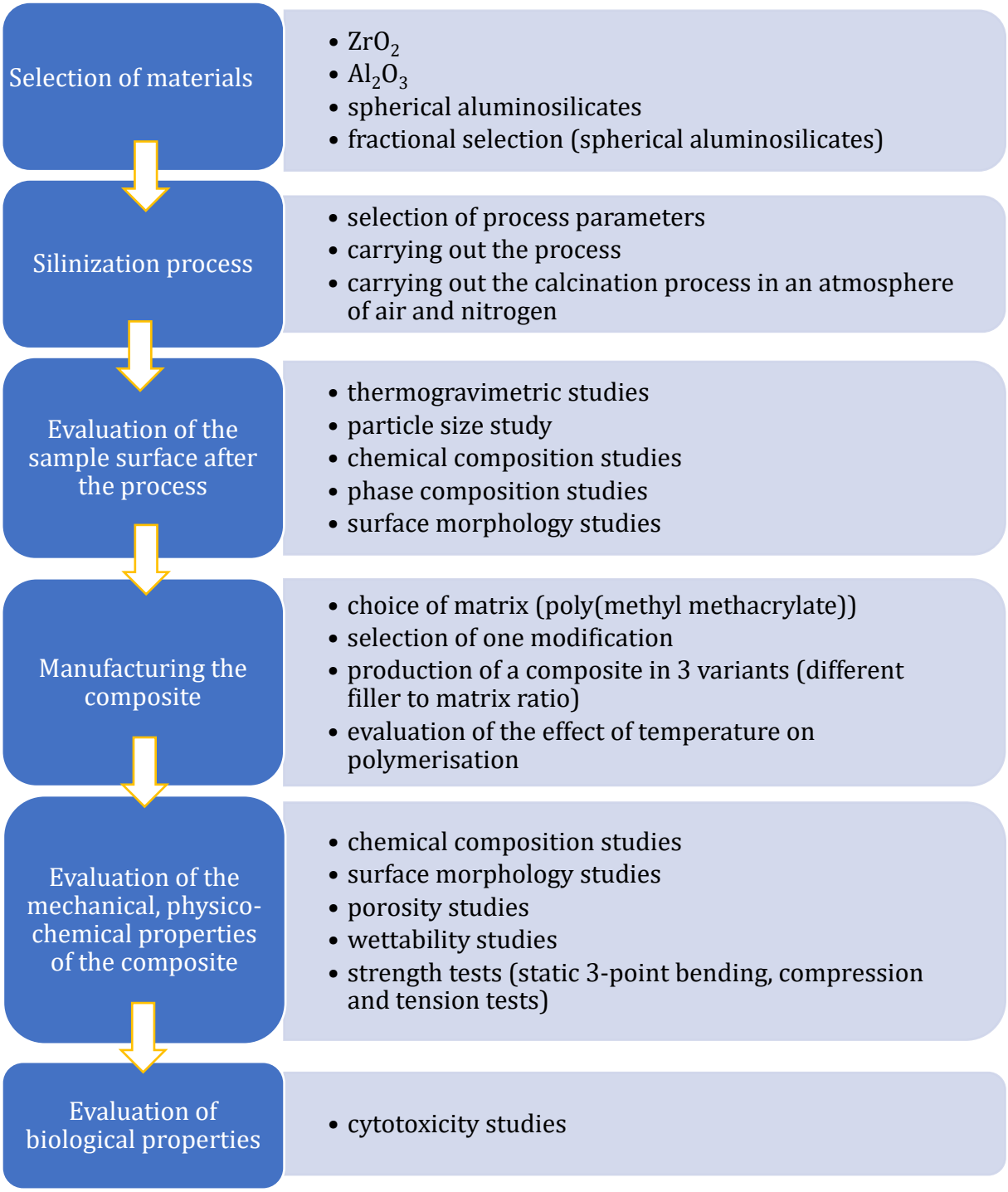

Fig. 16. Diagram of the completed research plan

2. Materials

Three materials in powder form were used for the study. Aluminum oxide (Al_2O_3) (CAS: 1344-28-1, Acros Organics, Geel, Belgium), zirconium oxide (ZrO_2) (CAS: 1314-23-4, Acros Organics, Geel, Belgium), and spherical aluminosilicates (origin: GRES-2 Powerplant, Kazakhstan). Cenospheres were cleaned with sonicated demineralized water and those with visible defects or fouling were removed. Three fractions were selected for further study due to the literature review. The fractions (approximately 90 μm, 150 μm and 212 μm) were separated using a linear vibrating sieve (Multiserw Morek,LPzE-2e, Marcyporeba, Poland).

Polymethylmethacrylate-based bone cement was used as the matrix for the composite. The selected bone cement consists of a powder and a liquid of the composition shown in the Tab. 9.

Tab. 9. Chemical composition of bone cement

Powder		Liquid	
Methyl Polymethacrylate	17.52 g	Methyl Methacrylate	9.88 ml
Benzoyl Peroxide	0.48 g	N,N dimethyl p-toluidine	0.12 ml
Barium Sulphate Ph. Eur.	2.00 g	Hydroquinone	18-20 ppm

2.1 Development of the silinization process

The silanization process involves three key steps:

1. **Surface Cleaning and Etching**: This step prepares the surface by removing contaminants and creating a reactive surface.
2. **Application of the Silanizing Agent**: A silane compound is applied, which forms chemical bonds with the surface.
3. **Calcination**: The treated surface undergoes heat treatment to enhance bonding and stability.

Considering the variety of silanizing agents available, the modifications illustrated in Fig. 17. were specifically selected to optimize performance in this process.

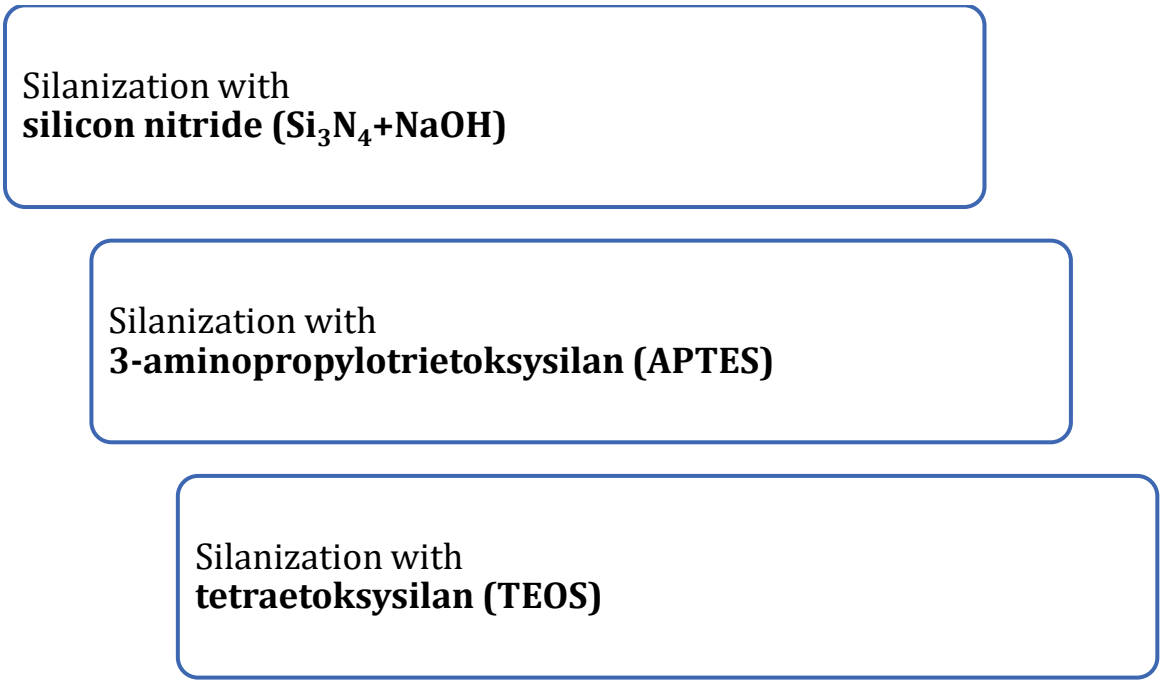

Fig. 17. Diagram showing the selection of silanization processes

2.1.1. Cleaning and etching the surface

Surface preparation for each of the three powders: Al_2O_3, ZrO_2, Cenospheres (90µm, 150µm, 212µm) were done the same way. Initially, the powders were cleaned and verified for visible dirt or defects. Each of the powders was measured on a laboratory balance (RADWAG, AS 160/C/2), and then the etching process was carried out with so-called Caro Acid. The acid was prepared from H_2SO_4 (Cas: 7664-93-9, 95% Acros Organics, Geel, Belgium) and H_2O_2 (Cas: 7722-84-1, 30%) in a ratio of 3:1 in a beaker on a magnetic stirrer (speed about 350 rpm) (LABWARE uniSTIRRER 3).

After about 10 min of combining the substances, the previously measured powder was added. The digestion process continued for 15 min with continuous stirring (350 rpm). The powder was then filtered on a 70-quantity filter under vacuum using a water pump (2x 500cm^3). After pH analysis, neutralization was performed with ammonia water (CAS: 1336-21-6, Chempur, Piekary Śl., Poland). Until neutralization, the procedure was repeated on a magnetic stirrer at 250 rpm. After re-filtration, the samples were dried at 100°C for 24 hours in a dryer (Pol-Eko Aparatura) (Fig. 18).

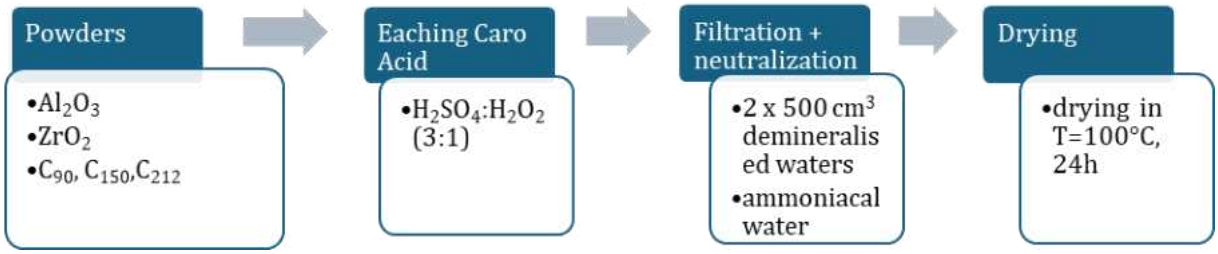

Fig. 18. Diagram showing the process of functionalization of powder surfaces

2.1.2. Application of silanizing agent

2.1.2.1. Silanization with silicon nitride (Si_3N_4+NaOH)

Previously prepared specimens (Al_2O_3, ZrO_2 and C_{90}, C_{150}, C_{212}) were weighed using a laboratory scale (RADWAG, AS 160/C/2) after the etching process. A sodium hydroxide solution (10M) (CAS: 1310-73-2, Chempur, Piekary Śl., Poland) was then prepared and placed on a magnetic stirrer (approximately 350 rpm) (LABWARE uniSTIRRER 3). After 15 minutes, 10 wt% silicon nitride (Si_3N_4) (CAS: 12033-89-5, Sigma Aldrich) was added, and the beaker was left on the magnetic stirrer. After an additional 30 minutes, the pre-measured sample was added (this process was repeated separately for each powder type). The stirring process continued on the magnetic stirrer (at approximately 250 rpm). A critical aspect of the procedure is ensuring that the sample is immersed in a volume three times its own size. After 24 hours, the process was completed, and the sample was placed in an ultrasonic cleaner (Ulsonix Ultrasonic Cleaner, proclean 10.0DSP) for 20 minutes. The sample was then rinsed, and the powder was filtered through a quantitative filter paper 70 under vacuum using a water pump (2x 500cm^3). Finally, the samples were dried at 100°C for 24 hours in a laboratory dryer (Pol-Eko Aparatura) – Fig. 19.

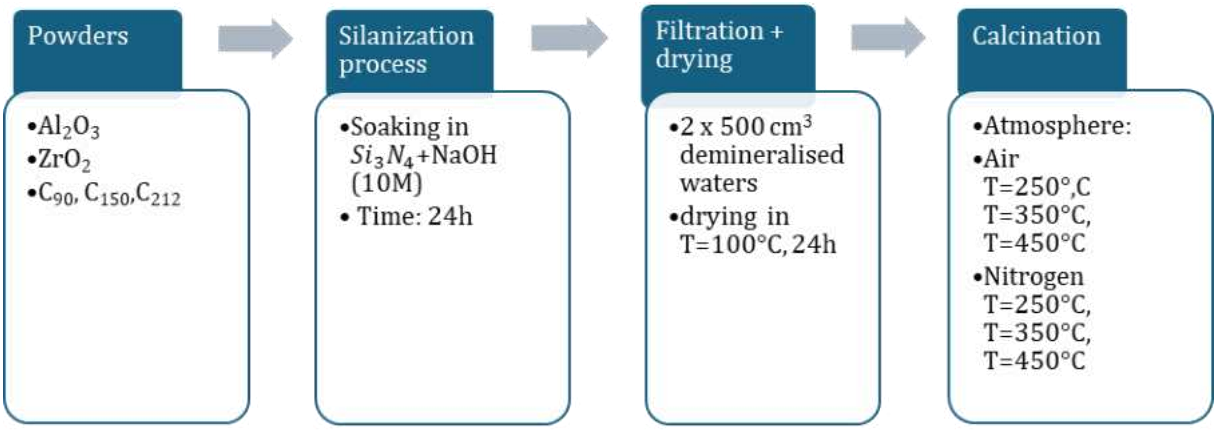

Fig. 19. Diagram showing silanization process using silicon nitride Si_3N_4 with sodium hydroxide (NaOH)

2.1.2.2. Silanization with 3-aminopropylotrietoksysilan (APTES)

Previously prepared samples (Al_2O_3, ZrO_2 and C_{90}, C_{150}, C_{212}) after the digestion process were weighed on a laboratory balance (RADWAG, AS 160/C/2). Then a suspension was prepared with propanol (CAS: 67-63-0, Chempur, Piekary Śl., Poland), the ratio to the sample was (1:5). The prepared suspension was set on a magnetic stirrer (speed of about 250 rpm) (LABWARE uniSTIRRER 3), the duration of stirring was 1h. After the time, the sample was rinsed, and the powder was filtered on a volume 70 filter under vacuum using a water pump (2x 500cm^3).

The samples were dried at 100°C for 24 hours in an oven (Pol-Eko Apparatus). A suspension was prepared from 3-aminopropyltriethoxysilane (APTES) (CAS: 919-30-2, Sigma Aldrich) with propanol in a ratio of (1:10). The suspension was placed on a magnetic stirrer at (speed about 350 rpm) After 15 min, a pre-measured sample was added (the process was repeated separately for each type of powder). The silanization process took 12h, after which time, the sample was placed in an ultrasonic cleaner (Ulsonix Ultrasonic Cleaner, proclean 10.0DSP) for 20min. Then the sample was rinsed, and the powder was filtered on a volume 70 filter under vacuum using a water pump (2x 500cm^3). The samples were dried at 80°C for 24h in a dryer (Pol-Eko Apparatus) – Fig. 20.

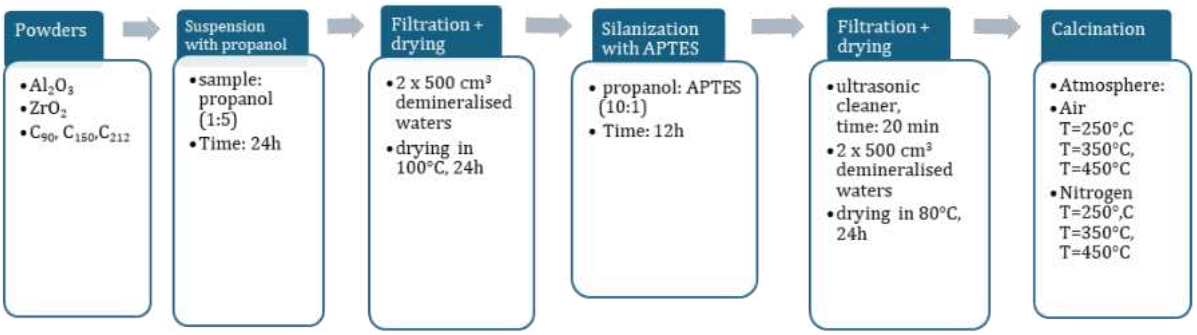

Fig. 20. Diagram showing silanization process using 3-aminopropylotrietoxysysilane (APTES)

2.1.2.3. Silanization with tetraethoxysilane (TEOS)

Previously prepared samples (Al_2O_3, ZrO_2 and C_{90}, C_{150}, C_{212}) after the digestion process were weighed on a laboratory balance (RADWAG, AS 160/C/2). A solution was prepared with 25wt% ethanol (CAS: 64-17-5, POL-AURA, Morąg, Poland) and 15 wt% tetraethoxysilane (TEOS) (CAS: 78-10-4, Sigma Aldrich). The pH was raised to 4 za using

acetic acid (64-19-7, Warchem, Zakręt, Poland). The suspension prepared in this way was placed on a magnetic stirrer (speed about 250 rpm) (LABWARE uniSTIRRER 3), the stirring time being 1.5h at an elevated temperature of 50°C. The sample was then placed in an ultrasonic cleaner (Ulsonix Ultrasonic Cleaner, proclean 10.0DSP) for 20min. The sample was then rinsed, and the powder was filtered on a volume 70 filter under vacuum using a water pump (2x 500cm^3). The samples were dried at 80°C for 24h in a dryer (Pol-Eko Apparatus) – Fig. 21.

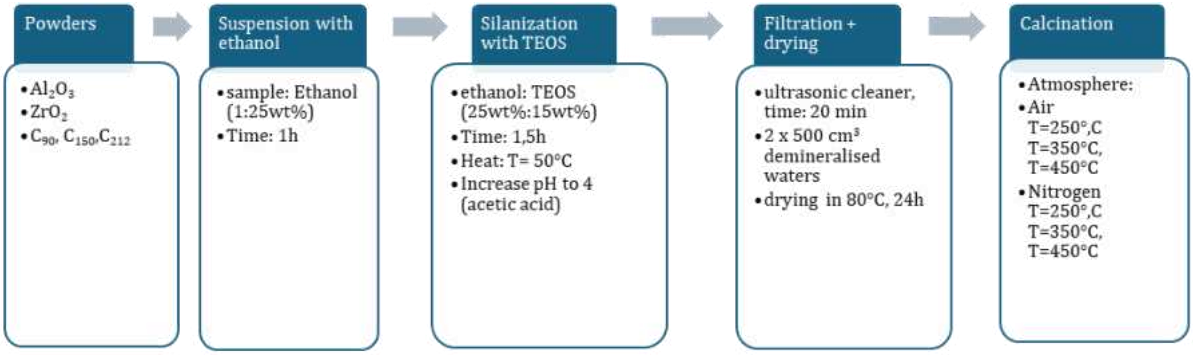

Fig. 21. Diagram showing silanization process using tetraethoxysilane (TEOS)

2.1.3. Calcination process

The calcination process was reflected, for each variant presented. Two types of calcination atmosphere were chosen air and nitrogen. Temperatures were declared at T=250°C, T=350°C and T=450°C. The calcination process in the air atmosphere was carried out in a high-temperature furnace (Renfert, Magma). On the other hand, the calcination process in a nitrogen atmosphere was carried out in a tubular high-temperature furnace (type PRC 75/150 WM from CZYLOK (Poland)). The process characteristics for both selected atmospheres are presented below. The process consisted of gradually heating the sample (the temperature step was set at T=9°C/min) and holding the sample at the predetermined temperature for 1.5 h. After this time, there is a spontaneous cooling of the furnace and removal of the sample (Fig. 22.).

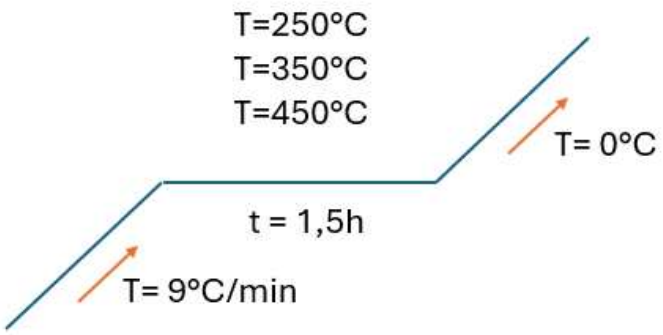

Fig. 22. Diagram showing the process of calcination

3. Manufacturing of the composite

The proposed bone cement modification includes the production of bone cement with spherical aluminosilicate fillers after silanization with Si_3N_4 with a selected fraction of 150μm. Three more variants of modified composite were produced by adding 20, 30 and 40% by weight, respectively, of cenospheres. The variants tested are shown in Tab. 9.

- **CK** - bone cement based on poly(methyl methacrylate).
- **GK** - aluminous spherical silicates after modification with Si_3N_4.

Tab. 9. Type of samples selected for testing

	CK	CK+GK 20%	CK+GK 30%	CK+GK 40%
Proportion by weight	20g/10 ml	16g+4g/10 ml	14g+6g/10 ml	12g+8g/10 ml

The total polymerization time was 10 min, at room temperature T=24°C. The relationship between temperature and time is shown in Fig. for which the manufacturer made such observations:

- The Sticky, Insertion and Polymerization phases correspond to average values.
- A deviation of ± 30 sec. is possible in the sticky and implant insertion phases.
- A deviation of ± 90 sec. Is possible in in the polymerization phase.
- Relative proportion of the powder and liquid components (as percent mass): 67%(powder)/ 32,2% (liquid) - by weight 2,1g (powder)/ 1ml (liquid).

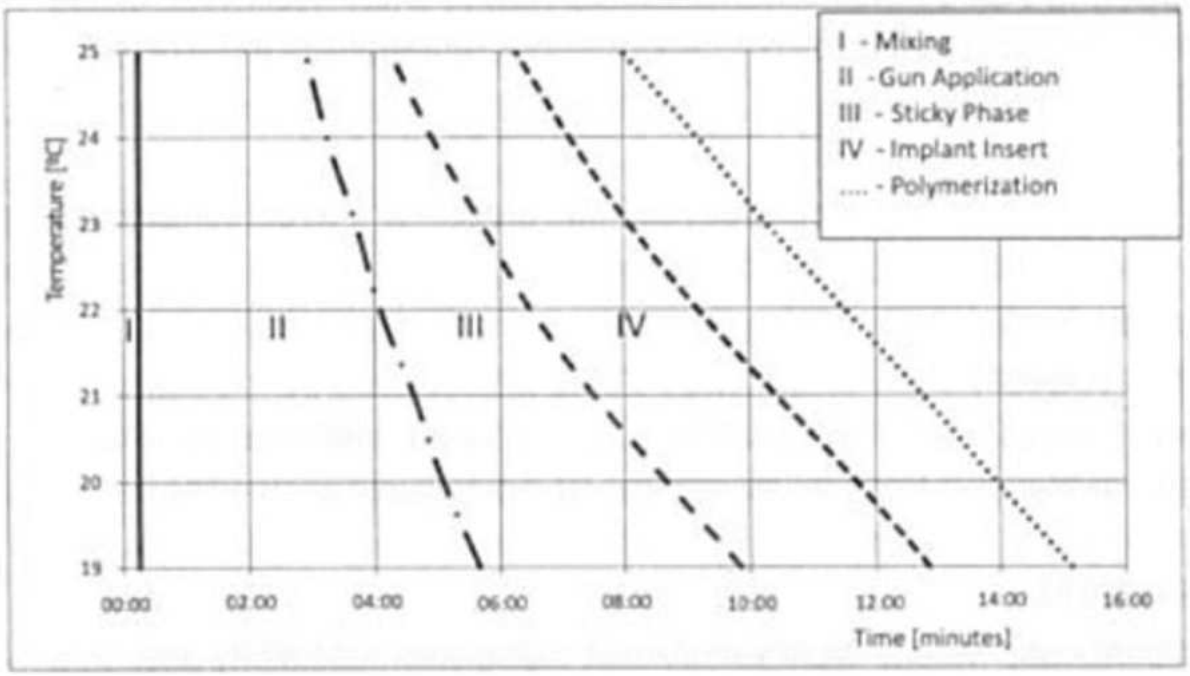

Fig. 23. Relation between working time and temperature for using bone cement (I – Mixing, II- Gun application, III - Sticky phase, IV - Implant insert), information in product

4. Methods

4.1 Thermogravimetric analysis

The thermal analysis demonstrates the changes in sample mass as the temperature increases, providing insights into the material's behavior during heating. Two devices were utilized for the tests: a Thermogravimetry Analyzer SII TGA/DTA 7300 EXSTAR series, and a Setsys 24 Evolution Setaram (Setaram, France). The measurements were conducted in an air atmosphere (75 ml.min^{-1}) in the temperature range of 20 to 1000 ºC, with a temperature-increasing rate of 10º/min. The sample mass was about 10 mg. The study was carried out for Al_2O_3 and ZrO_2 samples and spherical aluminosilicates (C_{90}, C_{150}, C_{212}) after surface modification with silicon nitride with sodium hydroxide (Si_3N_4 +NaOH) treatment.

4.2 Particle size study

The particle size (PS) was determined using the HORIBA Laser diffraction particle size analyzer LA-950 instrument (Kyoto, Japan). The PS analysis was carried out for an aluminosilicate sample with a fraction of about 150 μm. After all types of modification. Particle size distributions were evaluated via the Origin software.

4.3 Chemical composition study

The chemical composition for 150-μm fraction spherical aluminosilicates, using three modifications (Si_3N_4+NaOH, APTES and TEOS), was confirmed by X-ray photoelectron spectroscopy (XPS) in ultra-high vacuum (base pressure of 8.5×10^{-9} Pa). The study was carried out using a PREVAC EA15 semi-spherical electron energy analyzer, which was equipped with a 2D-MCP detector, and a PREVAC XR-40B monochromatic X-ray source (Al-Kα line, energy 1486.60 eV).

Overview spectra were collected with the transition energy (PE) set at 200 eV (with a scanning step of 0.8 eV), and for individual energy regions at 100 eV (with a scanning step of 0.06 eV). All measurements were performed at a normal start angle and using a curved analyzer output slit (0.8 × 25 mm) to achieve high energy resolution.

Calibration of the binding energy scale was performed based on the Au 4f region (84.0 eV) of the gold-coated sample, which took place in the same sampling step. The spectra were analyzed using CASA XPS® software (version 2.3.25), which used built-in algorithms for fitting. The out-of-focus components were fitted using the product of Gaussian (30%) and Lorenz (70%) functions. The background was subtracted using the Shirley function.

4.4 Phase composition study

Phase analysis (qualitative and quantitative) of the starting powders (C_{212}, C_{150}, C_{90}) and after modification (Si_3N_4+NaOH, APTES and TEOS) were carried out based on the X-ray diffraction method. The study was carried out using an X-ray diffractometer. X-ray powder diffraction (XRD) analysis was carried out using an Ultima IV diffractometer (RIGAKU, Japan) equipped with a scintillation detector, CuKα radiation and NiKβ filter. Powder samples were sampled using a Bragg-Brentano system under ambient atmosphere, standard sample holder and conditions of 40 kV, 40 mA, scan rate of 3.0°/min. Phase analysis was evaluated by the PDF-2 Release 2022 database. Phase analysis was also performed using an X'pert pro X-ray diffractometer (Panalytical, Almelo, Netherlands) equipped with a cobalt-lamp X-ray source (XRD). X-ray phase diffraction was measured according to the Bragg-Brentano geometry. The obtained diffractograms were analyzed using X'pert high score plus software (v.3.0e) with a dedicated database of inorganic crystal structures - ICSD (Fiz, Karlsruhe, Germany).

4.5 Fourier Transform Infrared Spectroscopy analysis

The IR spectra were collected using FT-IR spectrometer Nicolet iS50 (ThermoScientific, USA) with DTGS detector. The measurement parameters were the following: spectral region 4000-400 cm^{-1}, spectral resolution 4 cm^{-1}; 64 scans; Happ-Genzel apodization. The IR spectra of samples were measured by ATR (Attenuated Total Reflectance) technique.

4.6 Microstructure analysis

Comparative images of the bone cement were captured using a LEICA M205A microscope, highlighting the differences before and after modification with spherical aluminosilicate.

Microscopic observations and qualitative analysis of alumina, zirconium oxide, spherical aluminosilicate powders before and after silanization, and a composite based on spherical aluminosilicates were carried out by scanning electron microscopy (SEM) on a Tescan Vega 4 equipped with an EDS X-ray dispersive spectrometer – Oxford Instruments. The conditions of the test carried out: high vacuum, SE detector, voltage 5 keV. The morphology of the alumina and zirconium oxide samples after modification with silicon nitride was determined using an SEM EVO MA10 (Zeiss, Oberkochen, Germany) equipped with an EDS spectrum analyzer. The bone cement samples were sputtered with a gold layer using a sputter coater (Bal-Tec, SCD 050, Sputter Coater). The duration of sputtering was 60s.

4.7 Porosity studies

The specific surface area (SBET) and the pore diameter distribution were determined based on the low-temperature nitrogen adsorption analysis, which was performed using the Quantachrome Autosorb IQ device at liquid nitrogen temperature (77 K). The specific surface area was determined using the BET (Brunauer-Emmett-Teller) method, while the pore diameter distribution was determined using the BJH (Barrett, Joyner and Halenda) method.

4.8 Polymerization temperature tests

The polymerization process during the creation bone cement in the unmodified state (CK) and after modification with spherical aluminosilicate fraction 150μm (CK+ GK20%, CK+GK30%, CK+GK40%) were carried out. The tests were carried out in a water capillary with a temperature of about T=37±1°C. The mixed powder and liquid bone were

introduced into a 10x20 mm vessel, and then a measuring probe was immersed to verify the temperature over time. The temperature was measured continuously with a probe thermometer (EPAG Thermometer, PRAGMATICO). Three measurements were made, for bone cement and its modification. All measurements carried out were performed at an air temperature of T=23±1°C.

4.9 Wettability tests

Surface wettability was evaluated by the sitting drop method using an Attention Theta Flex optical tensiometer (Biolin Scientific) with OneAttention software. A 2 mm^3 droplet of distilled water was used for the test. The measurement lasted 60 s, with a sampling frequency of 1 Hz. Three measurements were made for initial state of bone cement (CK) and after modification with spherical aluminosilicate fraction 150μm (CK+GK20%, CK+GK30%, CK+GK40%).

4.10 Mechanical properties tests for bone cement

The mechanical strength of the bone cements, before and after modification were evaluated based on the results of tensile strength, compressive and flexural tests. All tests conducted were performed at an air temperature of 20±1°C.

4.10.1 Static tensile test

The static tensile test was performed according to the recommendations of standard: EN ISO 527-1:1998 [21], DIN53455 [21,60] and ASTM D638 [21,60] at a tensile rate of 25mm/min, using an MTS Insight 2 testing machine with a 2 kN load cell and MTS TestSuite software. The distance between the grips was 60 mm. An observation area during rupture was determined on the 75x10x3mm paddle-shaped specimens, this included a 35x5x3mm constriction area (Fig 24).

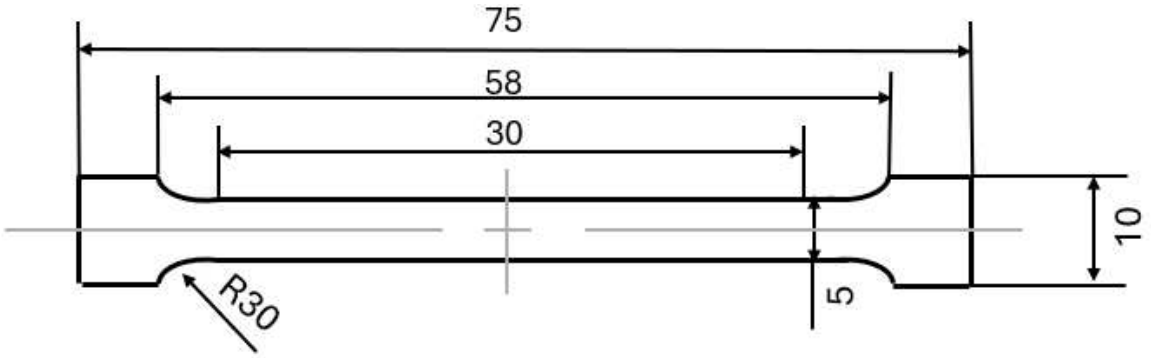

Fig. 24. Sample type 1BA for strength tests

From the tests, Young's modulus E [MPa], maximum breaking force Fmax [N], tensile strength Rm [MPa] and elongation at break A [%] were determined. Static tensile strength was carried out for bone cement in the initial state (CK) and after modification with spherical aluminosilicate fraction 150μm (CK+ GK20%, CK+GK30%, CK+GK40%). Five samples were tested for each variant.

4.10.2 Static uniaxial compression test

A static uniaxial compression test was carried out by the recommendations of ISO 5833 [21] and ASTM D695-91 [21] in the direction parallel to the growth direction at a constant speed of 1 mm/min on an MTS Criterion Model 43 testing machine. The tests were performed at room temperature. The measurement was carried out for cylindrical specimens with a diameter of 6 x 12 mm in bone cement in the initial state and after modification with spherical aluminosilicate fraction 150μm (CK+ GK20%, CK+GK30%, CK+GK40%). Five specimens were tested for each variant. The following were determined from the tests:

- maximum loading force F_{max} [N],
- compressive strength R_c [MPa],
- elastic modulus E [MPa].

4.10.3 Static three-point bending test

The static three-point bending test was carried out according to the recommendations of PN-79/C89027 [21] and ISO 5583 [21] at constant speed of v= 5 mm/min on an MTS Criterion Model 45 testing machine. The distance between the crossbars was l = 60 mm and the diameter of the rollers on which the specimen was placed was d = 5mm. The test was carried out for specimens with a length of L = 10 mm and width D = 3.3 mm in the initial state (CK) and after modification with spherical aluminosilicate fraction 150μm (CK+ GK20%, CK+GK30%, CK+GK40%). During the test, maximum loading force F_g [N], bending strength R_g [MPa], elastic modulus E [MPa] were determined. The bending test was performed on 5 samples of each variant.

4.11 Biological studies – cytotoxicity

The method considered extracts. The material samples were placed in pure medium for 24 hours. In this case, the medium from above the samples was mixed with pure cell medium in the ratio:

- 1 mL of medium from above the sample (10:0);
- 0.9 mL of sample extract and 0.1 mL of pure medium (9:1);
- 0.8 mL of sample extract and 0.2 mL of pure medium (8:2);
- 0.7 mL of sample extract and 0.3 mL of pure medium (7:3);
- 0.6 mL of sample extract and 0.4 mL of pure medium (6:4);
- 0.5 mL of sample extract and 0.5 mL of pure medium (5:5);
- 0.4 mL of sample extract and 0.6 mL of pure medium (4:6);
- 0.3 mL of sample extract and 0.7 mL of pure medium (3:7);
- 0.2 mL of sample extract and 0.8 mL of pure medium (2:8);
- 0.1 mL of sample extract and 0.9 mL of pure medium (1:9);
- 1 mL pure medium (0:10).

The prepared solutions were then placed in a culture vessel and in an incubator (37 °C, 5 % CO_2), and after 24 and 48 hours, the supernatant was collected into 2 mL Eppendorf tubes and centrifuged (5 min, 1000 rpm), 200 µl of solution was collected each into two Eppendorf tubes intended for and tested for LDH content. The level of LDH secreted from the tested samples was analyzed. The LDH assay was performed according to the manufacturer's protocol (CytoTox 96® Non-Radioactive Cytotoxicity Assay, G1780, Promega Corporation, Madison, WI, USA) and Cobas Integra analyzer (ROCHE).

5. Results

5.1 Thermogravimetric analysis

The results from the thermogravimetric analysis of Al_2O_3, ZrO_2, and aluminosilicates modified with silicon nitride are shown in Fig. 5. As can be seen, all samples are thermally stable up to 1000°C.

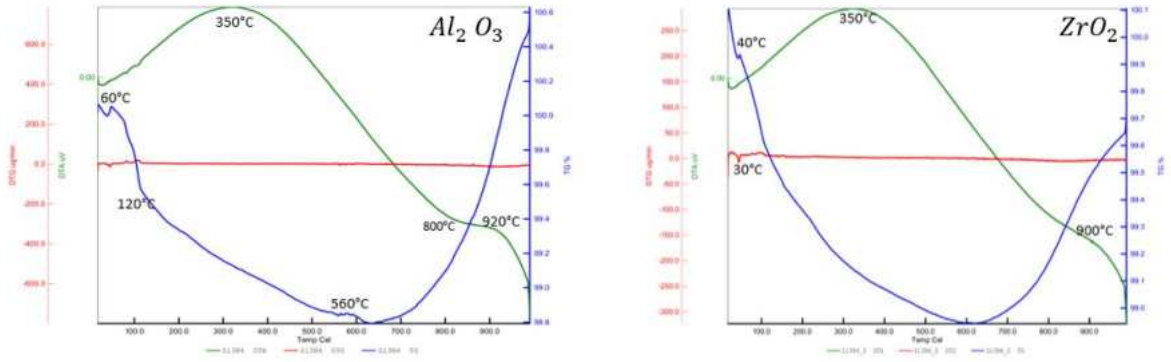

Fig. 25. Thermogravimetry results for alumina Al2O3 and zirconium oxide ZrO2 after modification with silicon nitride

The thermogravimetry results for aluminosilicates C_{90}, C_{150}, C_{212} were shown on the Fig26, Fig27, and Fig28, respectively.

For a complete characterization of the process during thermal treatment for aluminosilicate materials, it was found that kaolinite loses bound water from hydroxyl groups surrounding aluminum atoms to form an amorphous phase, metakaolin, at about 400C. It remains unchanged until 950±1000°C, when a rapid reorganization of the oxide ions in the lattice structure transforms into a spinnel-like form of g-oxide of aluminum and further mullite. Where the final form of aluminosilicates is a mixture of cristobalite and crystallized mullite [93]. The reaction of Si_3N_4 with NaOH produces Na_4SiO_4, which is bound to cenospheres (aluminosilicates), and show an endothermic effect at around 300°C, when gases and water are released from the glassy mas. After exceeding 900C, the aluminosilicate was likely transformed into a residual share of spinel or into the final phase i.e. mullite was formed with a residual occurrence of silicon nitride, which shows rapid oxidation at such temperatures.

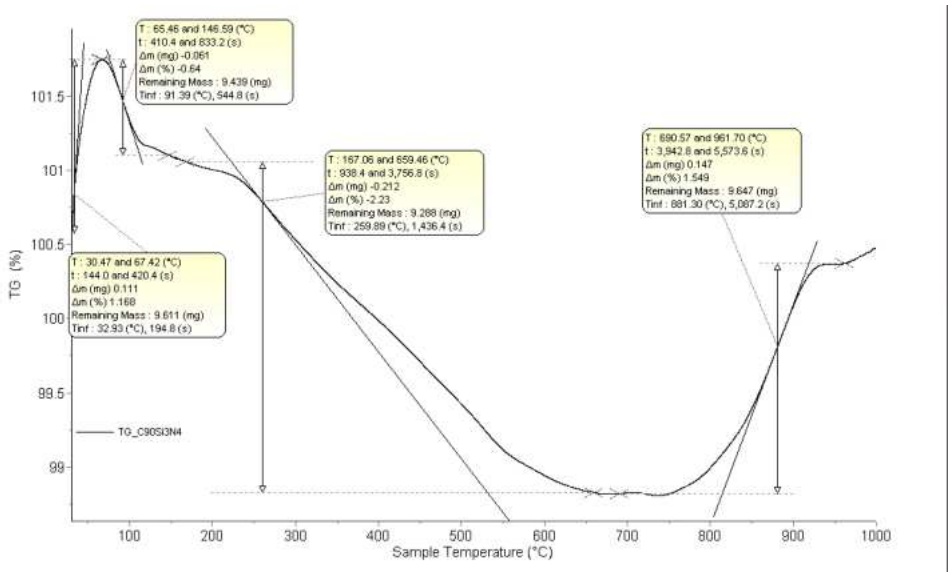

Fig. 26. Thermogravimetry results for aluminosilicates (C_{90}) modification with silicon nitride

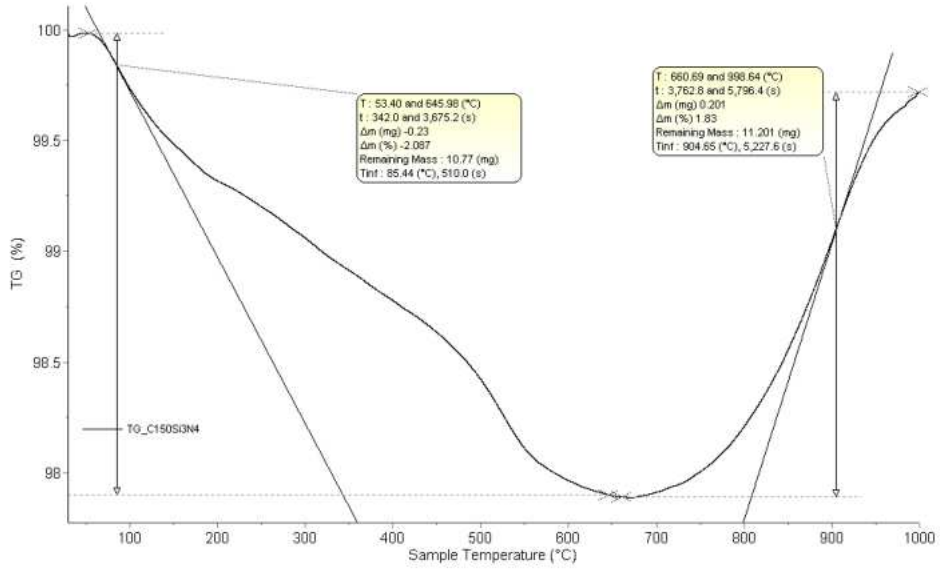

Fig. 27. Thermogravimetry results for aluminosilicates (C_{150}) modification with silicon nitride

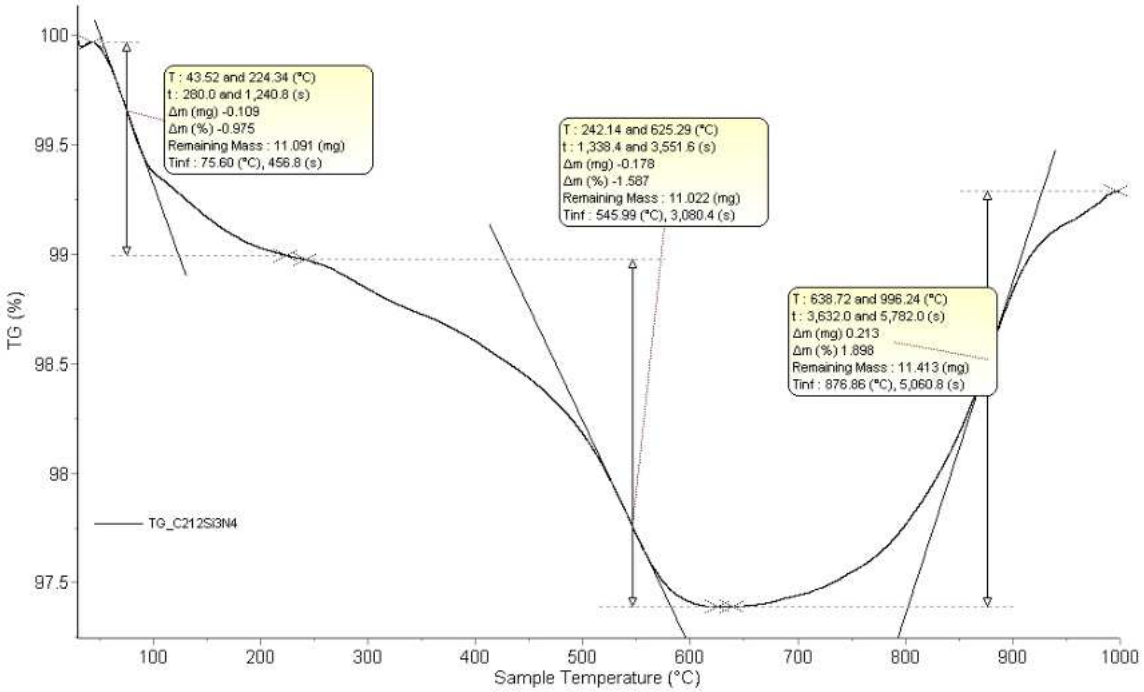

Fig. 28. Thermogravimetry results for aluminosilicates (C_{212}) modification with silicon nitride

5.2 Particle size study

Particle size distributions (PSD) in volumetric content are shown in Fig. 169, particle size parameters (PS) were evaluated. The graph shown is biomodal in nature. Caro 150, represented by the red curve, shows a predominant cumulative particle size at approximately 101.5 µm, indicating a significant presence of larger particles. In contrast, C150_Si3N4 (green curve) features smaller particle sizes, peaking at around 0.3 µm, 15.2 µm and 88.6 µm, suggesting a diverse range of particle sizes that may enhance the material's reactivity and bonding characteristics. C150_APTES (blue curve) exhibits a mean particle size of approximately 67.5 µm, while C150_TEOS (black curve) presents a relatively uniform distribution with a mean size of 88.6 µm.

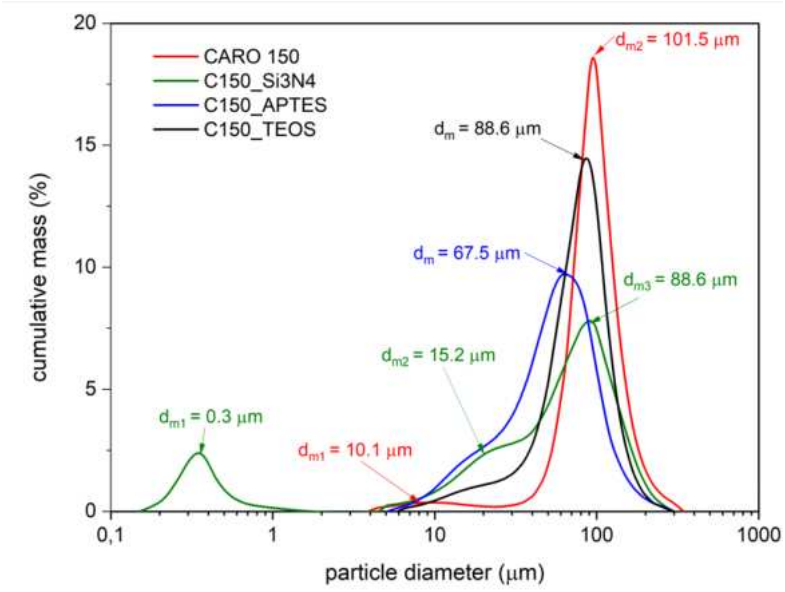

Fig. 169. Particle size distribution for spherical aluminosilicate with a fraction of about 150 µm, for all modifications

5.3 Chemical composition study

The XPS method was used to determine the chemical composition of the surface layer for 150 µm fraction spherical aluminosilicates, for three modifications using (Si_3N_4+NaOH, APTES and TEOS). The surface layers, for each of the samples, revealed the presence of elements viz: Si, N, O, Fe, Na, Mg, Al. For the surfaces of the samples modified in this way, their overview spectra were also recorded - (Fig. 30-32)

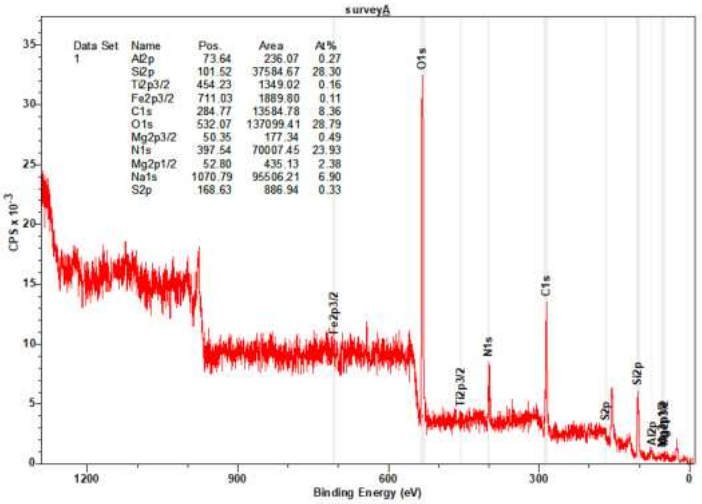

Fig. 30. X-ray photoelectron spectroscopy (XPS) plot, for modification with silicon nitride (Si_3N_4+NaOH)

Silicon occurred in two chemical states: the main Si2p line came from pure silicon with an energy of 101.52eV [95], while the weak line with an energy of 397.54 eV [96] came from Si_3N_4. For aluminum, the metallic state dominated with an energy of 73.62 eV - the Al2p line[95]. Oxygen occurred mainly in association with silicon - SiO_2. The frosty C1s line can be attributed to several chemical states. The main line with an energy of 284.77eV indicates the presence of a C=C/C-Si type mixture. Other weak lines in the maximum with energies much higher than 285.30 eV can be attributed to a chemical compound containing oxygen or carbonate formed in the modification process. Nitrogen, on the other hand, in addition to the presence of a compound with silicon Si_3N_4, also showed a line with an energy of 454.23 eV. This line can be associated with TiN. Magnesium was present in two chemical states: Mg2p1/2, with an energy of 52.80, came from MgO, while the weak line Mg2p2/3, with an energy of 50.35 eV, came from $Mg(CH_3COO)_2$. In addition, the performance of detailed spectra allowed the identification of chemical compounds and the quantitative contribution to the surface layer. All results in Tab. 12.

Tab. 12. Chemical composition of the surface layer of spherical aluminosilicates of 150µm fraction modified with Si_3N_4 +NaOH determined by XPS method

Element	Atomic concentration [%]	Chemical compound
Al	0.27	Al
Si	28.30	SiO_2, Si_3N_4
C	8.36	C=C/C-Si, $Mg(CH_3COOH)_2$, surface contamination
O	28.79	SiO_2, MgO, $Mg(CH_3COOH)_2$, surface contamination
N	23.93	Si_3N4, TiN
Ti	0.16	TiN
Mg	2.87	MgO, $Mg(CH_3COOH)_2$

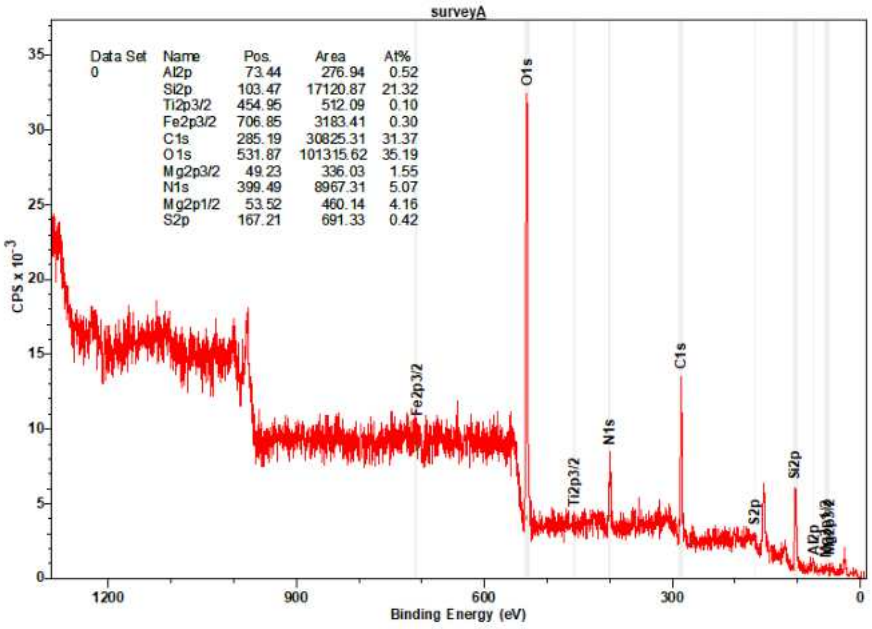

Fig. 31. X-ray photoelectron spectroscopy (XPS) plot for modification with 3-aminopropyltriethoxysilane (APTES)

Silicon occurred in a single chemical state: the main Si2p line came from the silicon compound SiO_2 with an energy of 103.47eV [95, 96]. For aluminum, the metallic state dominated with an energy of 73.44 eV - the Al2p line [95]. Oxygen occurred mainly in the silicon compound SiO_2. The frosty C1s line can be attributed to several chemical states. The head line with an energy of 285.19eV indicates the presence of a C-C/C-H type mixture. Other weak lines in the maximum with energies much higher than 285.30 eV can be attributed to chemical compounds containing oxygen or carbonate formed in the modification process. In contrast, the nitrogen line with an energy of 399.49 eV this one can be associated with many chemical compounds, such as organic compounds containing NH_3 groups. The line with an energy of 454.95 can be bound to TiN [95]. Magnesium was found in two chemical states: Mg2p1/2, with an energy of 53.52eV, came from MgO, while the weak line Mg2p2/3, with an energy of 49.23 eV, came from $Mg(CH_3COO)_2$. In addition, the performance of detailed spectra allowed identification of the chemical compounds and the quantitative contribution to the surface layer. All results were presented in Tab. 13.

Tab 13. Chemical composition of the surface layer of spherical aluminosilicates with 150µm fraction modified with APTES determined by XPS method

Element	Atomic concentration [%]	Chemical compound
Al	0.52	Al
Si	21.23	SiO_2
C	31.37	C=C/C-H, $Mg(CH_3COOH)_2$, surface contamination
O	35.19	SiO_2, MgO, $Mg(CH_3COOH)_2$, surface contamination
N	5.07	NH_3,TiN
Ti	0.10	TiN
Mg	5.71	MgO, $Mg(CH_3COOH)_2$

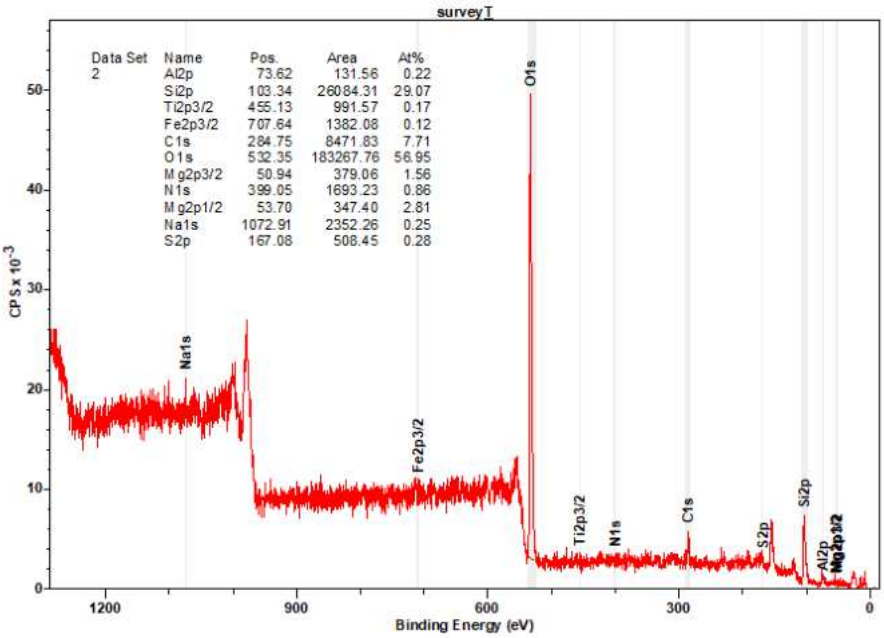

Fig. 172. X-ray photoelectron spectroscopy (XPS) plot, for modification with Tetraethoxysilane (TEOS)

Silicon occurred in one chemical state: the main Si2p line came from the silicon compound SiO_2 with an energy of 103.24 eV [95]. For aluminum, the dominant metallic state was the Al2p line, with an energy of 73.62 eV [95]. Oxygen occurred mainly in the silicon compound SiO_2 at an energy of 532.35 eV. The measured C1s line can be attributed to several chemical states. The main line with an energy of 284.75 eV indicates the presence

of a C-C/C-H type mixture. Other weak lines in the maximum with energies much higher than 285.30 eV can be attributed to a chemical compound containing oxygen or carbonate formed in the modification process. In contrast, the nitrogen line with an energy of 399.05 eV this one can be associated with many chemical compounds, such as organic compounds containing NH_3 groups. The line with an energy of 455.13 can be bound to TiN [95]. Magnesium was found in two chemical states: Mg2p1/2, with an energy of 53.70 eV, came from MgO, while the weak line Mg2p2/3, with an energy of 50.94 eV, came from $Mg(CH_3COO)_2$. In addition, the performance of detailed spectra allowed identification of the chemical compounds and the quantitative contribution to the surface layer. All results in Tab. 14.

Tab 14. Chemical composition of the surface layer of 150μm fraction of TEOS-modified spherical aluminosilicates determined by XPS method

Element	Atomic concentration [%]	Chemical compound
Al	0.22	Al
Si	29.07	SiO_2
C	7.71	C=C/C-H, $Mg(CH_3COOH)_2$, surface contamination
O	56.95	SiO_2, MgO, $Mg(CH_3COOH)_2$, surface contamination
N	0.86	NH_3, TiN
Ti	0.17	TiN
Mg	4.37	MgO, $Mg(CH_3COOH)_2$

5.4 Phase composition study

Phase composition analysis was performed for all powders, with each modification showing the samples' phase changes. XRD patterns show the phase changes that were observed for the materials: Al_2O_3, ZrO_2, and aluminosilicates (C_{90}, C_{150}, C_{212}), using the different modifications (Si_3N_4+NaOH, APTES or TEOS). XRD pattern presented on *Fig.* of showed the presence of corundum and silicon nitride and the effect of this modification on the intensity of the reflections, which were read as silicon nitride Si_3N_4.

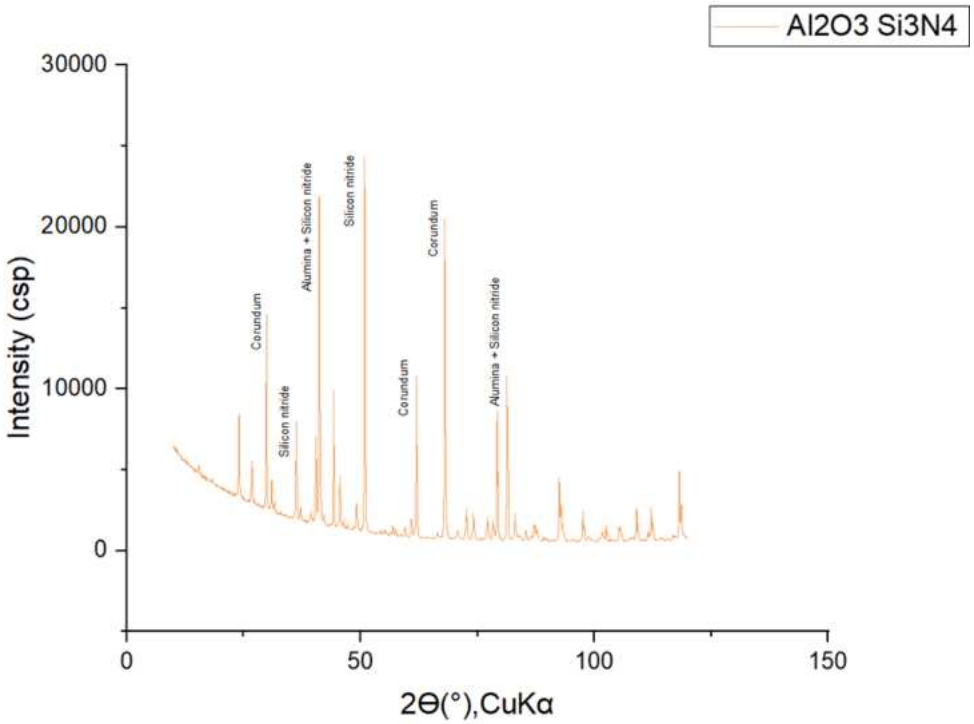

Fig. 33. XRD pattern of Al_2O_3 after Si_3N_4 modification

Fig. 34 shows analysis of the phase composition of zirconium oxide showing the presence of zirconium oxide and Si_3N_4, based on data sheets.

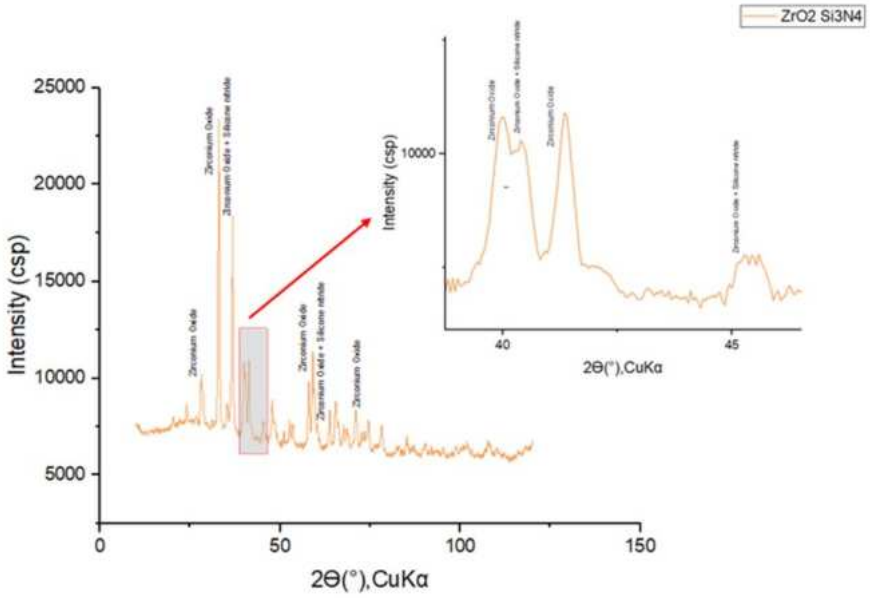

Fig. 34. XRD pattern of ZrO_2 after Si_3N_4 modification

Fig. 35. shows the XRD phase analysis for aluminosilicates. From the results, we find the occurrence of a mullite (M) and quartz (Q) phase, which are typical for microspheres. Moreover, the occurrence of reflections corresponding to Si_3N_4 was observed.

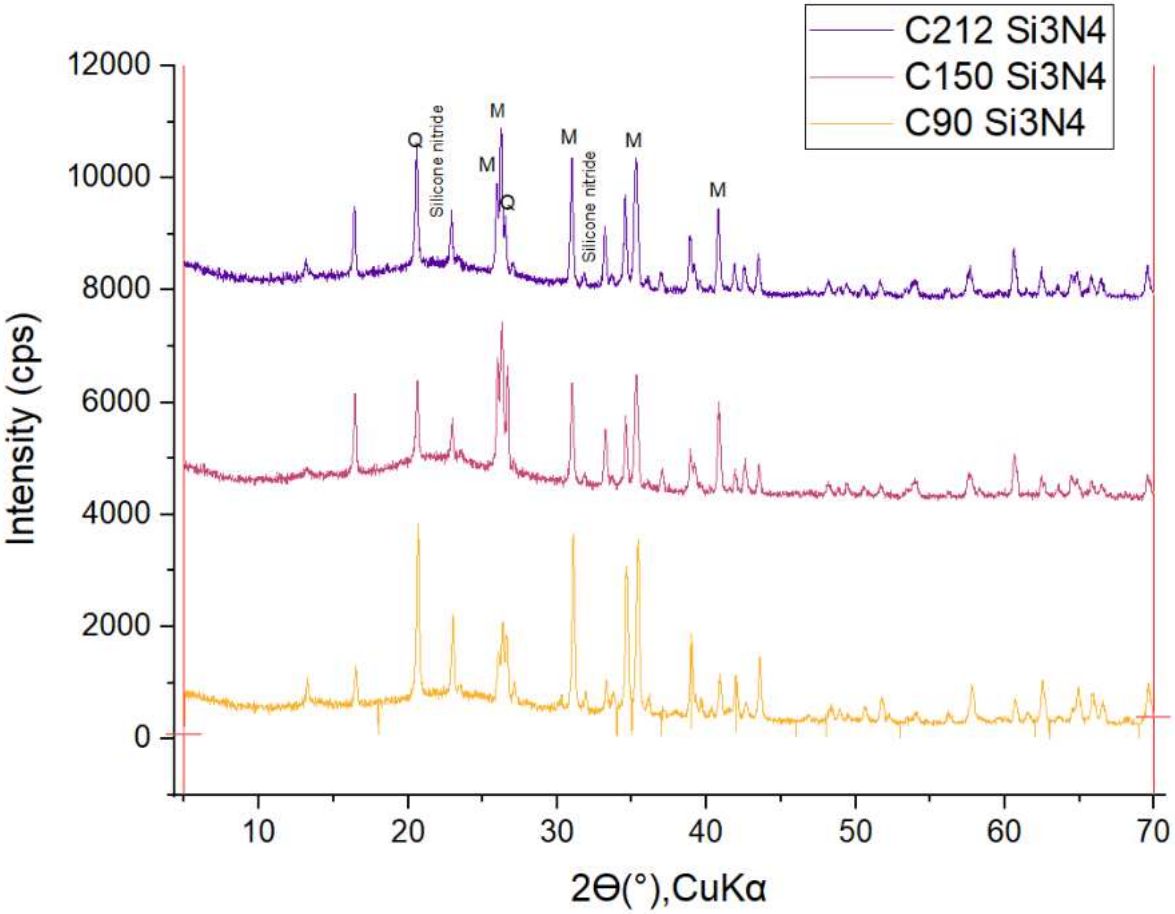

Fig. 35. XRD patterns of cenospheres after Si_3N_4 modifications

Figure 36 presents the results of the phase composition for zirconium oxide, did not see a significant effect on the variation for zirconium oxide, but noted the contribution of modification and the occurrence of characteristic reflections confirming the characteristics according to the data sheets. Fig. 37 for alumina, the phase composition characteristic of modification was also found.

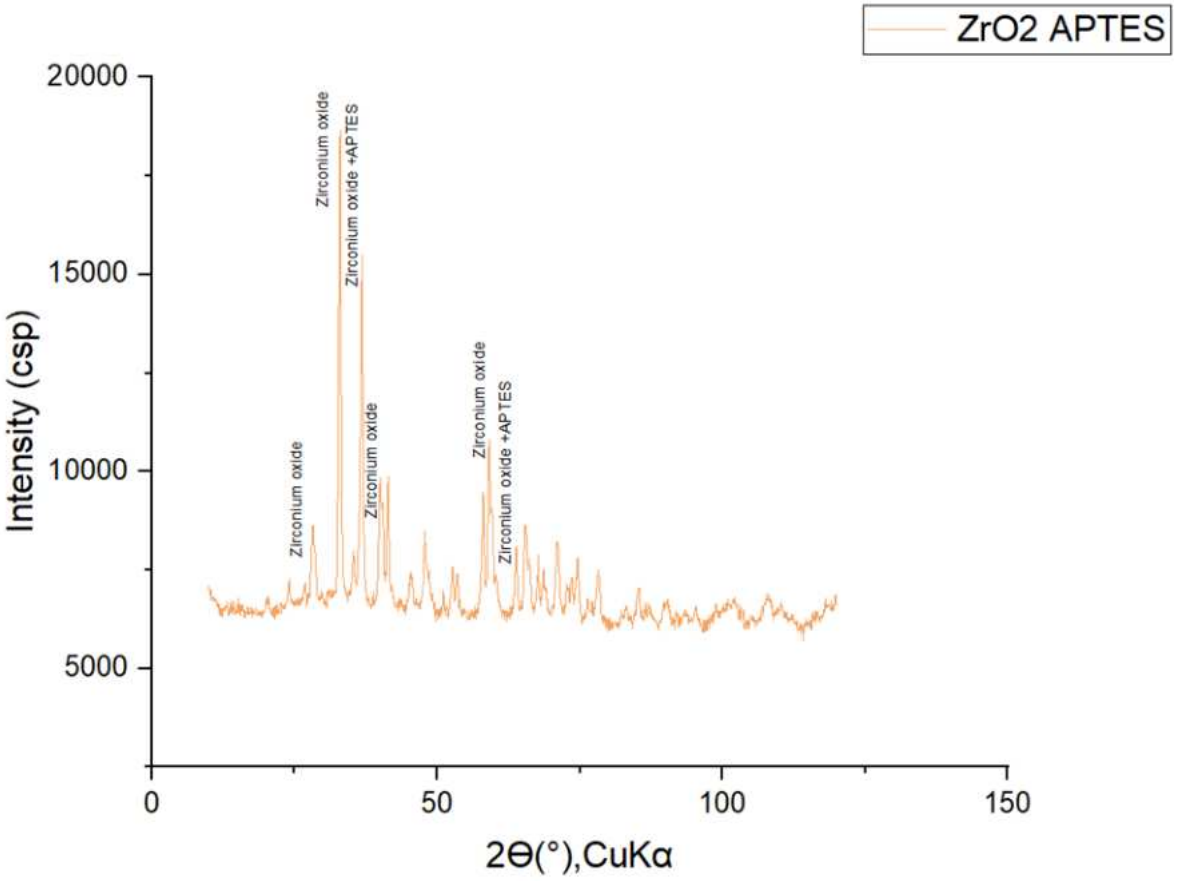

Fig. 36. XRD pattern of ZrO_2 after APTES modification

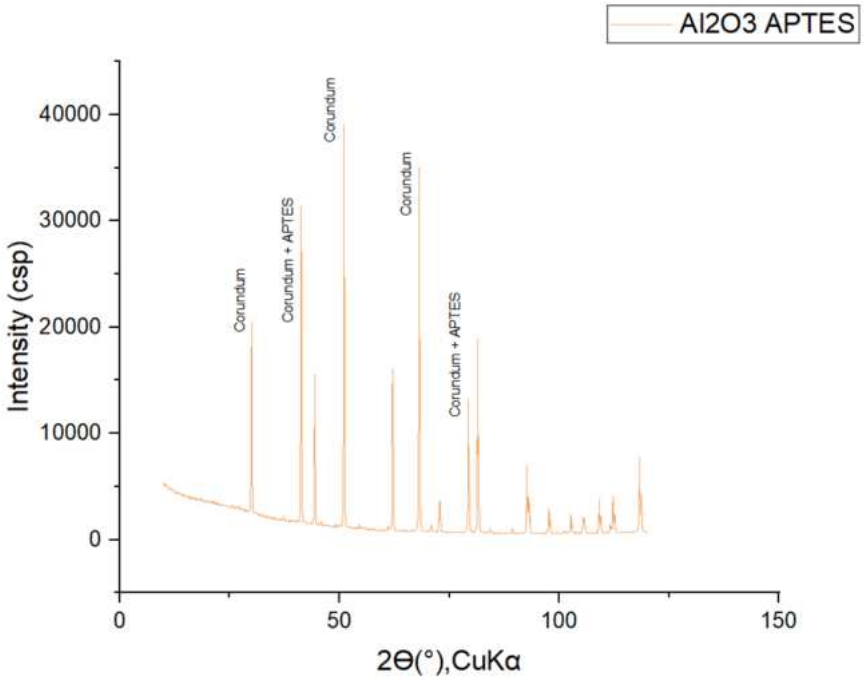

Fig. 37. XRD pattern showing the presence of modification phases for alumina

Fig 38 as in the case of modifications with silicon nitride, no major changes were observed between the proposed fractions. For cenospheres of fractions 150 μm and 90μm, Q was found, in contrast to fraction 212 μm, where only the phase M was seen. Due to the change in the nature of the reflection of about 2θ = 27°, it can be concluded that the effect of the modification is comparable to the modification with silicon nitride.

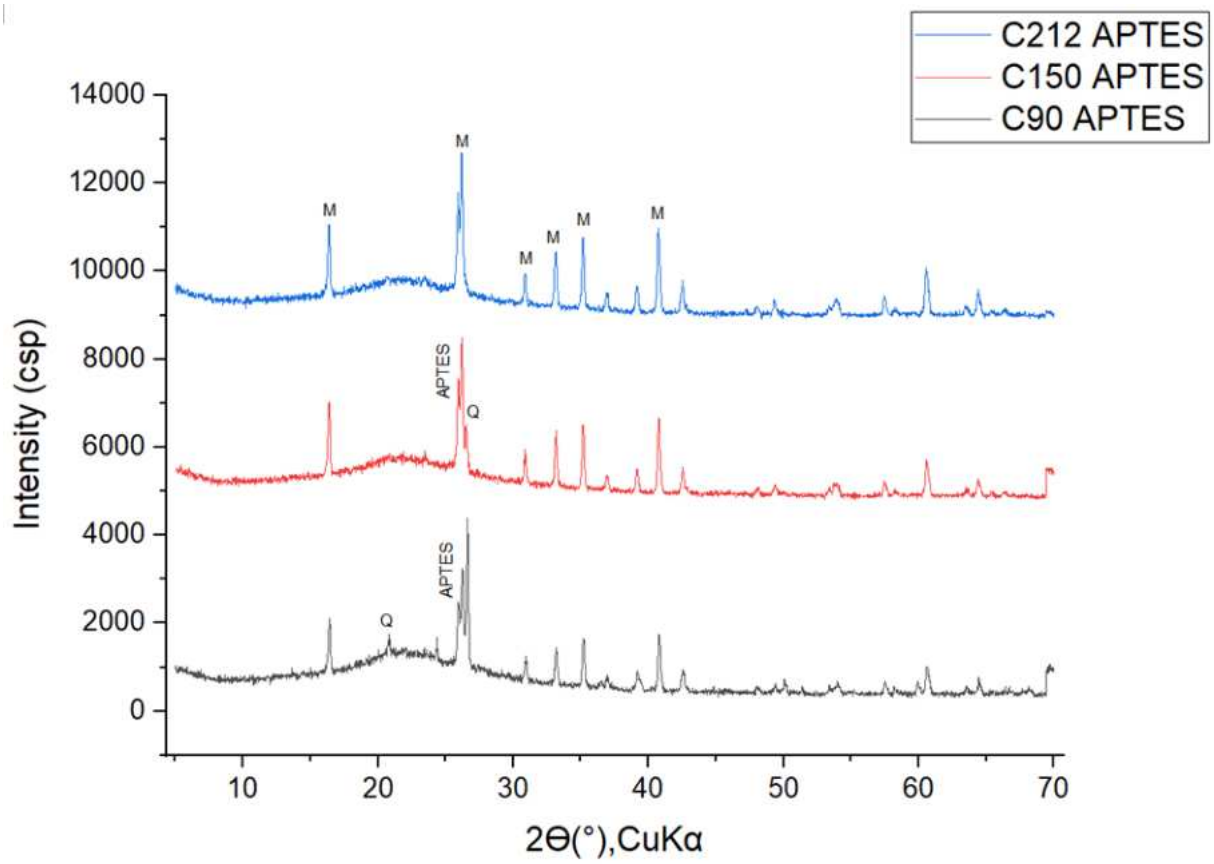

Fig. 38. XRD patterns of cenospheres after APTES modification

Fig. shows XRD pattern of ZrO_2 modified with TEOS due to the organic nature just like the modification with APTES, on the approximate graph, we can see reflections characteristic of the occurrence of different types of silicon.

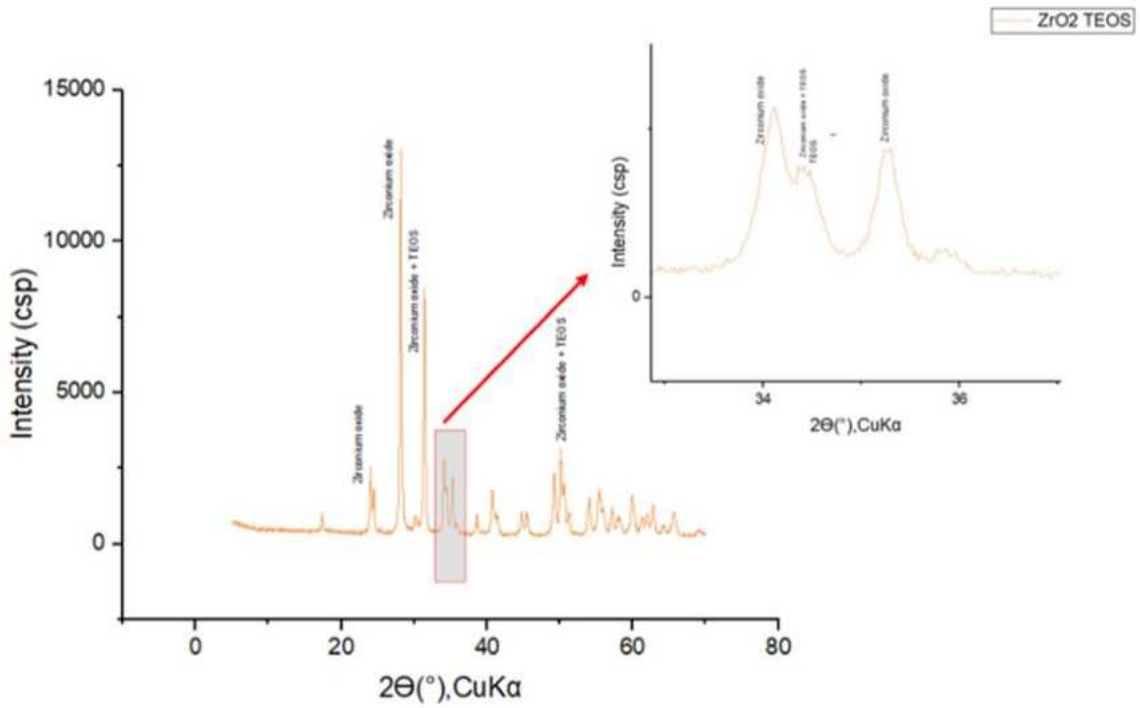

Fig. 39 XRD pattern of zirconium after TEOS modification.

XRD pattern of samples Al_2O_3 after APTES modification is illustrated on Fig 40. The intense reflections was assigned to corundum and TEOS.

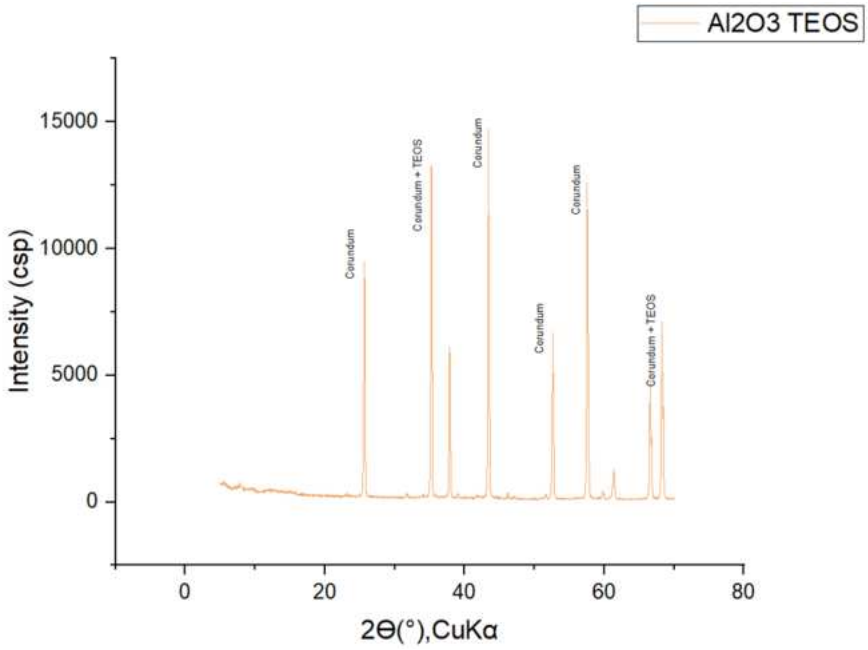

Fig. 40. XRD pattern of Al_2O_3 after TEOS modification

Fig 41shows the representation of the modification of TEOS aluminosilicates were not noted changes between fractions 150 μm and 212 μm, only for fraction 90 μm was

noted the revelation of a reflex defining quartz. Modification with TEOS, can show its presence by building into the phase composition of mullite creating synergies.

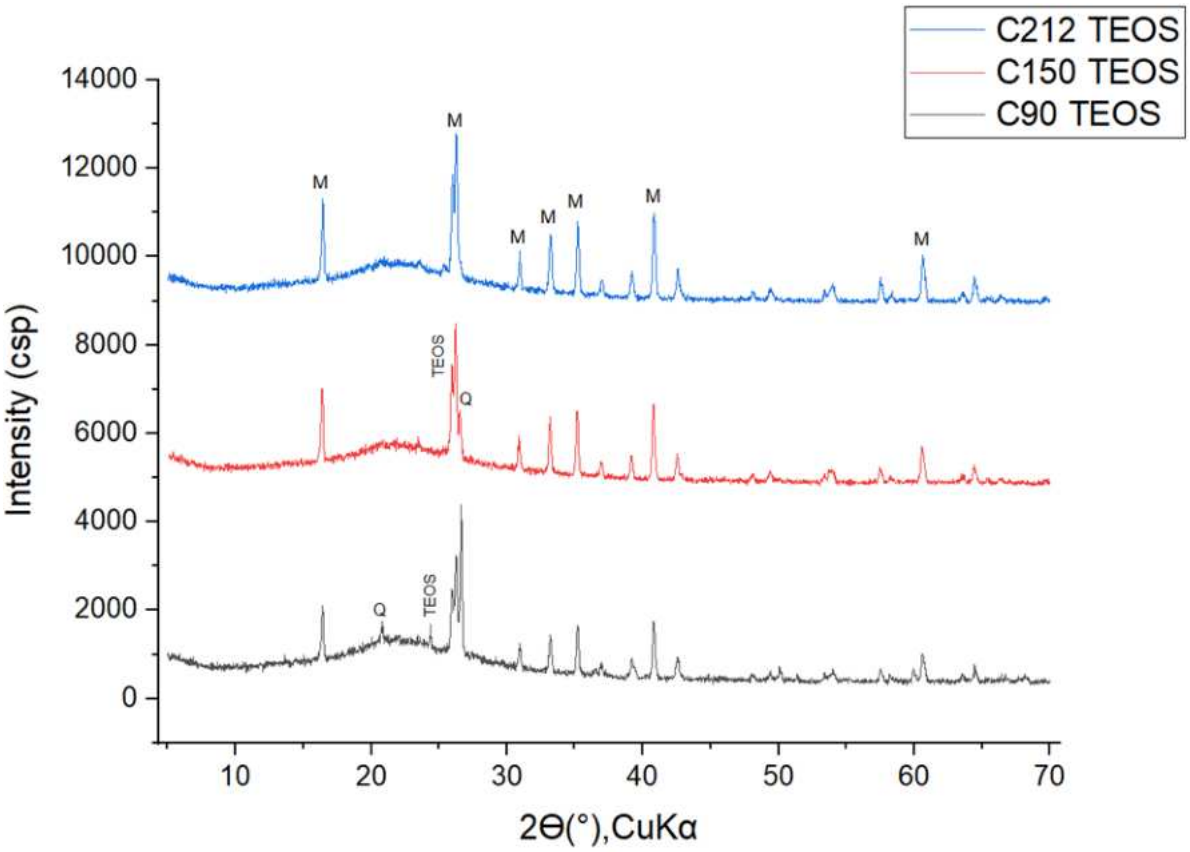

Fig. 41. XRD pattern of cenospheres after TEOS modification

5.5 Fourier Transform Infrared (FTIR) spectroscopy analysis

Tests for infrared spectroscopy were performed for all samples and after each modification considering the calcination process. The results presented, especially for the modification with silicon nitride (Si_3N_4 +NaOH), show a higher proportion of nitrogen groups relative to the other modifications. Only for this modification differences were observed with respect to the control sample and the process. Examples of FTIR spectra for alumina, zirconium oxide and spherical aluminosilicates after modification (Si_3N_4 +NaOH, APTES, TEOS) and after calcination in two different atmospheres are shown in Figures 42- 50.

.

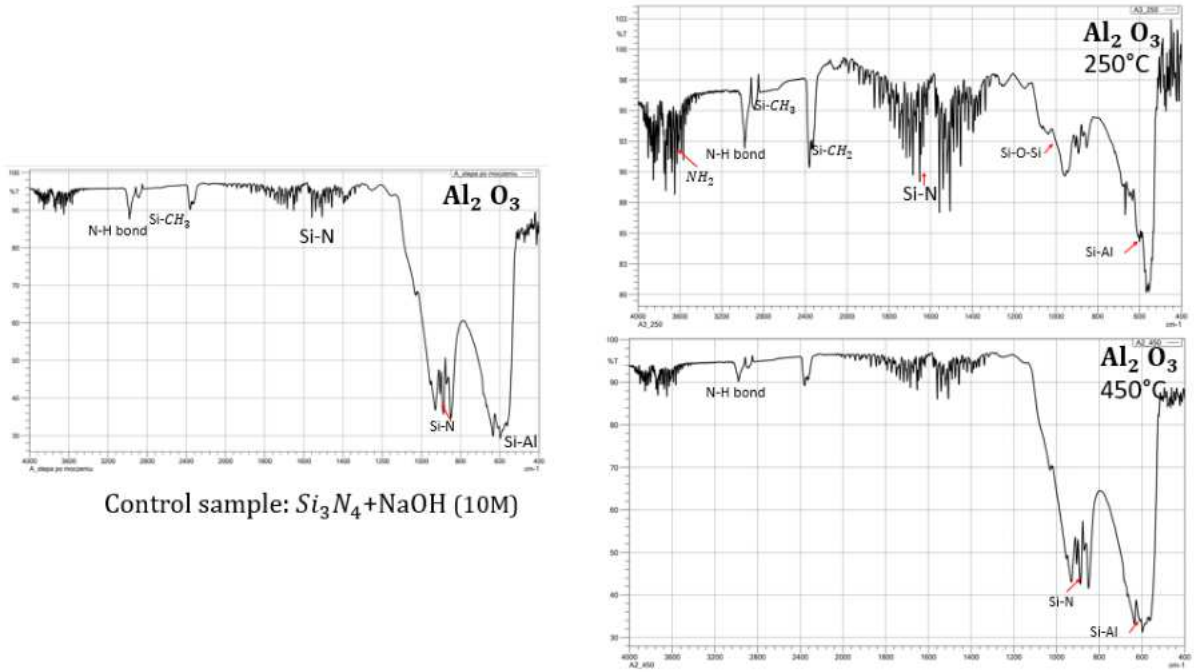

Fig. 42. FTIR spectra for alumina sample after modification with Si_3N_4 +NaOH in air atmosphere

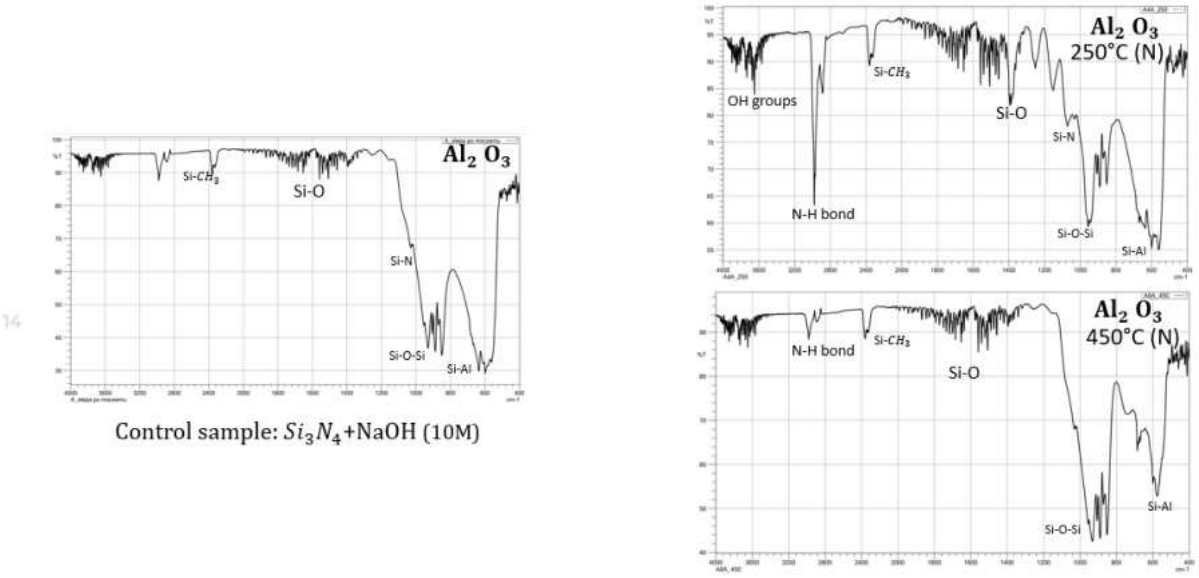

Fig. 43. FTIR spectra for alumina sample after modification with Si_3N_4 +NaOH) in nitrogen atmosphere

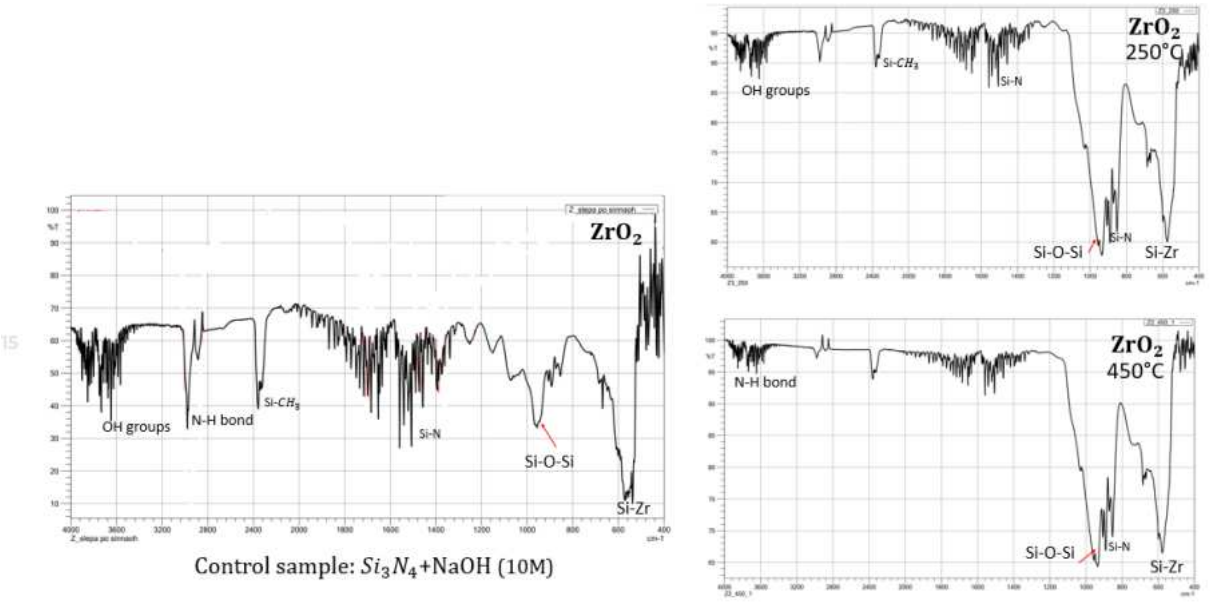

Fig. 44. FTIR spectra for zirconium oxide sample after modification with Si_3N_4 +NaOH in air atmosphere

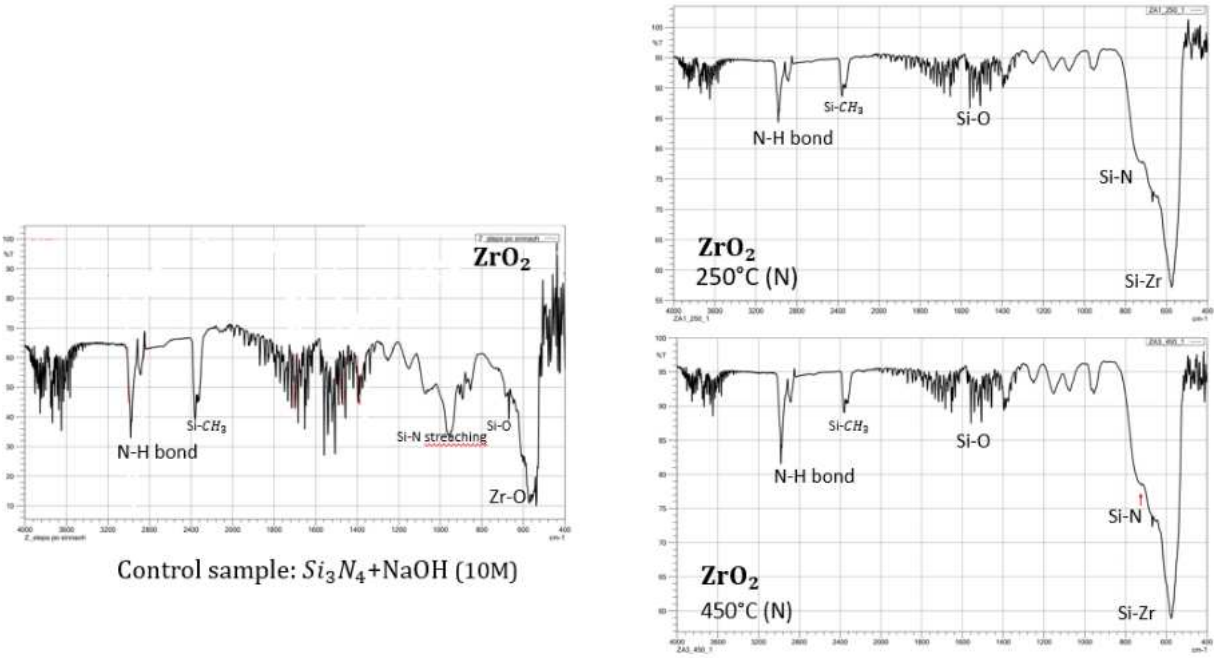

Fig. 45. FTIR spectra for zirconium oxide sample after modification with Si_3N_4 +NaOH in nitrogen atmosphere

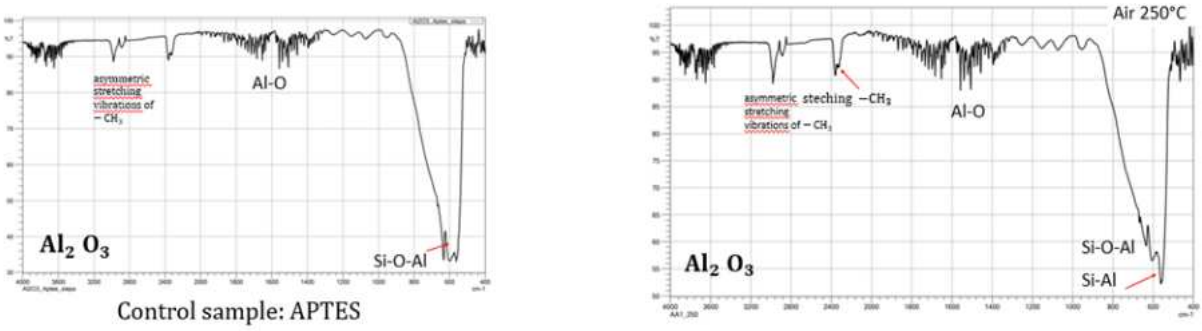

Fig. 46. FTIR spectra for alumina sample after modification with (APTES) in air atmosphere

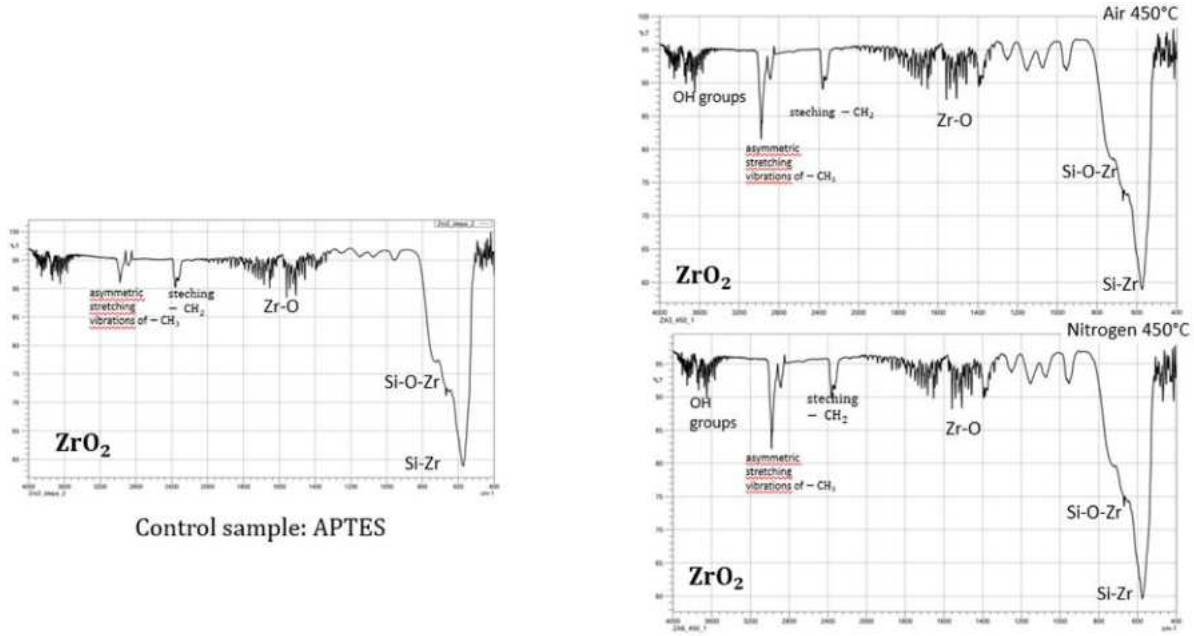

Fig. 47. FTIR spectra for zirconium oxide sample after modification with (APTES) in air atmosphere

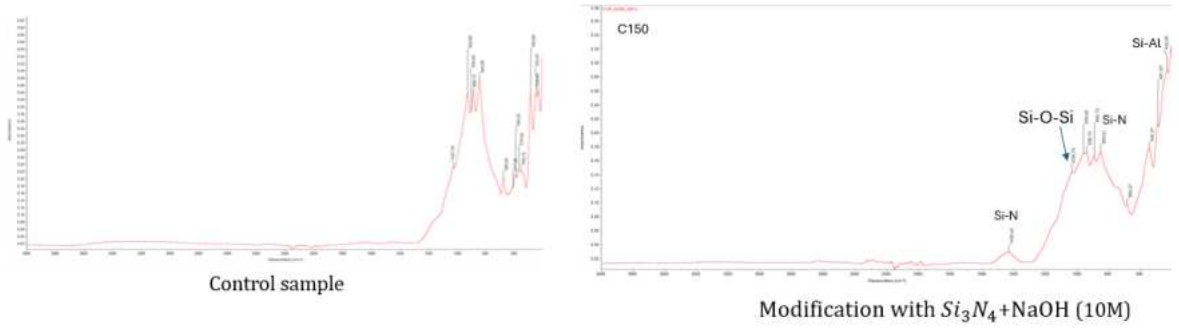

Fig. 48. FTIR spectra for aluminosilicate (C_{150}) sample after modification with Si_3N_4 +NaOH in nitrogen atmosphere

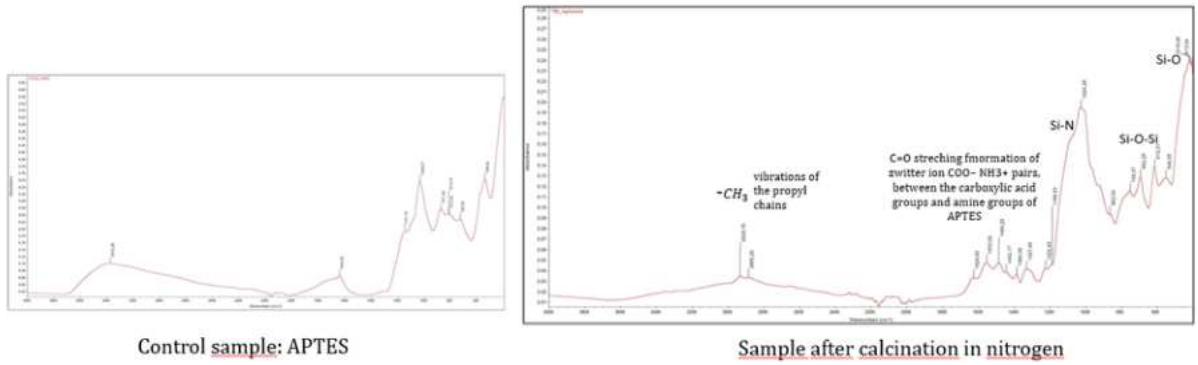

Fig. 49. FTIR spectra for aluminosilicate (C_{150}) sample after modification with (APTES) in nitrogen atmosphere

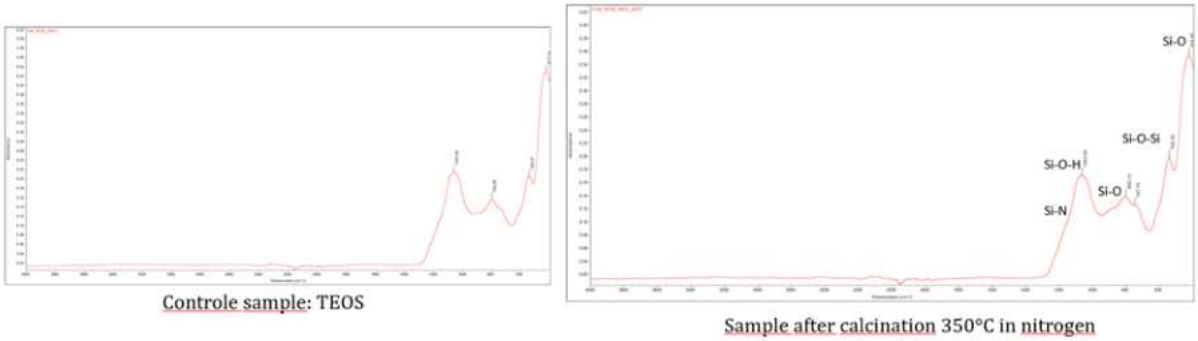

Fig. 50. FTIR spectra for aluminosilicate (C_{150}) sample after modification with (TEOS) in nitrogen atmosphere

5.6 Microstructure analysis

Test results for aluminum oxide (Al_2O_3) after modification with Si_3N_4

Analysis of the surface morphology carried out using SEM showed changes in the surface tomography for the alumina samples after surface modification in both air and nitrogen atmospheres. In both cases, the chemical compound Si_3N_4 was found - Fig. 50 and 51. The distribution of silicon and nitrogen on the surface of the sample was differentially distributed, as confirmed by EDS studies. The even distribution of these elements favorably affects the chemical bonding to the matrix.

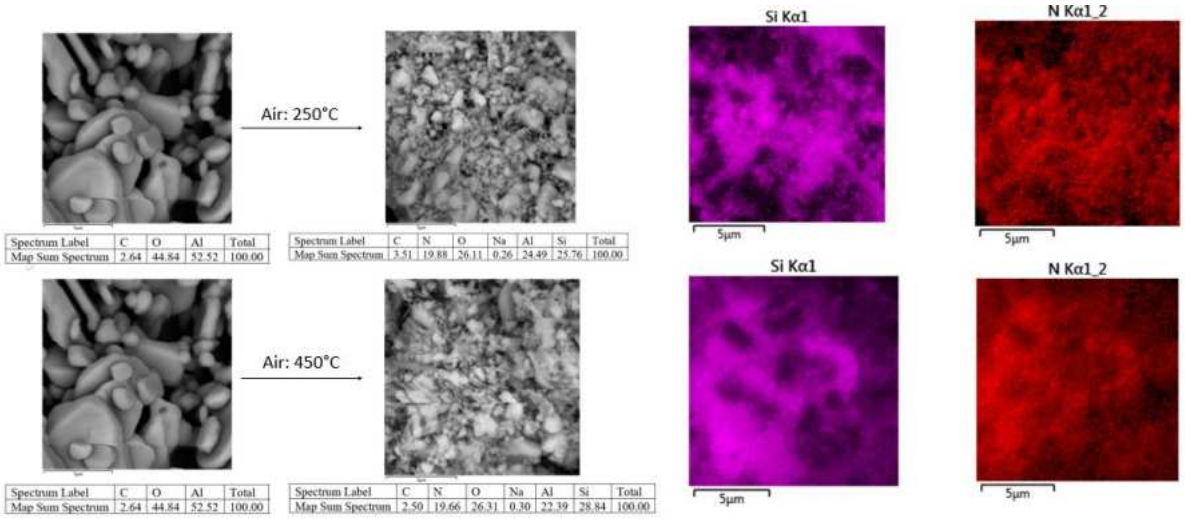

Fig. 51 SEM/EDS imaging results for aluminum oxide (Al_2O_3) after modification with Si_3N_4+ NaOH with air atmosphere

In the case of samples modified in an atmosphere of nitrogen, there was no increase in its share of the surface layer – Fig. 52.

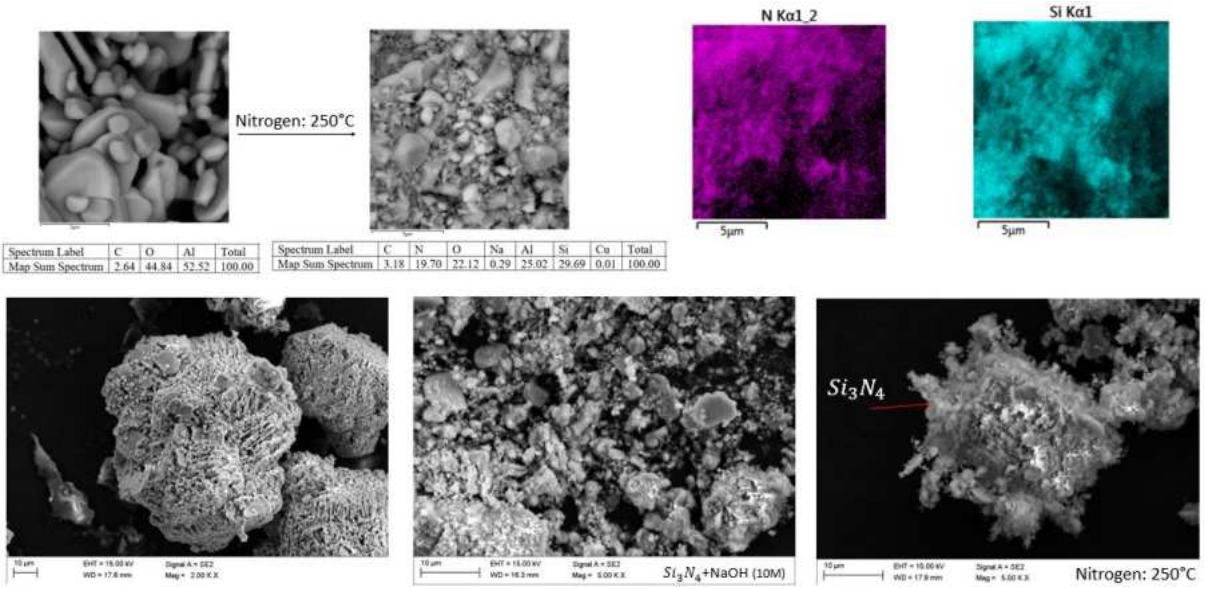

Fig. 52. SEM/EDS imaging results for aluminum oxide (Al_2O_3) after modification with Si3N4+ NaOH with nitrogen atmosphere

Test results for zirconium oxide (ZrO_2) after modification with Si_3N_4

Analysis of the surface morphology carried out using SEM showed changes in the surface tomography for the zirconium oxide samples after surface modification in both air and nitrogen atmospheres. In both cases, the chemical compound Si_3N_4 was found, (Fig. 53 and 54). The distribution of silicon and nitrogen on the sample's surface was differentially distributed, as confirmed by EDS studies. The even distribution of these

elements favourably affects the chemical bonding to the matrix.

In the case of zirconium oxide samples modified in a nitrogen atmosphere, there was no increase in its share of the surface layer – Fig. 55.

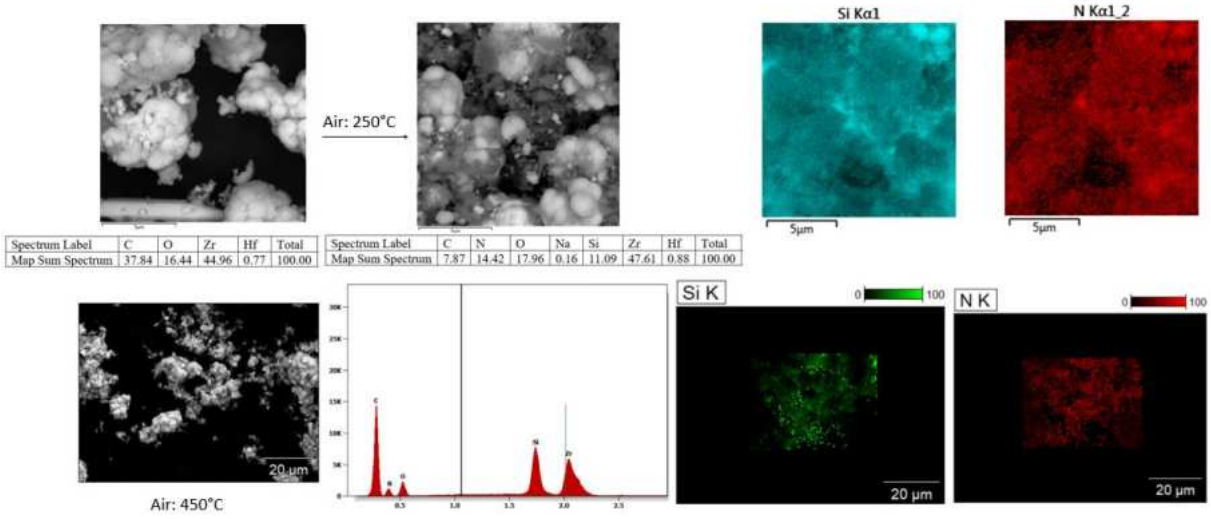

Fig. 53. SEM/EDS imaging results for zirconium oxide (ZrO_2) after modification with Si_3N_4+ NaOH with air atmosphere

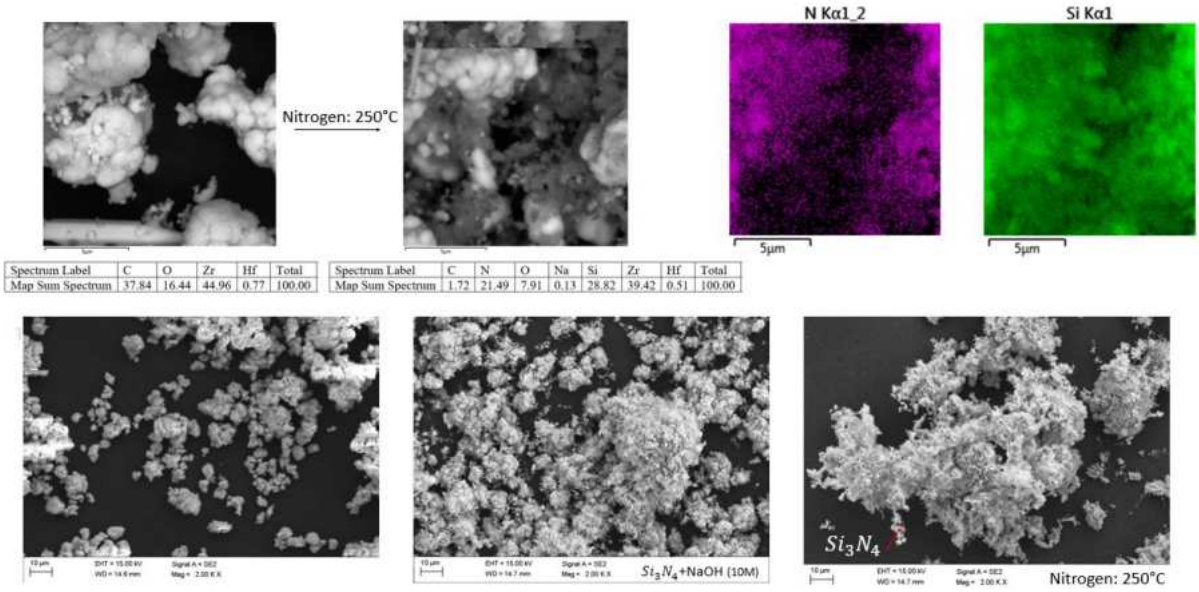

Fig. 54. SEM/EDS imaging results for zirconium oxide (ZrO_2) after modification with Si_3N_4+ NaOH with nitrogen atmosphere

Presented SEM analysis, showed a change in the surface morphology of spherical aluminosilicates after the application of Caro acid - Fig. 55. The surface topography shows greater surface unfolding which favorably affects the attachment of functional groups after the silanization process. The surface unfolding after the application of Caro acid may contribute to increased mechanical bonding to the matrix in the composite.

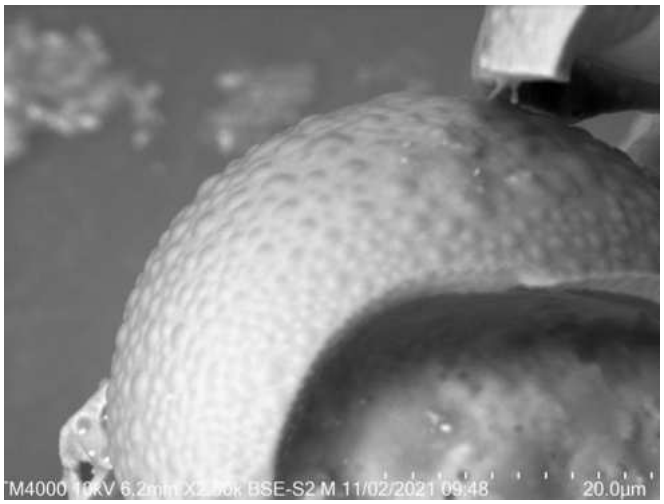

Fig. 55. SEM imaging results for surface topography after etching

Test results for spherical aluminosilicates (C_{150}) after modification with Si_3N_4+NaOH

Analysis of the surface morphology carried out using SEM showed changes in the surface tomography for spherical aluminosilicate (C_{150}) samples after surface modification with Si_3N_4+NaOH in an air atmosphere. The chemical compound Si_3N_4 was found on the surface of the sample – Fig. 56. The distribution of silicon and aluminum on the sample surface was uneven, which was confirmed by EDS studies. The locally increased occurrence of these elements favorably affects the chemical bonding to the matrix.

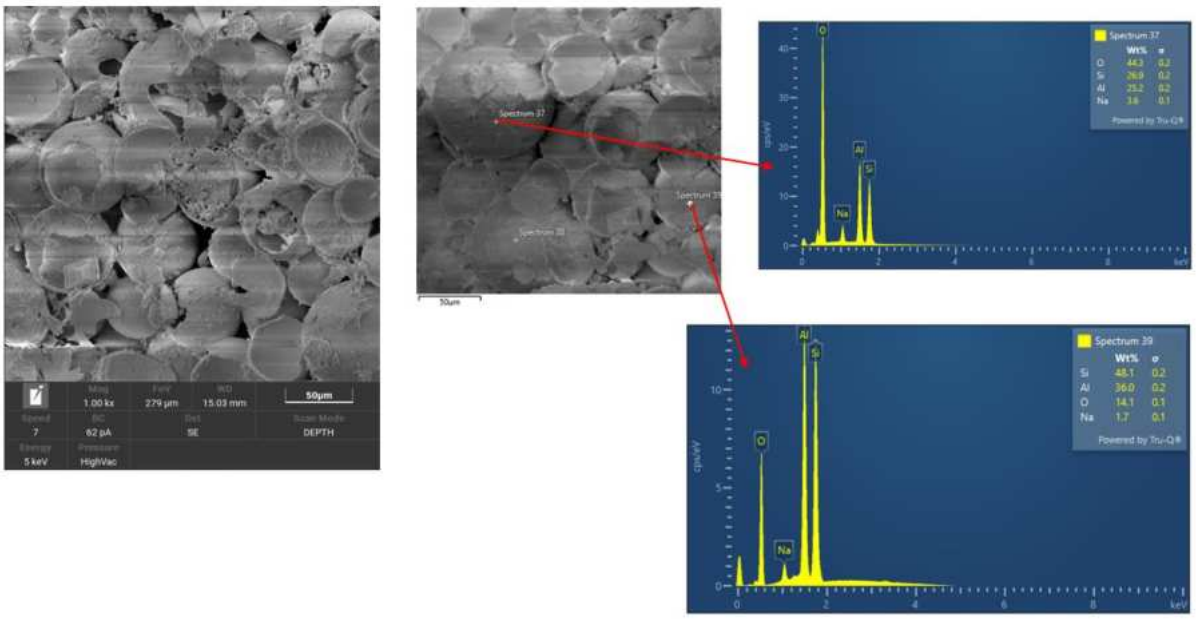

Fig. 56. SEM/EDS imaging results for aluminium silcates (C_{150}) after modification with Si_3N_4+ NaOH with air atmosphere

Test results for spherical aluminosilicates (C_{212}) after modification with Si_3N_4+ NaOH

SEM/EDS analysis revealed the presence of silicon and nitrogen on the surface of spherical aluminosilicate (C_{212}) after modification with Si_3N_4+ NaOH - Fig 57. Areas of occurrence of the various elements were revealed, and thus confirmed their contribution across the surface.

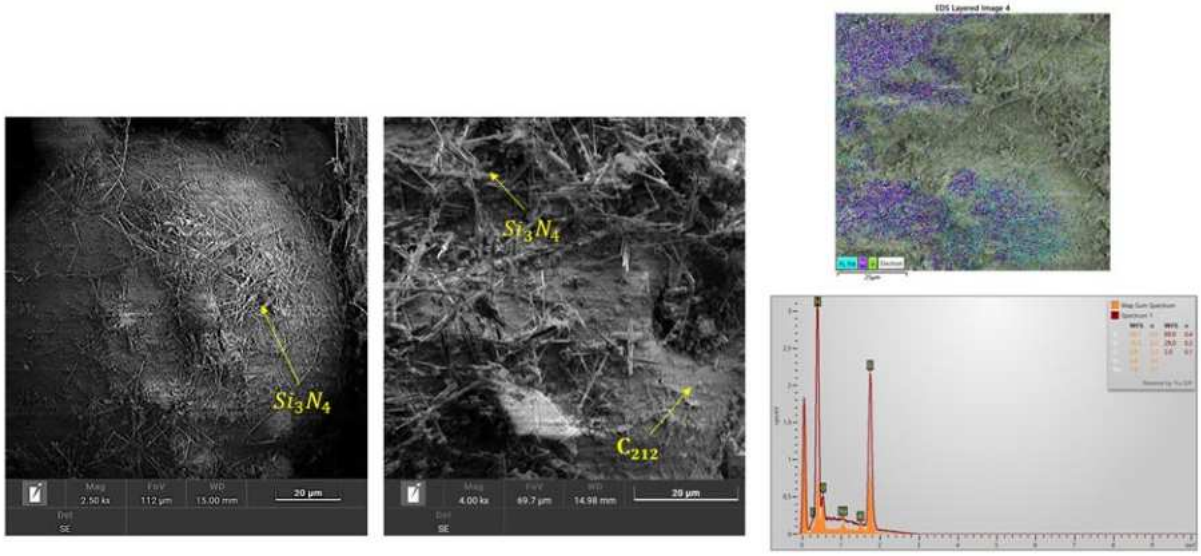

Fig. 57. SEM/EDS imaging results for aluminum silicates (C212) after modification with Si_3N_4+ NaOH with air atmosphere

Test results for zirconium oxide (ZrO_2) after modification with APTES

SEM analysis of the surface morphology showed changes in the surface tomography for the zirconium oxide sample after surface modification with APTES in a nitrogen atmosphere. Silicon was found on the sample surface - Fig. 58. The distribution of silicon on the surface of the sample was uneven, as confirmed by EDS studies. The locally increased occurrence of these elements favorably affects the chemical bonding with the matrix.

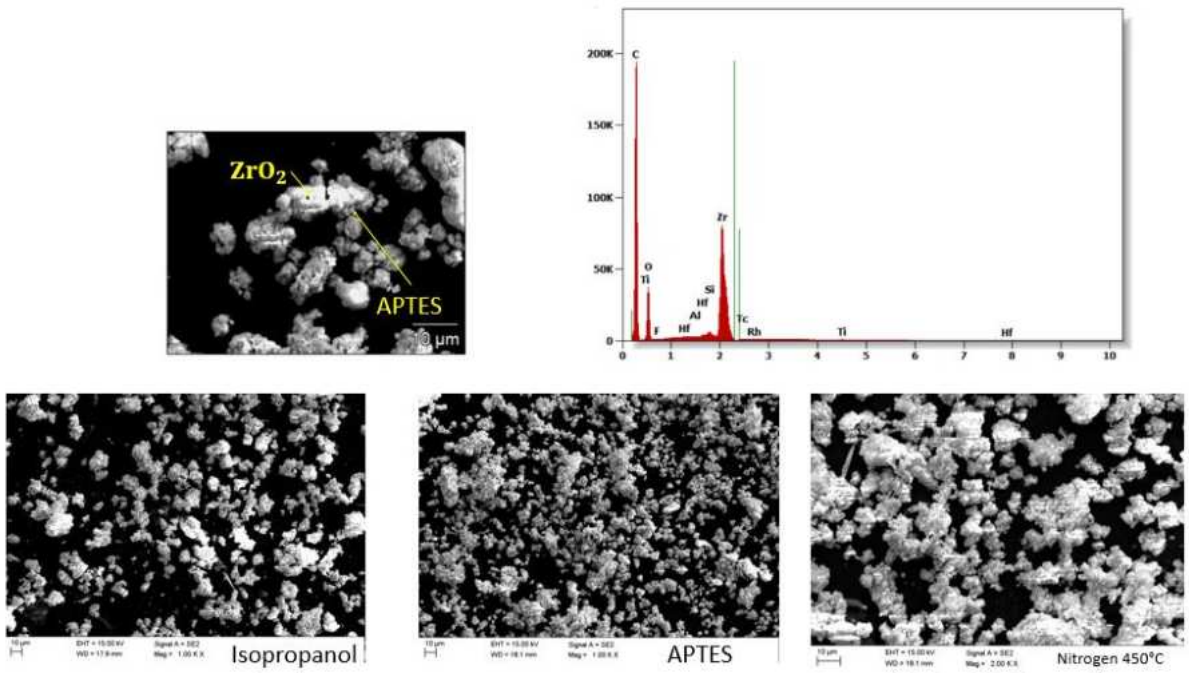

Fig. 58. SEM/EDS imaging results for zirconium oxide after modification with APTES in nitrogen atmosphere

Test results for aluminium oxide (Al_2O_3) after modification with APTES

SEM analysis of the surface morphology showed changes in surface tomography for the alumina sample after surface modification with APTES in a nitrogen atmosphere. Silicon was found to be present on the surface of the Fig. 59 sample in decidedly smaller amounts than for zirconium oxide. The distribution of silicon on the surface of the sample was uneven, which was confirmed by EDS studies. Despite the reduced proportion of silicon, still the occurrence of related elements after modification with APTES can favorably affect the chemical bonding with the matrix.

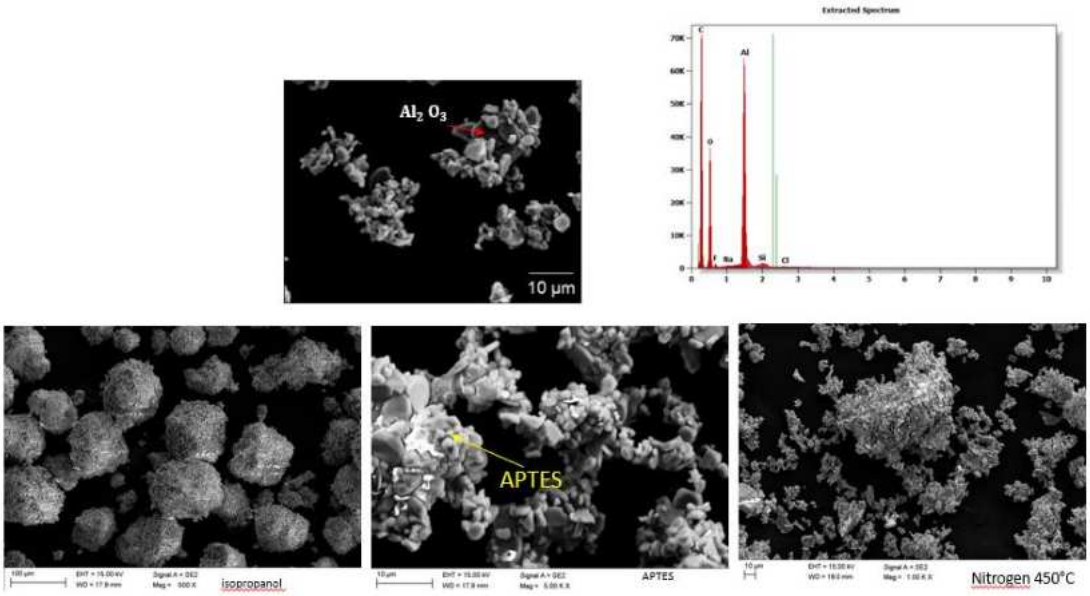

Fig. 59 SEM/EDS imaging results for aluminium oxide after modification with APTES in nitrogen atmosphere

Test results for aluminoslicates (C_{150}) after modification with APTES

Analysis of the surface morphology carried out using SEM showed changes in the surface tomography for the spherical aluminosilicate (C_{150}) sample after surface modification with APTES in an air atmosphere. Silicon was found on the surface of the Fig. 60 sample. As well as confirmed by EDS studies the distribution on the entire surface of the sample. Demonstrating the presence of silicon on the surface of the sample after modification with APTES may favorably influence the chemical bonding with the matrix.

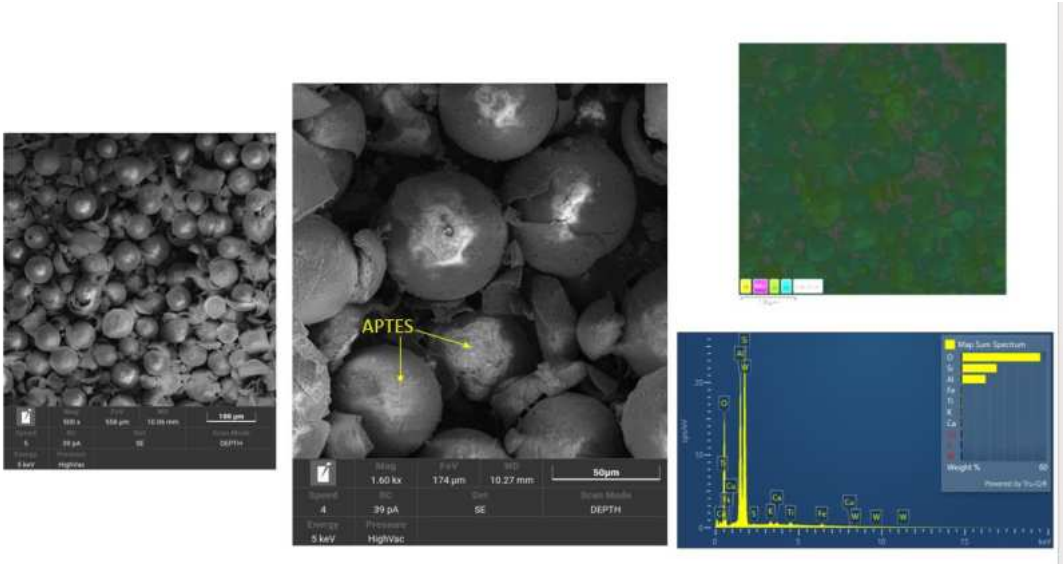

Fig. 60. SEM/EDS imaging results for aluminiumsilicates (C_{150}) after modification with APTES in air atmosphere

Test results for aluminoslicates (C_{150}) after modification with TEOS

Analysis of the surface morphology carried out using SEM showed changes in the surface tomography for the spherical aluminosilicate (C_{150}) sample after surface modification with TEOS in an air atmosphere. Silicon was found on the surface of the Fig. 61 sample. However, due to the nature of the modifier, it is not distributed over the entire surface of the sample. Differences in silicon concentration were shown by EDS analysis. Despite the differences in the proportion of silicon on the surface of the sample, the modification may contribute to an increase in the proportion of chemical bonds in the matrix.

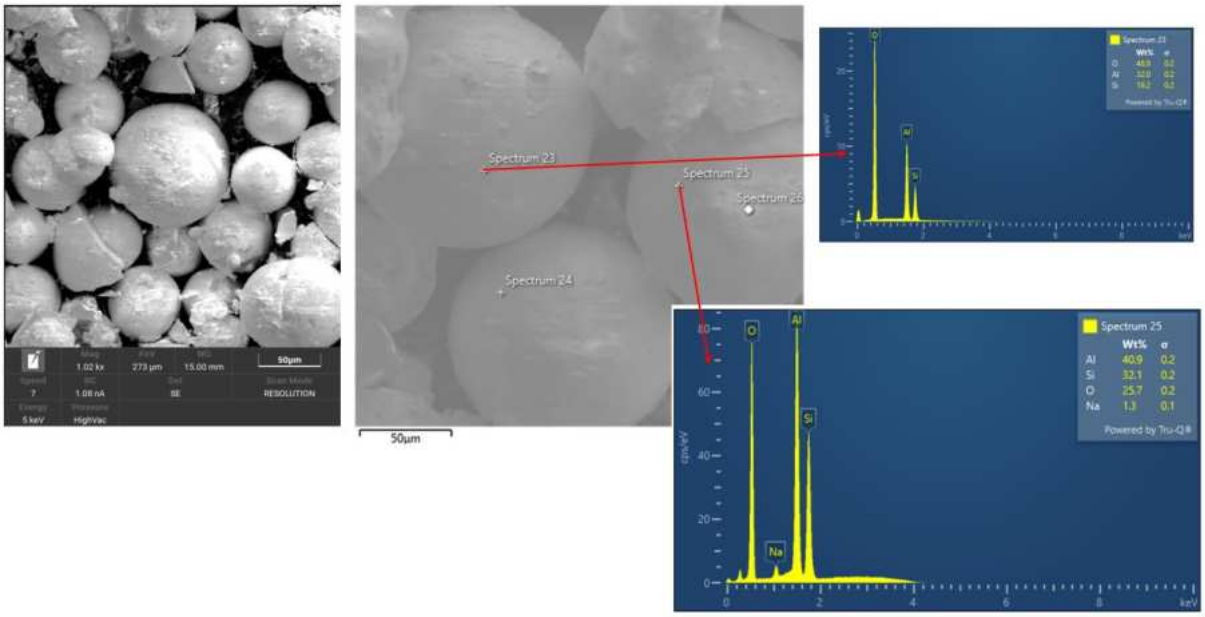

Fig. 61. SEM/EDS imaging results for aluminiumsilicates (C_{150}) after modification with TEOS in air atmosphere.

5.7 Porosity studies

To gain a more precise understanding of the porous structure of bone cement and bone cement modified with silicon nitride for spherical aluminosilicate, nitrogen adsorption isotherms were detected (Fig. 62). Analysis of the pore volume distribution curves, calculated using the Barrett-Joyner-Halenda (BJH) method, reveals that both samples are generally nonporous materials with a minimal contribution of mesopores of 3 – 4.5 nm in diameter. Additionally, the specific surface area (S_{BET}) of both materials is

notably low: 0.4 m^2/g for the bone cement and undetectable due to too low porosity for the bone cement modified with silicon nitride.

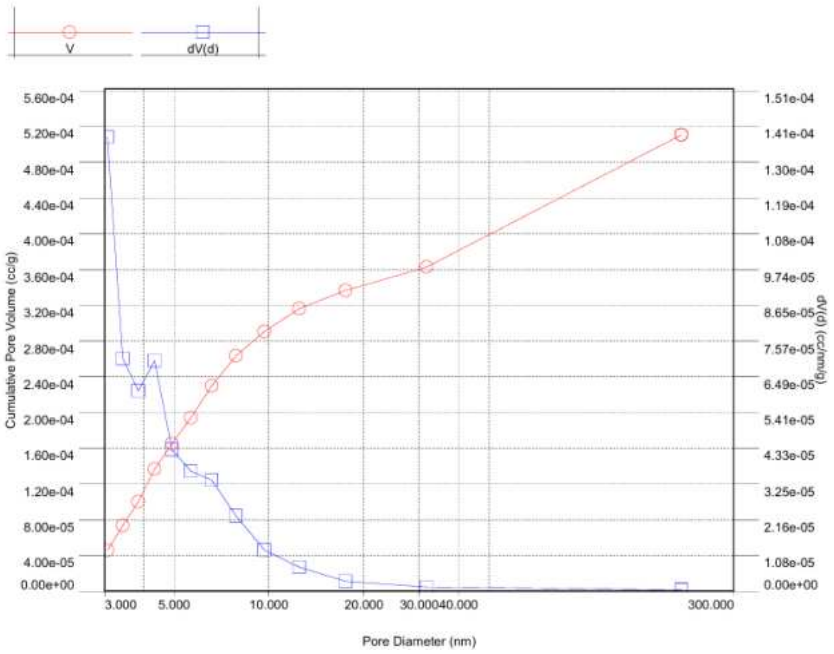

A)

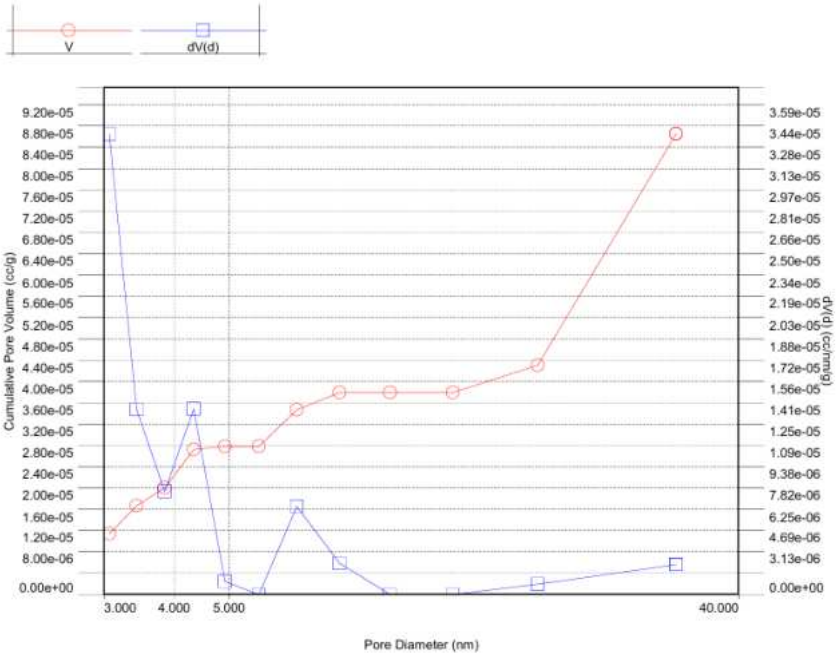

B)

Fig. 62. Pore size distribution in bone cement (A) and bone cement modified with silicon nitride (B)

5.8 Microstructural studies of bone cement

Microscopic images of Fig 63 and 64 already showed an apparent change in the surface morphology of the produced spherical aluminosilicate (C_{150}) bone cement. Sample A shows a homogeneous surface, in contrast to sample D, where more porosity and various types of inclusions on the surface are visible, suggesting the presence of aluminosilicate.

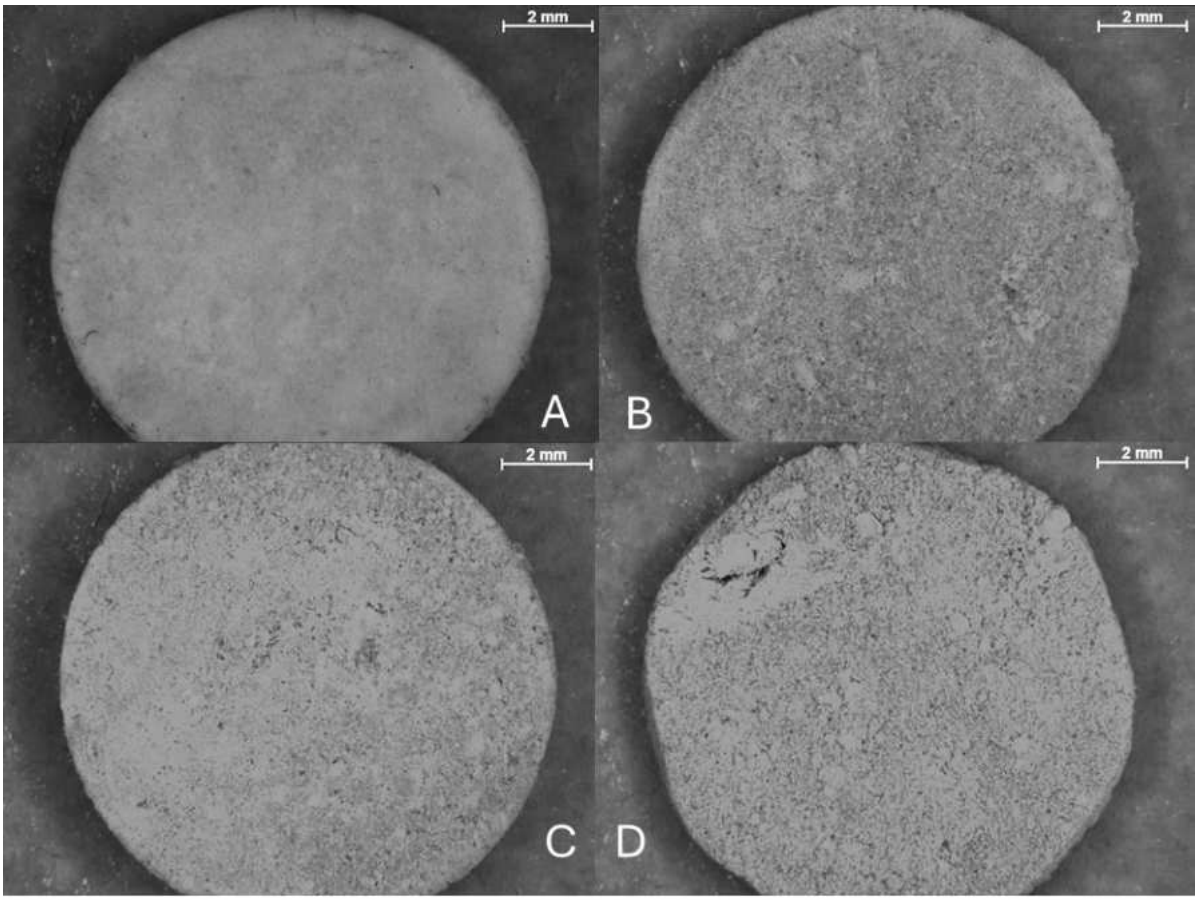

Fig. 63.64 Surface of sample: A - bone cement, B - bone cement after modification with 20% GK, C - bone cement with 30% GK, D - bone cement with 40% GK, GK-aluminosilicates

Microscope images taken on a digital microscope reveal the characteristics of the connection between bone and bone cement before and after modification with aluminosilicate. Fig. 65 shows the connection between bone and commercially available bone cement, and Fig. 66 shows the connection between bone and bone cement after modification with aluminosilicate. On each of the variants one can see the penetration of the cement into the pores of the bone which, may indicate good adhesion of the material with the substrate in this case bone.

Fig. 65. Image showing the connection between bone (HAp) and bone cement, where CK - bone cement

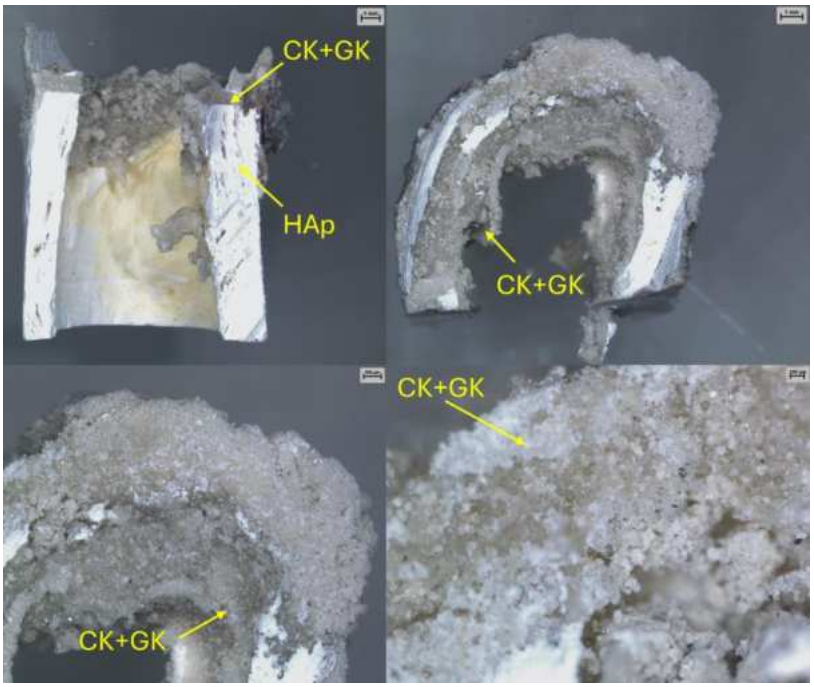

Fig. 66. Image showing the fusion of bone (HAp) with aluminosilicate bone cement (CK+GK), where GK – aluminosilicate

The results of the microstructural tests carried out are presented below. Analysis of the presented samples showed a change in the structure of bone cement after modification with spherical aluminosilicate. Qualitative analysis of the distribution of elements on the surface showed the presence of elements such as C, O, Ba, S, Si, Ca, Al. The highest percentage of carbon and oxygen is confirmed by the PMMA analyzed, the presence of Ba indicates confirmation of its presence in bone cement, which is added for X-ray imaging Fig. 67-69

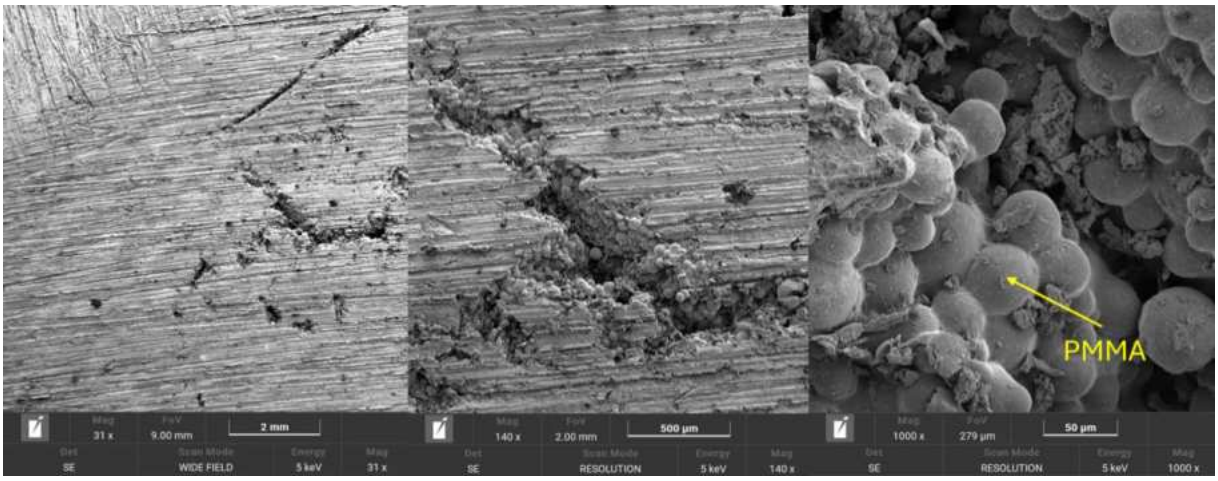

Fig. 67. Morphology of bone cement as a control sample. The cross-linked polymethylmethacrylate (PMMA) can be seen in detail, SEM, mag.: 31x, 140x, 1000x.

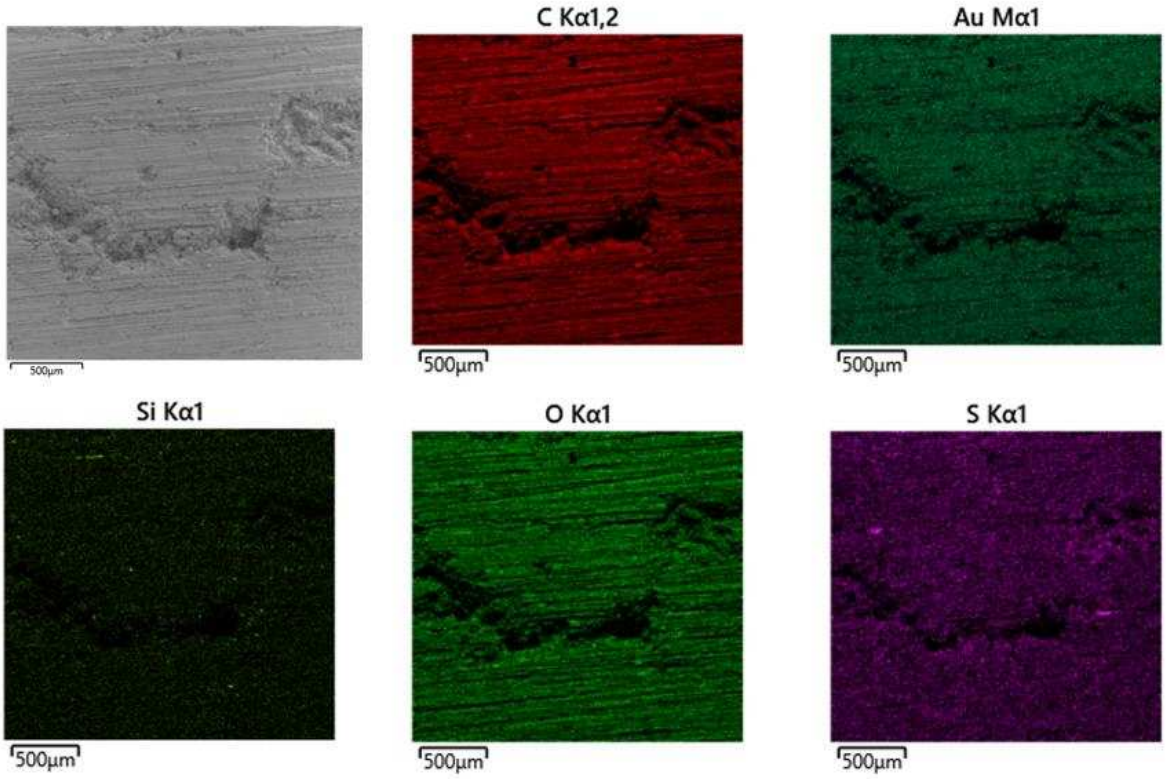

Fig. 68. EDS Mapping of bone cement, control sample.

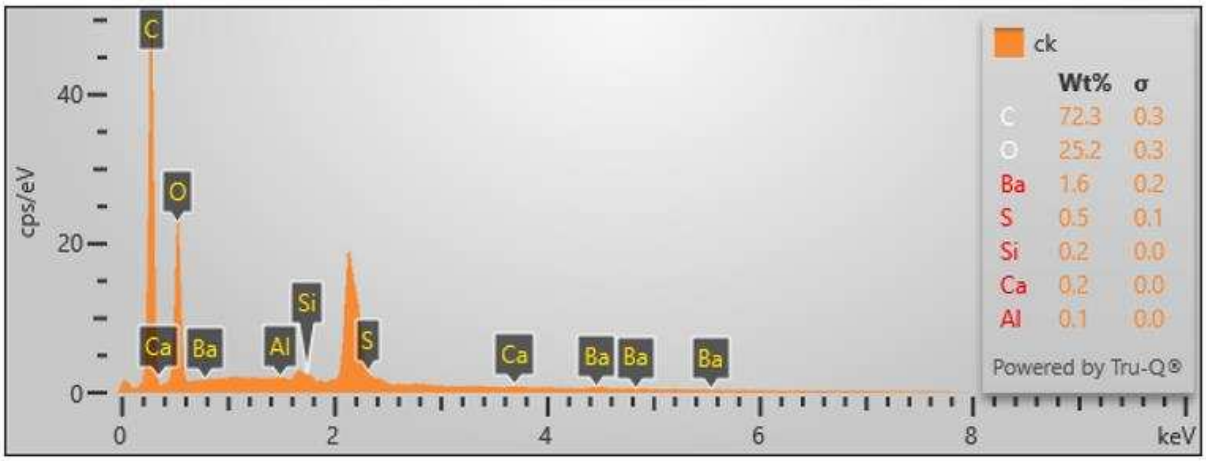

Fig. 69. Graph showing the percentage of a given element on the surface of the sample bone cement

Test results for bone cement (CK) after modification with spherical aluminosilicate at 20% (GK20%) - SEM/EDS

Analysis of the surface of the sample showed the proportion of aluminosilicates which demonstrates the acquisition of a connection to the matrix, in addition, the EDS spectrum shows the presence of the element silicon on the surface, confirming the stated purpose of Fig. 70-72.

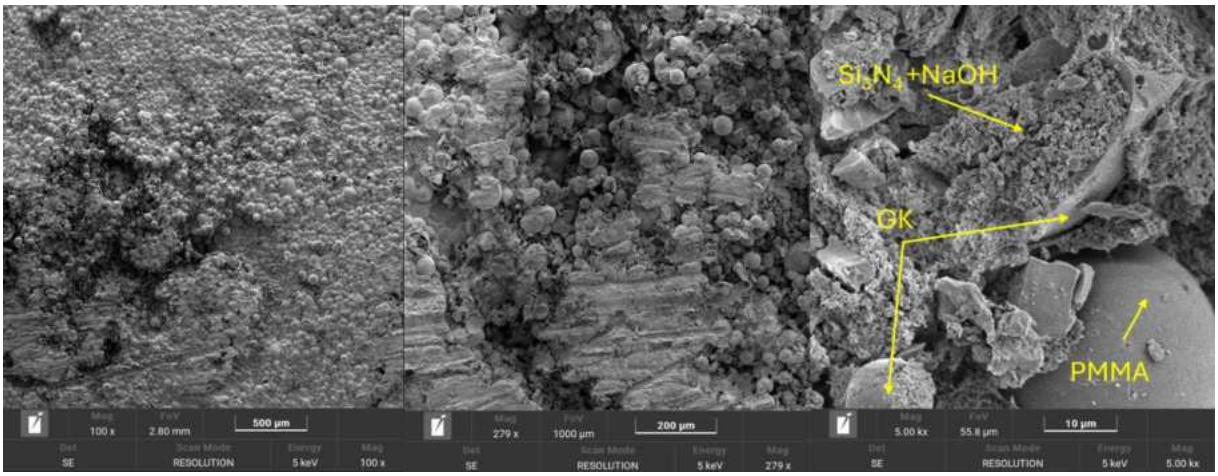

Fig. 70. Image shows bone cement with 20% spherical aluminosilicates (CK+GK20%)

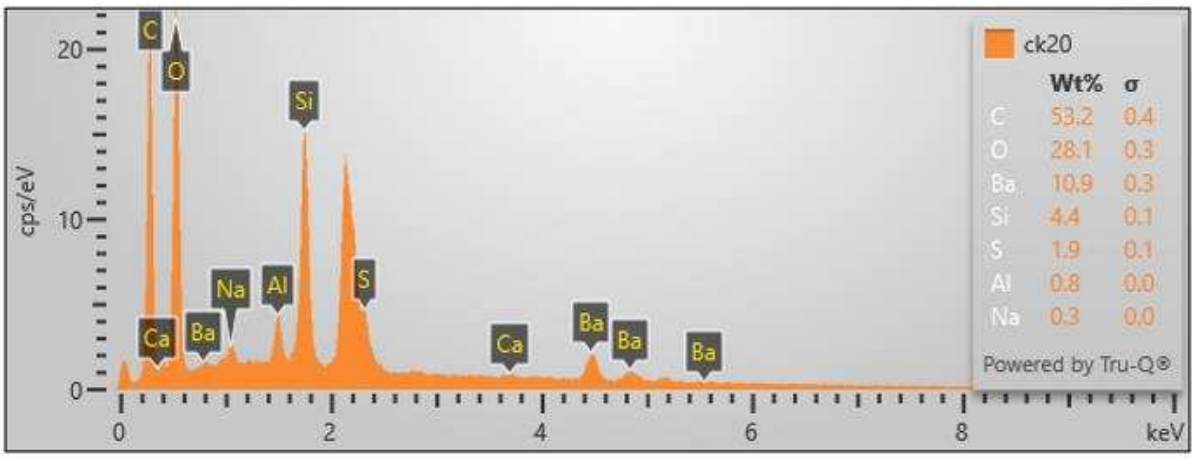

Fig. 71. Graph showing the percentage of a given element on the surface of a bone cement sample with 20% spherical aluminosilicate (CK+GK20%)

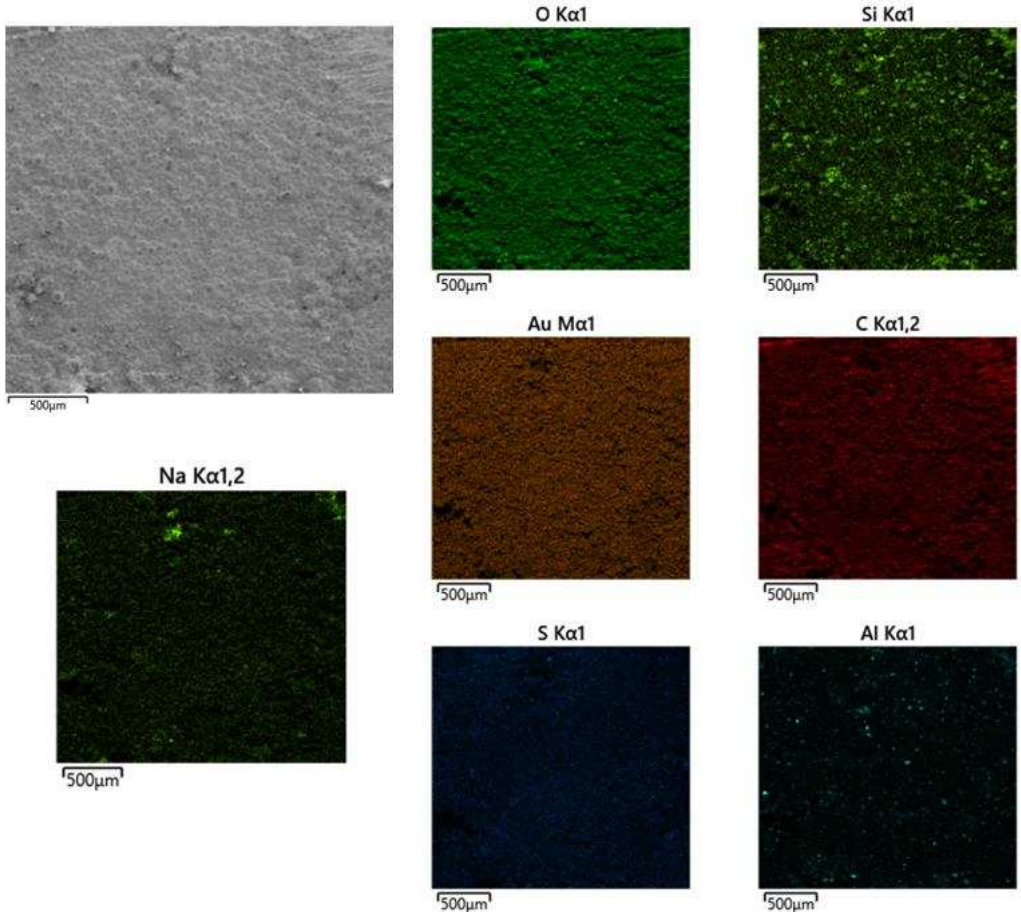

Fig. 72. Graphic representation of elemental proportions on the surface of a bone cement sample with 20% spherical aluminosilicate (CK+GK20%)

Test results for bone cement (CK) after modification with spherical aluminosilicate at 30% (GK30%) - SEM/EDS

SEM/EDS analysis, as for the previous sample, also showed the proportion of aluminosilicates in the matrix, which is confirmed by the EDS spectrum, confirming the silicon content on the sample surface. In addition, it is possible to observe a uniform distribution of this ring on the surface of the sample - Fig. 73-75.

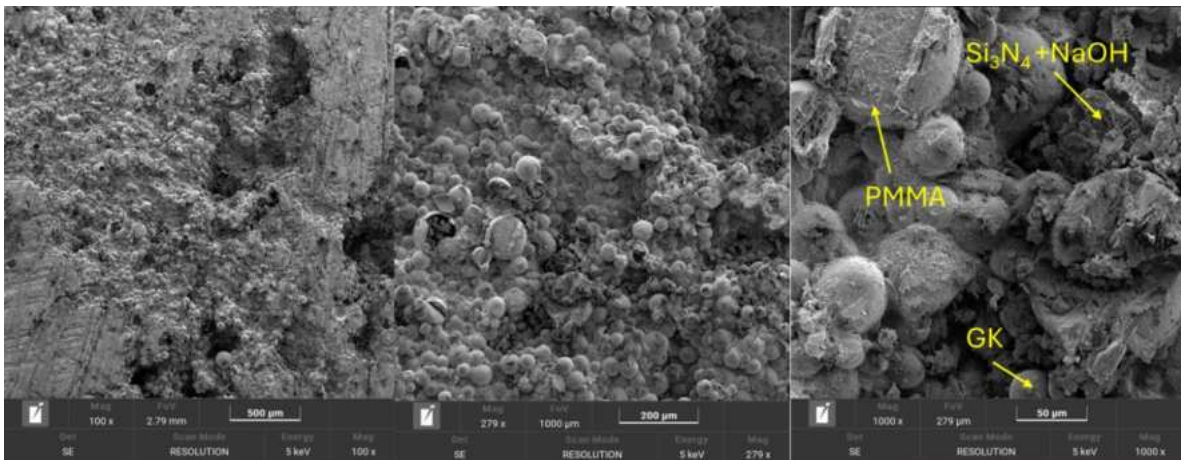

Fig. 73. Image shows bone cement with 30% spherical aluminosilicates (CK+GK30%)

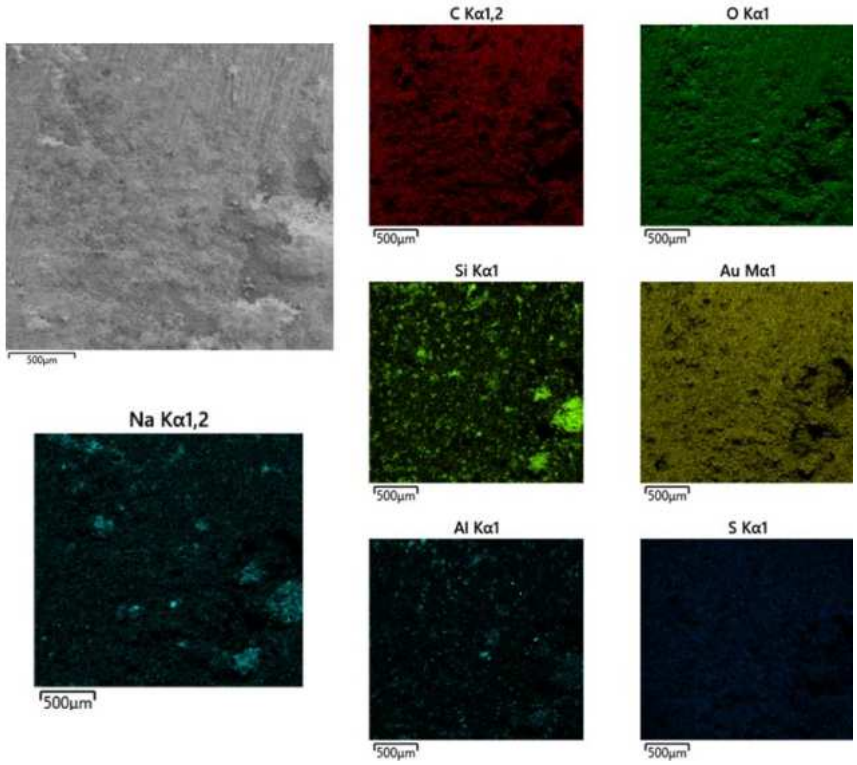

Fig. 74. Graphic representation of elemental proportions on the surface of a bone cement sample with 30% spherical aluminosilicate (CK+GK30%)

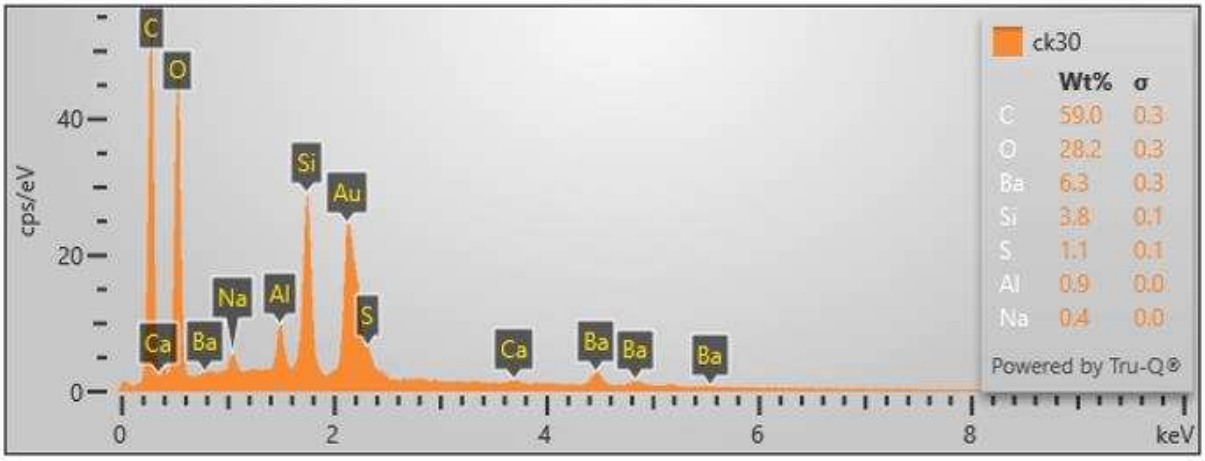

Fig. 75. Graph showing the percentage of a given element on the surface of a bone cement sample with 30% spherical aluminosilicate (CK+GK30%)

Test results for bone cement (CK) after modification with spherical aluminosilicate at 40% (GK40%) - SEM/EDS

Analysis of the EDS spectra showed the highest proportion of silicon on the surface of the sample, this is related to the highest proportion of filler in the matrix. In addition, microstructure analysis showed an even distribution of silicon on the sample surface - Fig 76-78.

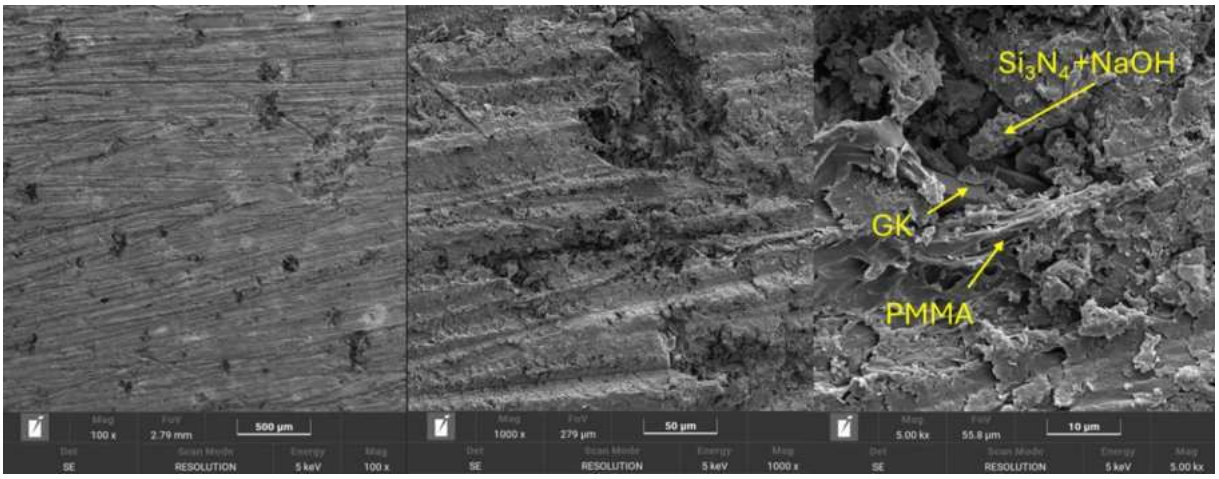

Fig. 76. Image shows bone cement with 30% spherical aluminosilicates (CK+GK30%)

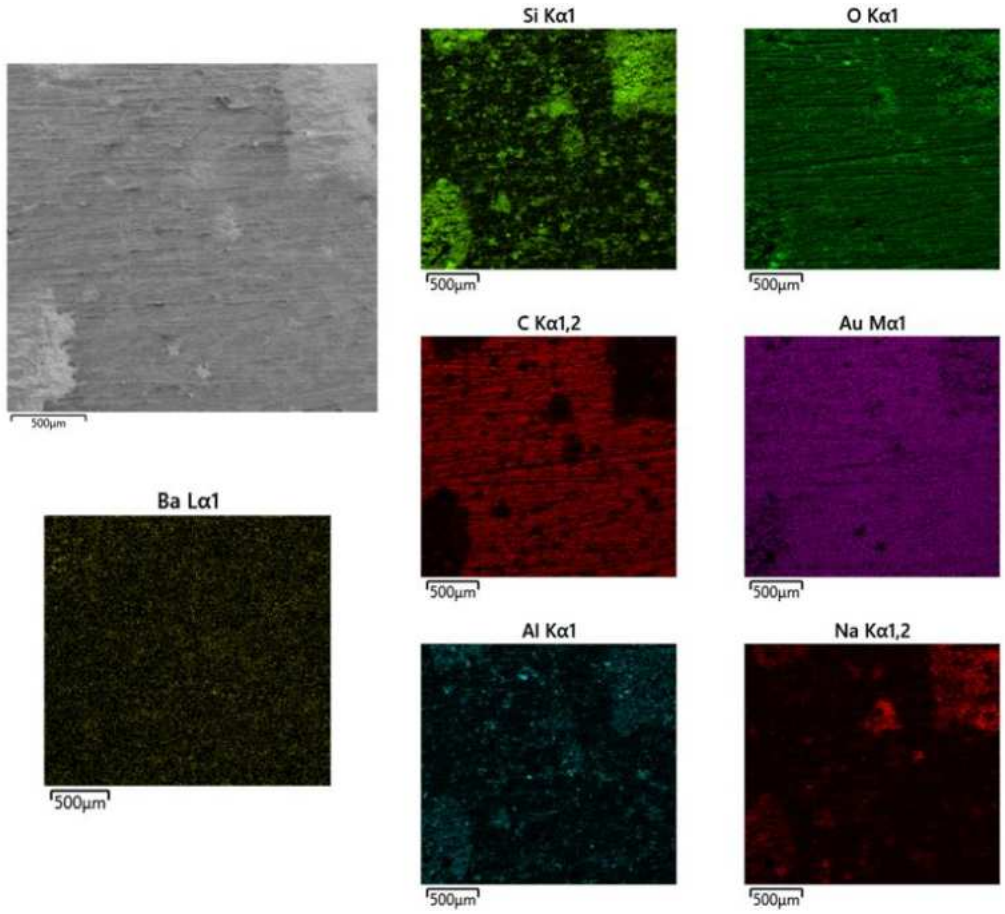

Fig. 77. Graphic representation of elemental proportions on the surface of a bone cement sample with 40% spherical aluminosilicate (CK+GK40%)

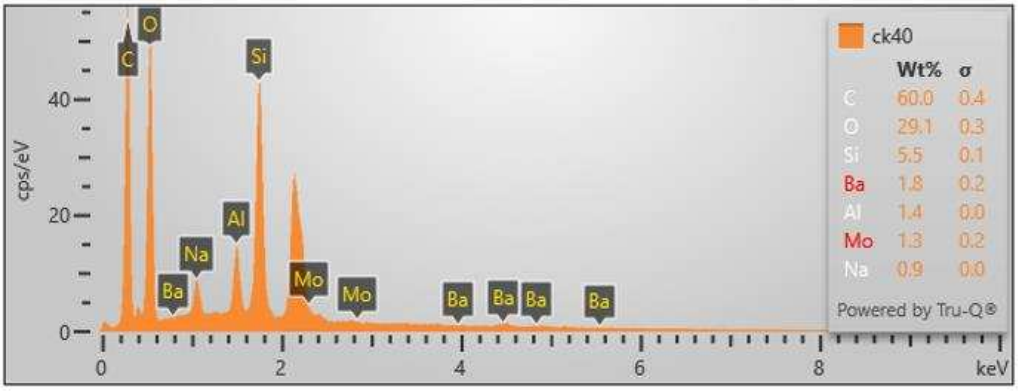

Fig. 78. Graph showing the percentage of a given element on the surface of a bone cement sample with 40% spherical aluminosilicate (CK+GK40%)

5.9 Polymerization temperature studies

Analysis of the results for determining the height of the temperature versus time showed very similar results in the three trials, demonstrating the stability of the process despite the modification used. Fig. 79 shows a slightly higher temperature of about 10°C

after modification compared to bone cement without modification. But between modifications, no significant differences can be seen in the process characteristics themselves, as well as in the temperature peak usually falling between 5 and 6 min of the process.

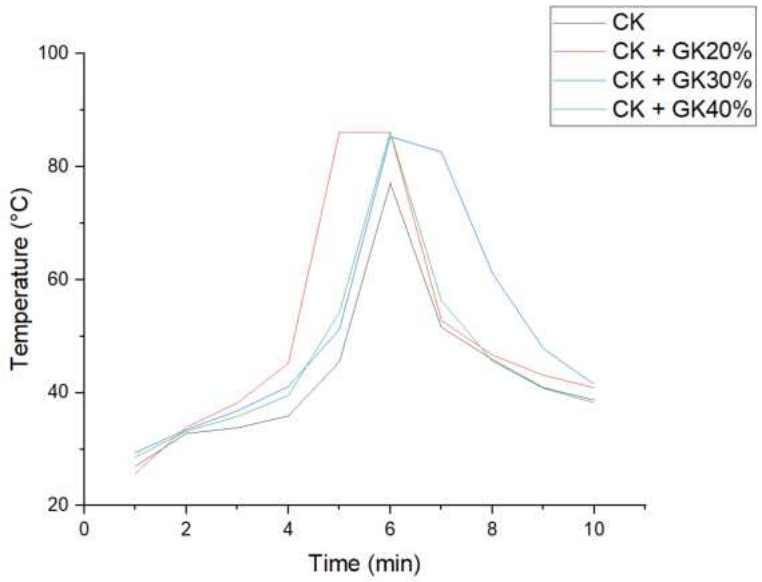

Fig. 79. First temperature measurement of bone cements before and after modification with aluminosilicates

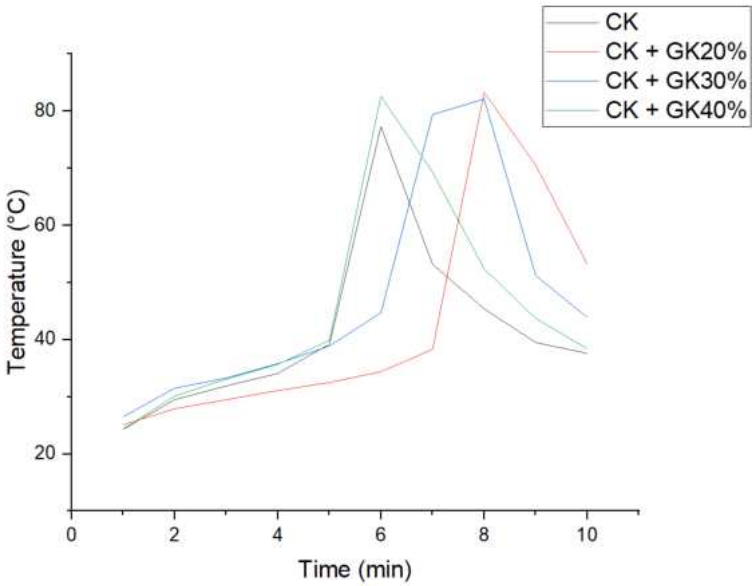

Fig. 80. Second temperature measurement of bone cements before and after modification with aluminosilicates

The tests shown in Fig. 80 reflect a similar situation to that of the first test, but now a slight shift is evident at the time of the largest temperature peak. The shift was observed for a sample with 30% and 40% spherical aluminosilicates.

On the other hand, the results shown in the Fig. 80 and 81 indicate a reduction in polymerization temperature for bone cement with spherical aluminosilicates. The lowest polymerization temperature was shown by the modification with 30% aluminosilicates. As with the second trial, we note a shift in the peak of the highest temperature between the 6th and 7th minutes of the process.

The study carried out, is comparable with the study carried out by A. Balin [21], which shows the behavior of characteristics of bone cement polymerization process after modification with spherical aluminosilicates. Based on the results, modification with 30% of aluminosilicates turned out to be the best option.

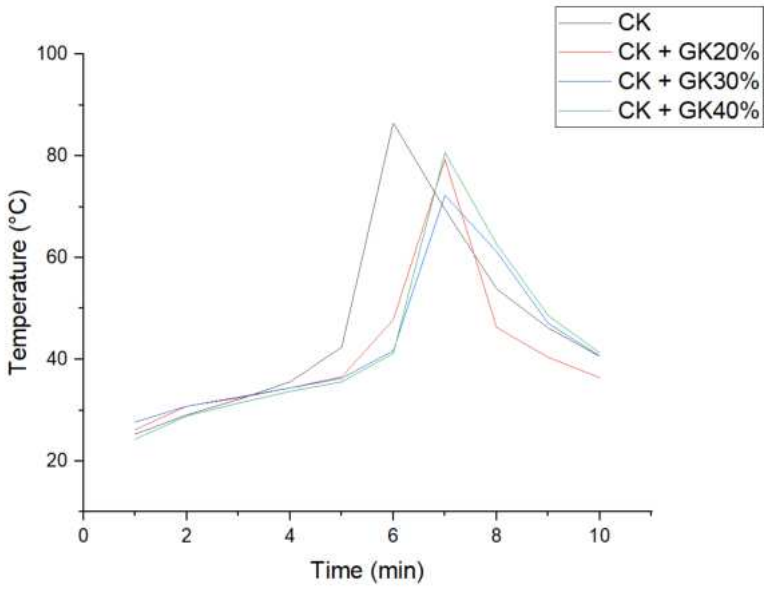

Fig. 81. Third temperature measurement of bone cements before and after modification with aluminosilicates

5.10 Wettability test

The results of wettability measurements (process diagram shown in Fig. 82) and sample drops applied to the surface of the samples before and after bone cement modification. The measurement for the bone cement without filler was 76°, while that for the sample with 30% GK filling was 85°. The surface of the bone cement before and after modification shows a hydrophilic character. The use of filler after modification with

silicon, influenced the increase in the value of the wetting angle. This is due to a change in the structure of the cement, i.e. a reduction in the proportion of pores.

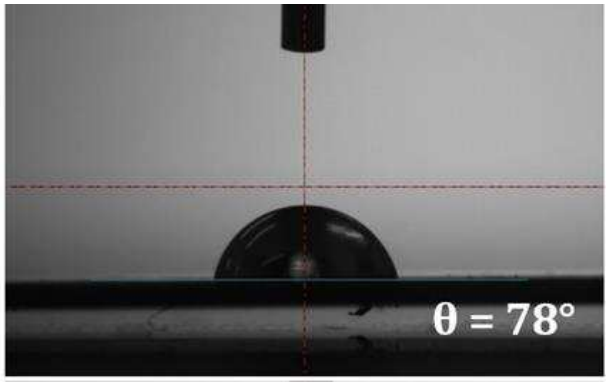

Fig. 82. Representative measurement of wetting angle

5.11. Mechanical properties tests result for bone cement

The mechanical strength of bone cement was evaluated by testing its tensile, compressive and 3-point bending strengths according to ISO 5833, DIN53455 and ASTM D638. Analysis of the results shows that the mechanical strength of the bone cement was influenced by the proportion of spherical aluminosilicate filler.

5.11.1. Static tensile test

The results obtained from conducting mechanical tests, in accordance with ISO 5833, for bone cement based on poly(methyl methacrylate) and after modification with spherical aluminosilicate filler, are presented in the Tab. 15. Based on the test results, the tensile strength Rm and Young's modulus Er were determined. The CK sample exhibits the highest peak load of 331±27 N and peak stress of 22.1±1.8 MPa, along with a strain at break of 2.2±0.15 % and a modulus of 1181±144 MPa, indicating robust mechanical performance. As the percentage of GK in the composites increases, mechanical properties show a notable decline. The CK+GK20% sample shows a peak load of 169±21 N and peak stress of 11.3±1.4 MPa, with a strain at break of 0.9±0.08 %and a modulus of 1445±250 MPa. For CK+GK30% sample records a peak load of 115±35 N and peak stress of 7.7±2.3 MPa, while the CK+GK40% sample shows the lowest values, with a peak load of 91±42 N and peak stress of 6.1±2.8 MPa. Additionally, the strain at break decreases with increasing GK content, indicating a reduction in ductility. Overall, these results suggest that while the addition of GK improves certain aspects of the material's modulus, it negatively impacts strength and strain capacity, highlighting a trade-off in mechanical properties with

varying composite compositions. After the control sample, the best results of the static tensile test showed bone cement with 20% aluminosilicate (CK-GK20%) – Fig. 83.

Tab. 15. The average value of test results for the static tensile test for each variant

Sample	Peak Load, F [N]	Peak Stress, σ [MPa]	Strain at Break, ε [%]	Modulus, E [MPa]
Ck	331±27	22.1±1.8	2.2±0.15	1181±144
Ck+GK20%	169±21	11.3±1.4	0.9±0.08	1445±250
Ck+GK30%	115±35	7.7±2.3	0.8±0.20	1115±143
Ck+GK40%	91±42	6.1±2.8	0.6±0.28	1175±84

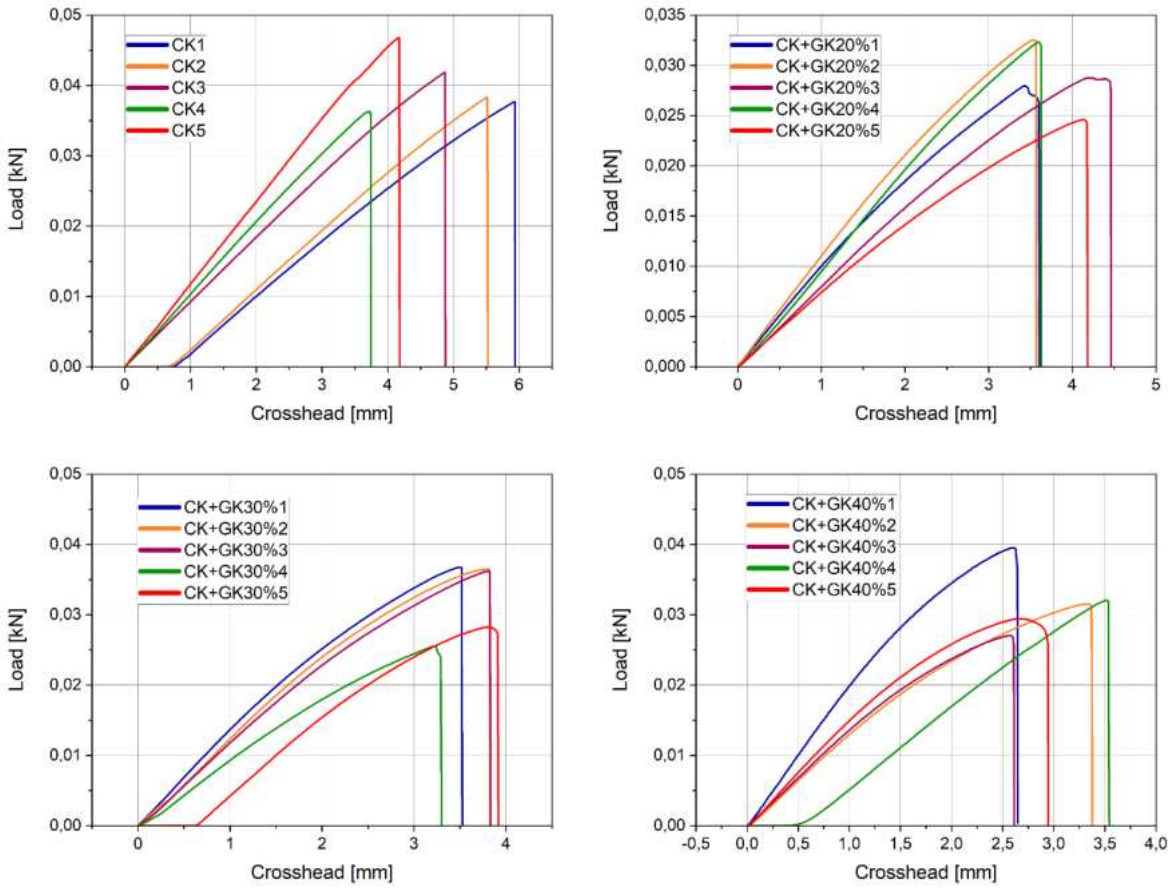

Fig. 83. Curves for the static tensile test of the composite

5.11.2. Static uniaxial compression test

Table 16 presents the mechanical properties of various composite samples, including peak load, peak stress, modulus, strain point, and yield stress. The CK sample serves as a baseline with a peak load of 1687±146 N and a peak stress of 23.4 ± 2.1MPa, along with a modulus of 580 ± 129 MPa. When 20% GK is added (sample CK+GK20%), the peak load seams to CK, 1638 ± 269 N, but the modulus decreases to 404 ± 120 MPa, indicating improved ductility. In contrast, the CK+GK30% sample shows a peak load of 1156 ± 235 N and peak stress of 16.3 ± 3.2 MPa, reflecting a loss in strength and modulus (297 ± 89,3MPa). The CK+GK40% sample demonstrates a peak load of 1231 ± 239 N and an improved modulus of 432 ± 126 MPa, indicating a better balance between strength and stiffness – Fig. 84.

Tab. 16. The average value of test results for the static compression test for each variant

Sample	Peak Load, F (N)	Peak Stress, Rc (MPa)	Modulus, E (MPa)	Stress at Yield, Rc $_{0,2}$ (MPa)	Stress at Offset Yield $\sigma_{y,}$ (MPa)
Ck	1687±146	23.4 ± 2.1	580 ± 129	22.5 ± 1.7	15.7 ± 2.6
Ck+GK20%	1638 ± 269	22.7 ± 3.7	404 ± 120	20.1 ± 4.9	16.4 ± 2.5
Ck+GK30%	1156 ± 235	16.3 ± 3.2	297 ± 89	13.9 ± 2.7	11.8 ± 2.7
Ck+GK40%	1231 ± 239	17.1 ± 3.3	432 ± 126	14.3 ± 7.8	14.0 ± 4.1

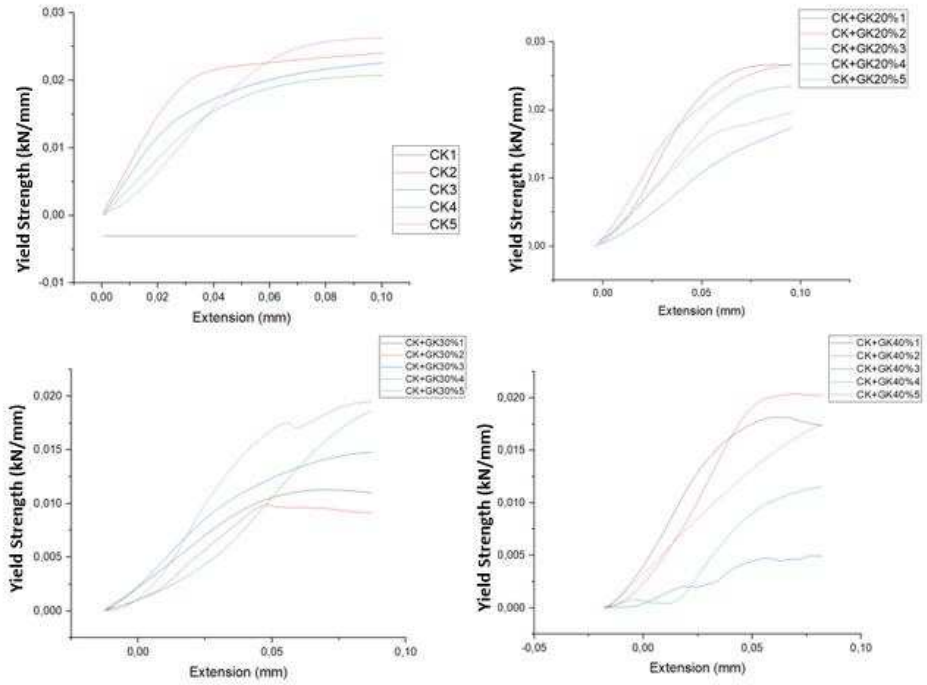

Fig. 84. Curves for the static compression test of the composite

5.11.3. Static 3-point bending tests

The results are shown in the Table 17 and Figure 84. The CK sample exhibits the highest peak load of 39.6 ± 3.6 N and peak stress of 34.0 ± 2.9 MPa, alongside a strain at break of 2.48 ± 0.20 % and a modulus of 1532 ± 229 MPa. With the addition of 20% GK (sample CK+GK20%), the peak load decreases to 28.6 ± 3.0 N, and peak stress drops to 24.16 ± 2.4 MPa, while the strain at break reduces to 2.06 ± 0.10%. The modulus value is 1488 ± 223 MPa, indicating enhanced stiffness. The CK+GK30% sample shows a peak load of 32.4 ± 4.9 N and peak stress of 25.90 ± 3.8 MPa, with a strain at break of 1.88 ± 0.16% and a high modulus of 1966 ± 179 MPa. For the CK+GK40% sample, the peak load remains at 28.2 ± 7.7 N, peak stress is 23.58 ± 6.5 MPa, and the strain at break decreases to 1.46 ± 0.19%, while the modulus increases further to 2344 ± 694 MPa. Fig 85

Overall, the addition of GK leads to a gradual decline in peak load and strain at break but results in higher modulus values, reflecting a trade-off between strength and stiffness across the composite formulations.

Tab. 17. The average value of test results for static 3-point bending test for each variant

Sample	Peak Load Fmax (N)	Peak Stress Rg (MPa)	Strain at Break e [%]	Modulus (MPa)	Stress at Brake (kN/mm²)
Ck	39.6 ± 3.6	34.00 ± 2.9	2.48 ± 0.20	1532 ± 229	0.094 ± 0.100
Ck+Gk20%	28.6 ± 3.0	24.16 ± 2.4	2.06 ± 0.10	1488 ± 223	0.0242 ± 0.002
Ck+Gk30%	32.4 ± 4.9	25.90 ± 3.8	1.88 ± 0.16	1966 ± 179	0.0241 ±0.004
Ck+Gk40%	28.2 ± 7.7	23.58 ± 6.5	1.46 ± 0.19	2344 ± 694	0.0236 ± 0.006

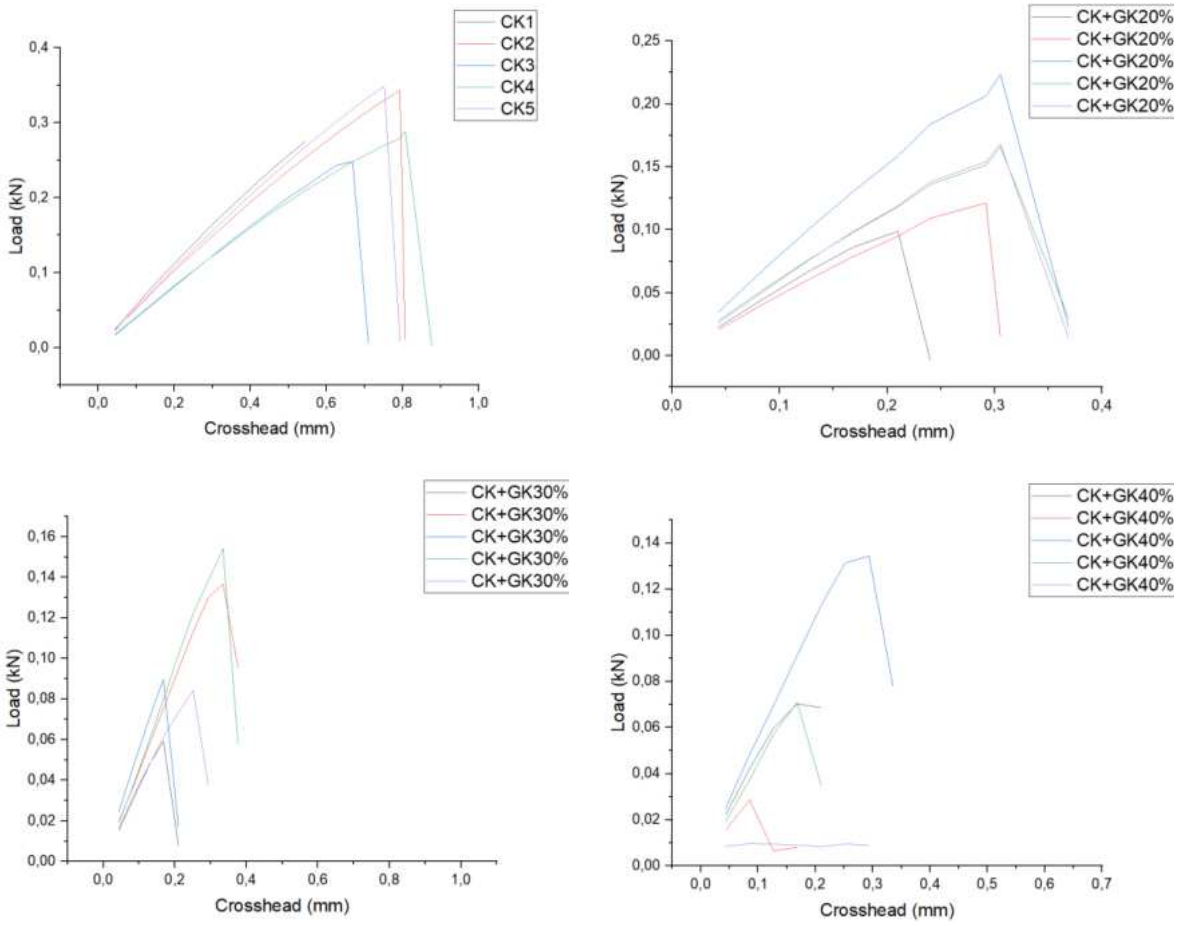

Fig. 85. Curves for the 3-point bending test of the composite

5.12. Biological tests - cytotoxicity

Figure 85 and Figure 86 show a graph of LDH lactate dehydrogenase levels. The tests shown were performed after 24h and 48h. For the results read after 24 hours, we do not have a significant difference between the negative control and the rest of the samples. We can see a slight increase in the release of LDH, this is an enzyme released from inside the cell as a result of the destruction of the cell membrane. For the results read after 24 hours Fig. 86, we do not have a significant difference between the negative control and the rest of the samples. We can see a slight increase in the release of LDH, this is an enzyme released from inside the cell as a result of the destruction of the cell membrane.

A different situation is observable in the test after 48h – Fig. 87. Significant differences can be seen between the pure medium and the medium after contact with the material. The worst variant turned out to be bone cement with an aluminosilicate filling of 20% (CK +20%), and bone cement (CK) as a control sample. The recommended materials were bone cement with clay-silicate fill of 30% (CK+ 30%) and bone cement with clay-silicate fill of 40% (CK +40%).

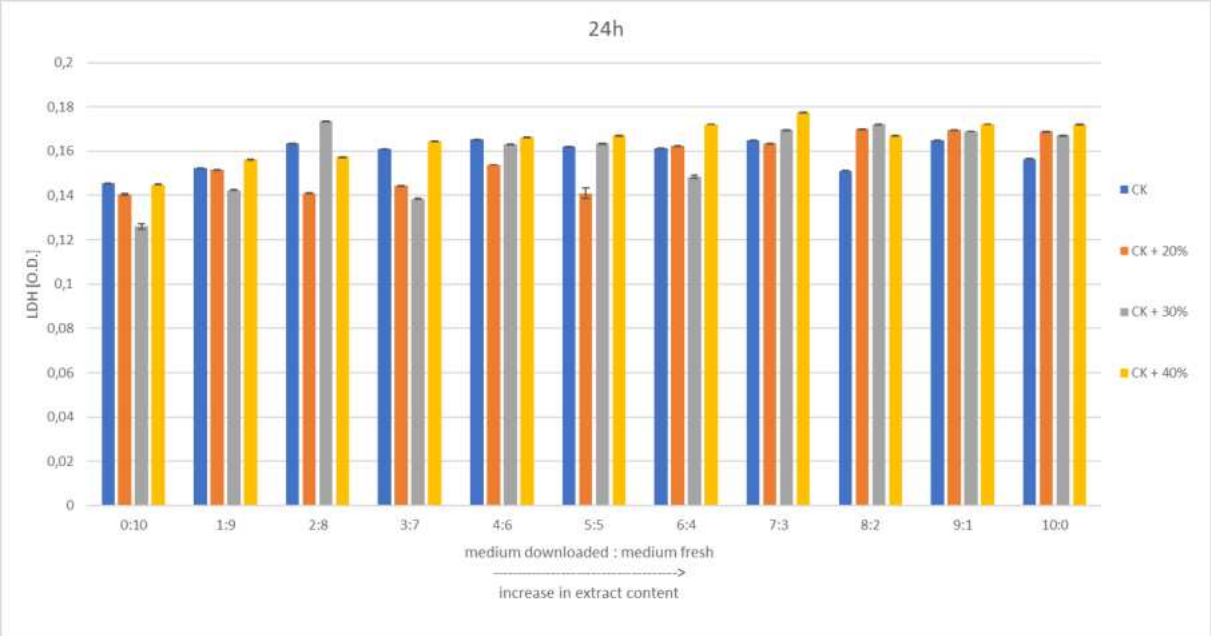

Fig. 86. LDH levels for direct contact samples tested after 24h

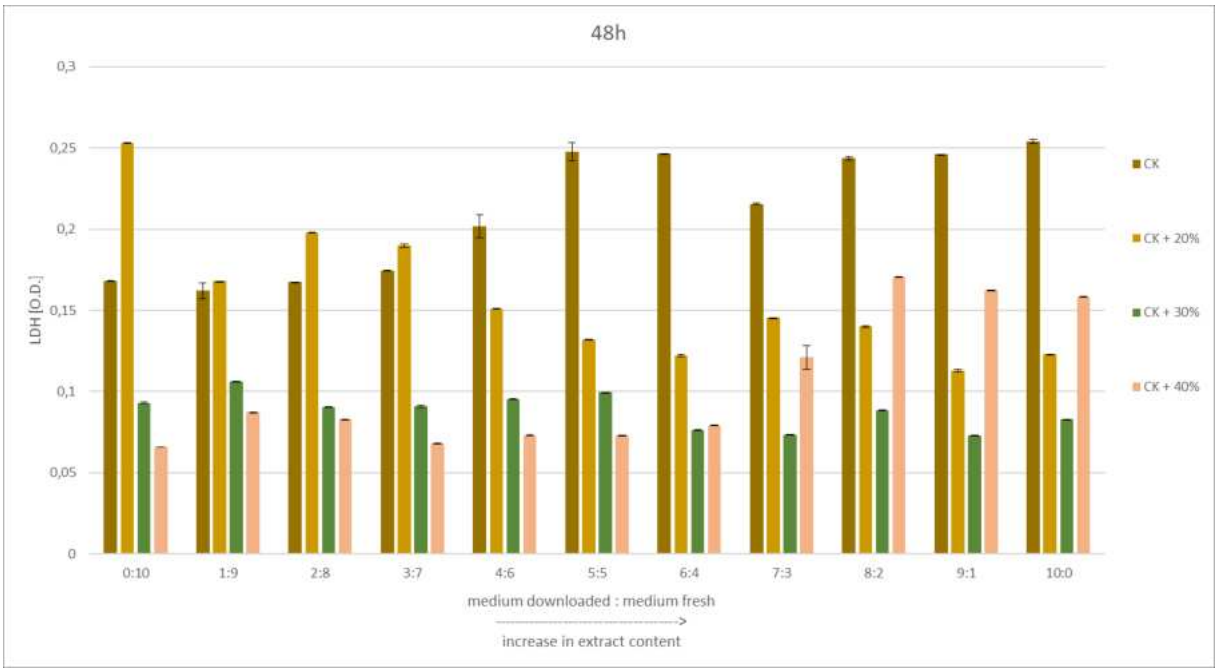

Fig. 87. LDH levels for direct contact samples tested after 48h

6. Discussion

Biomaterials, known in medicine as bone cements, are used primarily for fixing joint endoprostheses and filling bone defects. Other applications include procedures involving filling vertebrae in the spine with bone cement (vertebroplasty and kyphoplasty) and fracture stabilization. Depending on whether the cement is intended to perform a fixation or filling function, different requirements are placed on its strength properties. For cements intended for filling cavities, the compressive strength should be a minimum of 30 MPa, since this is the compressive strength of the spongy bone where it is used. On the other hand, for endoprosthesis fixation, cements should have a minimum compressive strength of 70 MPa [21]. Other requirements are common to both applications. The most important of these is biocompatibility (biocompatibility), that is, the absence of toxic, allergic, carcinogenic effects and the absence of causing infections in the body's environment [19,21]. However, the primary function of bone cements is to fix endoprostheses. Cements that fix endoprostheses play an important stabilizing role, filling the space between the prosthesis and the bone and transferring loads. In addition, bone cement should be resistant to abrasion and fracture, and above all, its polymerization process should be rapid [21]. Despite the availability of various materials, bone cements are still being modified to improve their strength properties and lower the polymerization temperature, which is a very big problem with polymer-based cements. In order to increase strength, the best filler would be a ceramic material, but those currently used, namely alumina and zirconium oxide, exhibit numerous problems related to the occurrence of various types of cracks, resulting in poor adhesion to the matrix. To address the unresolved issues, a silanization process of a new spherical aluminosilicate material was proposed as an alternative material to the currently used ceramics for fillings in composites used in biomedical engineering.

Hence, the aim of the dissertation was to develop a silanization process for spherical aluminosilicates to obtain amine, carboxyl, nitrogen functional groups to improve their adhesion with the matrix compared to those currently used (Al_2O_3 and ZrO_2) in bone cements. Three types of materials were used in this study, i.e. aluminum oxide (Al_2O_3), zirconium oxide (ZrO_2), spherical aluminosilicates with fractions (C_{90}, C_{150}, C_{212}). Each material was then subjected to a silanization process. The silanization process involved three types of modification using silicon nitride with hydroxide ($_{Si3N4}$+NaOH), 3-

aminopropyltriethoxysilane (APTES), tetraethoxysilane (TEOS). Then the degree of influence of the silanization process on the surface of a given material was characterized. After the silanization process, a detailed evaluation of the physicochemical properties of the aluminosilicates was carried out in order to select the best fraction and modification to be used as a filler for bone cement. Based on the results obtained from X-ray spectra analyses, the presence of characteristic phases for the component modifiers was confirmed. In the case of aluminum oxide (Al_2O_3) and zirconium oxide (ZrO_2), characteristic reflections identifying positions for modifications with silicon nitride were observed, while for spherical aluminosilicates only in the area of the identified mullite, a slight broadening of the reflection can be seen, which may, be a confirmation of the presence of phases originating from the given modifications. In order to identify the chemical composition of the surface layer of spherical aluminosilicates after the slianiazation process, XPS studies were conducted. The surface layer with Si_3N_4 modification was identified the following elements Al, Si, Mg, Ti, N, O, C The obtained overview spectra min. for the modification with silicon nitride showed that on the surface of the filler there are mainly silicon compounds, i.e. SiO_2, Si_3N_4, compounds with the participation of C=C/C-Si bonds which is also a phenomenon favorable to confirm the deposition of silicon and nitrogen groups in the process of silanization. For the other modifications also, the occurrence of silicon on the surface was registered but in a much lower percentage, which was also confirmed by SEM/EDS analysis of the distribution of this element on the sample surface.

Infrared spectroscopy (FTIR) analysis showed the presence of carboxyl, nitrogen and amine bonds and functional groups. The analysis presented here showed the highest proportion of nitrogen bonds for modification with silicon nitride (Si_3N_4+NaOH), not depending on the material used. The differences in intensity can be explained by the type of atmosphere during calcination and its temperatures T = 250°C and T = 450°C. The largest change was shown for Al_2O_3. For the organic modifications APTES and TEOS, no significant differences were shown with respect to temperature or calcination atmosphere. The analyzed spectra showed no increase in the proportion of the desired groups. Microstructure analysis showed the presence of each type of modification on the modified materials. EDS analysis confirmed the presence of silicon (Si) on the entire surface of the test sample, as well as other elements associated with the silanization process. Microstructure analysis showed the presence of modifications not only on the

surface of the spherical aluminosilicates, but also the incorporation of modifications into the structure or pores present in the material. This suggests the persistence of *Van der Walsa* bonds on the surface of the aluminosilicates, which may result in good bonding to the matrix without crack propagation. Thermogravimetric tests (TGA) confirmed the stability of the processes, and the measurement of the mass of the sample versus elevated temperature was Δ%1.83 at about 900°C, where there is a reorganization of the oxide ions in the lattice structure transforms into a spinel-like form of aluminum g-oxide and further mullite. The final form of aluminosilicates is a mixture of cristobalite and crystallized mullite. A particle distribution analysis was also carried out for spherical aluminosilicates with a fraction of 150 μm for each modification. A difference in particle size was shown depending on the modification. In addition, the presence of Si-O-Si groupings, characteristic of silica revealed by Fourier transform absorption spectroscopy (FTIR) measurements, allows further functionalization of the surface layer in a controlled manner, providing a kind of matrix for the implication of functional groups that improve its wettability, which is a beneficial phenomenon.

The study of the presented processes showed that silicon nitride modification is the best variant, which can be intended for further modification in the form of producing a new type of bone cement based on spherical aluminosilicates. For bone cement modification, in addition to the reference sample, i.e. bone cement - CK, 3 other variants with 20%, 30% and 40% of spherical aluminosilicates of 150 μm fraction were selected. The polymerization process was carried out according to the methodology announced in the paper, which made it possible to precisely determine the influence of the matrix setting time on the polymerization temperature, a key parameter during bone cement injection. Too high a temperature sustained for a long time can cause bone necrosis [21].

The results discussed indicate that the layer produced on the surface of spherical aluminosilicates with Si_3N_4+NaOH through the silanization process developed in the dissertation makes it possible to design a surface with properties that take into account the biophysical and biochemical characteristics of the bone tissue environment. To verify the suitability of the proposed surface layer for clinical applications, *in vitro* bioassays were conducted in the last stage of the work. The 24-hour test showed no significant differences between the negative control and the rest of the samples. There is a noticeable slight increase in the release of LDH. This is an enzyme released from inside the cell as a result of cell membrane destruction. On the other hand, after 48 hours, changes were

observed between the pure medium and the medium after contact with the material. In summary, the study showed that bone cement with 30% and 40% spherical aluminosilicates is the most favorable option compared to pure PMMA.

In addition, mechanical property tests carried out showed differences in the determined values for the different variants. It was found that as the percentage of filler in the form of spherical aluminosilicate increased, there was a decrease in the plastic properties relative to PMMA.

In summary, the research problems contained in the dissertation relate to unresolved complex problems in the field of biomedical engineering, especially biomaterials engineering, relevant to clinical applications. The research results obtained in the dissertation may also have a measurable application effect, providing a basis for the development of a new form of bone cement with spherical aluminosilicates for contact with bone tissue with commercialization potential. The research conducted in the dissertation provided valuable information on how to modify the surface of spherical aluminosilicates allowing them to be introduced as a filler into PMMA.

In summary, the conducted research confirmed the validity of the adopted thesis. The development of a silanization process for spherical aluminosilicates has made it possible to permanently combine them chemically and physically with a polymer matrix in composite materials, and thus is an alternative solution to the currently used fillers for bone cements dedicated to biomedical engineering applications.

7. Conclusions

The results obtained from the dissertation research made it possible to formulate the following generalizations of a cognitive and applied nature:

1. The use of peroxysulfuric acid ensured adequate surface development, which was observed during SEM studies thus providing a suitable active surface for carrying out the silanization process.
2. SEM and XPS analysis showed silicon deposition on the entire surface of the tested materials, which confirms the assumed thesis of the development of the silanization process.
3. Analysis of the results of infrared spectroscopy (FTIR) showed the presence of nitrogen compounds, amine and carboxyl groups, which will allow to increase the chemical bond between the filler and the matrix in the produced composite.
4. The use of spherical aluminosilicates in the composite reflected the polymerization curve, which shows invariability in the polymer crosslinking process.
5. Strength tests of bone cement and bone cement with spherical aluminosilicate showed similar flexural and compressive strengths.

IV. BIBLIOGRAPHY

1. J. Marciniak, Biomateriały, Wydawnictwo Politechniki Śląskiej, Gliwice 2002
2. https://ezdrowie.gov.pl/5583
3. https://www.synevo.pl/akademia-zdrowia/osteoporoza/
4. Sambrook, P. and C. Cooper, Osteoporosis. Lancet, 2006. **367**(9527): p. 2010-8
5. Johnell, O. and J.A. Kanis, An estimate of the worldwide prevalence and disability associated with osteoporotic fractures. Osteoporos Int, 2006. **17**(12): p. 1726-33.
6. Klotzbuecher, C.M., et al., Patients with prior fractures have an increased risk of future fractures: a summary of the literature and statistical synthesis. J Bone Miner Res, 2000. **15**(4): p. 721-39
7. https://www.riverheightsphysiotherapy.ca/Injuries-Conditions/Knee/Surgery/Revision-Arthroplasty-of-the-Knee/a~356/article.html
8. https://radiopaedia.org/cases/bone-cement-with-tumor-recurrence
9. https://www.certus.med.pl/pl/baza-wiedzy/leczenie-chorob-kregoslupa/wertebroplastyka
10. https://www.luxmed.pl/dla-pacjenta/uslugi/leczenie-i-zabiegi/wertebroplastyka-leczenie-zlamania-kregoslupa
11. http://onkologia24.com.pl/en/wertebroplastyka
12. https://www.aldemed.pl/neurochirurgia/pagesView,81,wertebroplastyka,PL
13. [https://www.poradnia.pl/wertebroplastyka-czyli-cementowanie-kregoslupa.html]
14. [https://pl.dental-tribune.com/news/wiekszosc-polakow-ma-braki-zebowe-i-choroby-przyzebia/]
15. Naseer, Amara & McLoughlin, Jacinta & Donoghue, Orna & Kenny, Rose & O'Connell, Brian. (2018). Oral health status of community dwelling adults aged 50 years and over in Ireland. A cross-sectional analysis of the Wave 3 TILDA cohort. HRB Open Research. 1. 26. 10.12688/hrbopenres.12891.1.
16. Raport IQS dla GSK „Corega Tracking", sierpień 2016
17. https://www.isbzdrowie.pl/2024/04/bezzebie-dotyka-ponad-9-milionom-polakow/
18. https://www.infodent24.pl/bizdentpost/rocznie-wszczepia-sie-w-polsce-juz-100-tys-implantow,105162.html
19. Hu M.H., Wu H.T.H., Chang M.C., Yu W.K., Wang S.T., Liu C.L.: polymethylmethacrylate augumentation of the pedicle screw: the cement distribution in the vertebral bod. Eur Spine J (2011) 20:1281–1288
20. https://dentalclub.fr/en/produit/inlay-onlay-overlay-march-2024/
21. Balin A. Cementy w chirurgii kostnej. Wydawnictwo Politechniki Śląskiej, Gliwice (2016).

22. Shafi B., Mery C., Binyamin G., Knight J., Gertner M. E.: Injectable Biomaterials in Surgery
23. Jayabalan M., Shalumon K.T., Mitha M.K.: Injectable biomaterials for minimally
24. Pijls, Bart & Sanders, Ingrid & Kujiper, Ed & Nelissen, Rob. (2020). Induction heating for eradicating Staphylococcus epidermidis from biofilm. Bone & Joint Research. 9. 192-199. 10.1302/2046-3758.94.BJR-2019-0274.R1.
25. Wekwejt, M., Świeczko-Żurek, B., & Szkodo, M. (2017). Requirements, modifications and methods of mechanical testing of bone cement – literature review. European Journal of Medical Technologies, 3(16), Article 3(16).
26. Spierings, Pieter. (2005). Testing and Performance of Bone Cements. 10.1007/3-540-28924-0_7.
27. Błażewicz S., Stoch L., Biomateriały, Warszawa, 2003, Akademicka Oficyna Wydawnicza Exit
28. Jerzy NOWACKI, Leszek A. DOBRZAŃSKI,Fabio GUSTAVO Implanty śródszpikowe w osteosyntezie kości długich Open Access Library, 2012, vol.11 (17)
29. [https://www.tecres.pl/index.php?go=cemexsystem]
30. Matos A., Gonçalves L., Rijo P., Vaz M., Almeida A., Bettencourt A. A novel modified acrylic bone cement matrix. A step forward on antibiotic delivery against multiresistant bacteria responsible for prosthetic joint infections. Mater. Sci. Eng. C, 38 (2014), s. 218-226.
31. Ormsby R., McNally T., O'Hare P., Burke G., Mitchell C., Dunne N. Fatigue and biocompatibility properties of a poly(methyl methacrylate) bone cement with multi-walled carbon nanotubes. Acta Biomater., 8 (2012), s. 1201-1212
32. Miola M., Bruno M., Maina G., Fucale G., Lucchetta G., Vernè E., Antibiotic-free composite bone cements with antibacterial and bioactive properties. A preliminary study. Mater. Sci. Eng. C, 43 (2014), s. 65-75.
33. Jiang, Hong-Jiang & Xu, Jin & Qiu, Zhiye & Ma, Xin-Long & Zhang, Zi-Qiang & Tan, Xun-Xiang & Cui, Yun & Cui, Fu-Zhai. (2015). Mechanical Properties and Cytocompatibility Improvement of Vertebroplasty PMMA Bone Cements by Incorporating Mineralized Collagen. Materials. 8. 2616-2634. 10.3390/ma8052616.
34. Ding X, Yuan Y, Lu H, Wang Y , Ji K, Lu H, Xu H, Zhou J Analysis of the Effect of Antibiotic Bone Cement in the Treatment of Diabetic Foot Ulcer through Tibia Transverse Transport Orthop Surg. 2022 Aug 5. doi: 10.1111/os.13412
35. Combe E.C.: „Wstęp do materiałoznawstwa." Wydawnictwo Medyczne S anmedica Warszawa, 1997.
36. Dalle B.G., Aschheim K.W.: „Stomatologia estetyczna. Kliniczne zastosowanie technik i materiałów." Podręcznik Wydawnictwo Czelej Lublin, 1998.

37. Kelly J.R., Nishimura I., Campbell S.D.: „Ceramics in dentistry: historical roots and current perspectives.” J. Prosthet. Dent. 1996; 75; 1: 18-35.
38. Kenneth J., Anusawice P.D.: „Postępy w technologii i właściwości porcelany i metal ceramiki.” Magazyn Storn. 1993; 3; (10): 30-33.
39. Kordasz P., Wolanek Z.: „Materiałoznawstwo protetyczno-stomatologiczne.” Podręcznik PZWL Warszawa 1976.
40. Shilinburg H.T., Hobo S., Whitsett L.D.: „Protezy stałe. Zarys postępowania klinicznego i laboratoryjnego.” Podręcznik Wydawnictwo Kwintesencja 1994.
41. Tejchman H., Wiśniewska E.: „Ocena przydatności niektórych materiałów stomatologicznych na podstawie badań klinicznych i bakteriologicznych.” Prot. Storn. 1996; XLIV; 2: 107-110.
42. Wilson H., Me Lean J., Brown D.: „Materiały stomatologiczne i ich kliniczne zastosowanie.” Podręcznik; Wydawnictwo Medyczne Sanmedica Warszawa 1995
43. Świeczko-Żurek B. Biomateriały. Gdańsk: Wydawnictwo Politechniki Gdańskiej 2009.
44. Marciniak J., Kaczmarek M., Ziębowicz A. Biomateriały w stomatologii. Gliwice: Wydawnictwo Politechniki Śląskiej 2008.
45. https://www.ceramit.pl/tlenek-glinu-al2o3
46. Małgorzata Lewandowska - Szumieł „Uwalnianie się glinu w warunkach in vivo z bioceramicznych wszczepów wykonanych z tlenku glinu Al203, Praca Doktorska, Warszawa 1992.
47. Ziębowicz A. Powłoka ZrO2 na podłożu stopów kobaltowych jako czynnik minimalizujący stomatopatie protetyczne. Gliwice: Wydawnictwo Politechniki Śląskiej; 2023.
48. K. Lasek, P. Okoński, E. Mierzwińska-Natalska, Tlenek cyrkonu – właściwości fizyczne i zastosowanie kliniczne, Protetyka stomatologiczna, tom 59, nr 6, s. 415-422.
49. H. Lada, Materiały inżynierskie w zastosowaniach biomedycznych, Wydawnictwo Politechniki Poznańskiej, Poznań, 2012.
50. A. Kolenda, Z. Jaegermann, E. Mierzwińska-Nastalska, Polimorfizm, otrzymywanie i degradacja tlenku cyrkonu – ujęcie źródłowe, Protetyka stomatologiczna, tom 66, 2016, s. 27-32.
51. L.A. Dobrzański, Podstawy nauki o materiałach i materiałoznawstwo, Materiały inżynierskie z podstawami projektowania materiałowego, Wydawnictwo Naukowo Techniczne, Warszawa, 2002.
52. https://www.metal-powder-dust.com/Rare-metals/zirconium-dioxide [dostęp dnia: 28.04.2020].
53. https://www.azonano.com/article.aspx?ArticleID=5012 [dostęp dnia: 28.04.2020].

54. https://www.americanelements.com/zirconium-oxide-1314-23-4 [dostęp dnia: 28.04.2020]
55. Ashby M.F., Jones H.D.R.: „ Materiały inżynierskie-kształtowanie struktury i właściwości, dobór materiałów.” Wydawnictwo Naukowo-Techniczne, Warszawa 1995
56. Błaszczyk D., Mielnik-Błaszczyk M.: „Ceramika dentystyczna.” Podręcznik; Wydawnictwo Ekoinżynieria Lublin 1998
57. C.A.M. Volpato, L.G.D.A. Garbelotto, M.C. Fredel, F. Bondioli, Application of Zirconia in Dentistry: Biological, Mechanical and Optical Considerations, Open Access, 2011.
58. E. Białożyt, M. Tysiąc-Miśta, A. Dwornicka, K. Olek, M. Cieślik, Uzupełnienia na bazie tlenku cyrkonu, Medical Tribune Stomatologia, 7-8, 2015.
59. Nakonieczny, Damian & Antonowicz, Magdalena & Paszenda, Zbigniew. (2020). Cenospheres and their application advantages in biomedical engineering -a systematic review. REVIEWS ON ADVANCED MATERIALS SCIENCE. 59. 10.1515/rams-2020-0011.
60. Nakonieczny, Damian & Nuckowski, Paweł & Matus, Krzysztof & Antonowicz, Magdalena & Heim, Thomas & Swinarew, Andrzej & Lemanowicz, Marcin. (2022). Cenospheres-Reinforced PA-12 Composite: Preparation,Physicochemical Properties, and Soaking Tests. Polymers. 14. 2332. 10.3390/polym14122332.
61. Wajda A., Kozioł M., Mikrosfery - pozyskiwanie, właściwości, zastosowania, Piece przemysłowe i kotły, "Inżynieria Środowiska", t. 1, 2015, s. 15-17
62. Navid Ranjbar, Carsten Kuenzel,Cenospheres: A review,Fuel,Volume 207,2017,Pages 1-12,ISSN 0016-2361,https://doi.org/10.1016/j.fuel.2017.06.059
63. Danish, Aamar & Mosaberpanah, Mohammad & Tuladhar, Rabin & Salim, Muhammad & Yaqub, Muhammad & Ahmad, Naveed. (2022). Effect of cenospheres on the engineering properties of lightweight cementitious composites: A comprehensive review. Journal of Building Engineering. 49. 104016. 10.1016/j.jobe.2022.104016.
64. Ranjbar, Navid & Künzel, Carsten. (2017). Cenospheres: A review. Fuel. 207. 1-12. 10.1016/j.fuel.2017.06.059.
65. B.R. Bharath Kumar, Mrityunjay Doddamani, Steven E. Zeltmann, Nikhil Gupta, M.R. Ramesh, Seeram Ramakrishna,Processing of cenosphere/HDPE syntactic foams using an industrial scale polymer injection molding machine, Materials & Design,Volume 92,2016,Pages 414-423,ISSN 0264-1275, https://doi.org/10.1016/j.matdes.2015.12.052.
66. Aamar Danish, Mohammad Ali Mosaberpanah, Rabin Tuladhar, Muhammad Usama Salim, Muhammad Arslan Yaqub, Naveed Ahmad, Effect of cenospheres on the engineering properties of lightweight cementitious composites: A comprehensive review, Journal of Building Engineering, Volume 49, 2022, 104016, ISSN 2352-7102,https://doi.org/10.1016/j.jobe.2022.104016.

67. Bareiro Ferreira, Oscar & Dos Santos, Luis Alberto. (2014). Tetraethylorthosilicate (TEOS) applied in the surface modification of hydroxyapatite to develop polydimethylsiloxane/hydroxyapatite composites. Colloids and surfaces. B, Biointerfaces. 115. 400-405. 10.1016/j.colsurfb.2013.12.027.
68. Yano, Haruka & Ikeda, Hiroshi & Nagamatsu, Yuki & Masaki, Chihiro & Hosokawa, Ryuji & Shimizu, Hiroshi. (2019). Correlation between microstructure of CAD/CAM composites and the silanization effect on adhesive bonding. Journal of the Mechanical Behavior of Biomedical Materials. 101. 103441. 10.1016/j.jmbbm.2019.103441.
69. Grzegorz Schroeder, Chemicznafunkcjonalizacja powierzchni dla potrzeb nanotechnologii, Praca zbiorowa, Cursiva 2011, ISBN 978-83-62108-07-7
70. Gao LZ, Bao Y, Cai HH, et al (2020) Multifunctional silk fabric via surface modification of nano-SiO2. Text Res J 90:1616–1627
71. Xie Y, Hill CAS, Xiao Z, et al (2010) Silane coupling agents used for natural fiber/polymer composites: A review. Compos Part A Appl Sci Manuf 41:806–819.
72. Boger A., Wheeler K.D., Schenk B. : Clinical investigations of polymethylmethacrylate cement viscosity during vertebroplasty and related in vitro measurements, Eur Spine J (2009) 18:1272–1278
73. Ćwikła, Grzegorz & Grabowik, Cezary & Kalinowski, Krzysztof & Paprocka, Iwona & Ociepka, Piotr. (2017). The influence of printing parameters on selected mechanical properties of FDM/FFF 3D-printed parts. IOP Conference Series: Materials Science and Engineering. 227. 012033. 10.1088/1757-899X/227/1/012033.
74. Nakonieczny, Damian & Antonowicz, Magdalena & Paszenda, Zbigniew. (2020). Surface modification methods of ceramic filler in ceramic-carbon fibre composites for bioengineering applications -A systematic review. Reviews on Advanced Materials Science. 59. 10.1515/rams-2020-0024.
75. Figure 1 (omicsonline.org)
76. Cheng F, Sajedin SM, Kelly SM, et al (2014) UV-stable paper coated with APTES-modified P25 TiO2 nanoparticles. Carbohydr Polym 114:246–252.
77. Souza KG da S, Cotting F, Aoki IV, et al (2020) Study of the wettability and the corrosion protection of the hybrid silane (3-aminopropyl) triethoxysilane (aptes) and (3-glycidyloxypropyl) trimethoxysilane (gptms) film on galvannealed steel. Rev Mater 25:1–18.
78. Meroni D, Lo Presti L, Di Liberto G, et al (2017) A close look at the structure of theTiO2-APTES interface in hybrid nanomaterials and its degradation pathway: An
79. Cheng F, Sajedin SM, Kelly SM, et al (2014) UV-stable paper coated with APTES-modified P25 TiO2 nanoparticles. Carbohydr Polym 114:246–252.

80. Zhang J, Zhang R, Zhao LH, Sun SQ (2012a) Synthesis of water-soluble γ-aminopropyl triethoxysilane-capped ZnO:MgO nanocrystals with biocompatibility. CrystEngComm14:613–619.
81. Abhijeet B. Muley, Ketan H. Mulchandani, Rekha S. Singhal,Chapter Three - Immobilization of enzymes on iron oxide magnetic nanoparticles: Synthesis, characterization, kinetics and thermodynamics,Editor(s): Challa V. Kumar,Methods in Enzymology,Academic Press, Volume 630,2020, Pages 39-79,ISSN 0076-6879, ISBN 9780128201435,https://doi.org/10.1016/bs.mie.2019.10.016.
82. https://www.scientificlabs.co.uk/product/organosilicon-reagents/86578-1L
83. Justyna Krzak i inni, Sol–gel surface functionalization regardless of form and type of substrate, [w:] Chaudhery Mustansar Hussain (red.), Handbook of nanomaterials for manufacturing applications, Elsevier, 2020, s. 111–147, DOI: 10.1016/b978-0-12-821381-0.00005-3
84. Huda Abdullah i inni, $(SiO_2)_{100-x}$-Ni_x (x = 2.5, 10.0) Composite-based photoanode with polymer gel electrolyte for increased dye-sensitized solar cell performance, „Ionics", 25 (7), 2019, s. 3387–3396, DOI: 10.1007/s11581-019-02886-w
85. Qian Guo i inni, Synthesis and characterization of spherical silica nanoparticles by modified Stöber process assisted by slow-hydrolysis catalyst, „Colloid and Polymer Science", 296 (2), 2018, s. 379–384, DOI: 10.1007/s00396-017-4260-0
86. Gaoyuan Ren, Hongjiu Su, Shudong Wang, The combined method to synthesis silica nanoparticle by Stöber process, „Journal of Sol-Gel Science and Technology", 96 (1), 2020, s. 108–120, DOI: 10.1007/s10971-020-05322-y
87. Marek Jasiorski, Krzysztof Maruszewski, Wiesław Stręk, Optical behaviour of sol-gel derived photonic structures formed by submicron silica spheres, „Materials Science", 20 (1), 2002, s. 51–56 [dostęp 2022-01-10]
88. Mercedes Perullini i inni, Effect of synthesis conditions on the microstructure of TEOS derived silica hydrogels synthesized by the alcohol-free sol–gel route, „Journal of Sol-Gel Science and Technology", 59 (1), 2011, s. 174–180, DOI: 10.1007/s10971-011-2478-8
89. Werner Stöber, Arthur Fink, Ernst Bohn, Controlled growth of monodisperse silica spheres in the micron size range, „Journal of Colloid and Interface Science", 26 (1), 1968, s. 62–69, DOI: 10.1016/0021-9797(68)90272-5
90. A. Venkateswara Rao, Sharad D. Bhagat, Synthesis and physical properties of TEOS-based silica aerogels prepared by two step (acid–base) sol–gel process, „Solid State Sciences", 6 (9), 2004, s. 945–952, DOI: 10.1016/j.solidstatesciences.2004.04.010

91. A. Venkateswara Rao i inni, Influence of temperature on the physical properties of TEOS silica xerogels, „Ceramics International", 25 (6), 1999, s. 505–509, DOI: 10.1016/S0272-8842(97)00085-0
92. Mayoral, María & Izquierdo, Maria Teresa & Andrés, Jose & Rubio, B. (2001). Aluminosilicates transformations in combustion followed by DSC. Thermochimica Acta. 373. 173-180. 10.1016/S0040-6031(01)00459-2.
93. Ryan M. Bock Manipulation of Silicon Nitride Biomaterial Surfaces for Enhanced Osteoconductivity and Bacteriostasis, Kyoto, Japan March 2017
94. C.D. Wagner, A.V. Naumkin, A. Kraut-Vass, J.W. Allison, C.J. Powell, J.R.Jr. Rumble, NIST Standard Reference Database 20, Version 3.4 (web version) (http:/srdata.nist.gov/xps/) 2003
95. C.D. Wagner, A.V. Naumkin, A. Kraut-Vass, J.W. Allison, C.J. Powell, J.R.Jr. Rumble, NIST Standard Reference Database 20, Version 3.4 (web version) (http:/srdata.nist.gov/xps/) 2003.
96. G. Beamson, D. Briggs, High Resolution XPS of Organic Polymers - The Scienta ESCA300 Database, Wiley Interscience, 1992, Appendices 3.1 and 3.2.
97. G. Beamson, D. Briggs, High Resolution XPS of Organic Polymers - The Scienta ESCA300 Database, Wiley Interscience, 1992, Appendices 3.1 and 3.2

Development of the Silanization Process for Spherical Aluminosilicates Dedicated as Filler for Polymers used in Medical Devices

Abstract

The topic of this dissertation concerns an issue related to improving the properties of materials used in the treatment of bone defects and the attachment of implants to bone. Correct filling of the defect should ensure stability and integration of the implant with the body minimizing the risk of complications. Currently used materials, i.e. aluminum oxide or zirconium oxide, despite their good mechanical properties, do not always guarantee a good connection with the matrix in the bone cement, which can lead to fractures.

The dissertation adopted the theme of developing a silanization process for three selected materials (Al_2O_3, ZrO_2 and spherical aluminosilicate with fractions C_{90}, C_{150} and C_{212}). Each of these materials was subjected to three modifications using silicon nitride with sodium hydroxide (Si_3N_4+NaOH), 3-aminopropyltriethoxysilane (APTES), Tetraethoxysilane (TEOS). One type of aluminosilicate with a 150μm fraction, after modification from silicon nitride with sodium hydroxide (Si_3N_4+NaOH), was selected on the basis of chemical composition, phase composition, microstructure, as well as thermogravimetric studies of the surface. The second part of the conducted research was the verification of the produced composite. For this purpose, chemical composition, surface morphology, porosity, wettability as well as strength tests were performed. Biological evaluation was also carried out by performing a cytotoxicity test.

The results of the aforementioned studies showed the beneficial effect of using spherical aluminosilicate filler in polymer matrix bone cements.

Opracowanie procesu silanizacji dla glinokrzemianów sferycznych dedykowanych jako napełniacz do kompozytów polimerowych stosowanych w wyrobach medycznych

Streszczenie

Tematyka rozprawy doktorskiej dotyczy zagadnienia związanego z poprawą własności materiałów stosowanych w leczeniu ubytków kostnych oraz mocowania implantów z kością. Prawidłowe wypełnienie ubytku ma zapewnić stabilność oraz integrację implantu z organizmem minimalizując ryzyko powikłań. Obecnie stosowane materiały tj. tlenek glinu czy tlenek cyrkonu, pomimo swoich dobrych własności mechanicznych nie zawsze gwarantują dobre połączenie z osnową w cemencie kostnym, co może doprowadzić do pęknięć.

W rozprawie doktorskiej przyjęto tematykę opracowani procesu silanizacji dla trzech wybranych materiałów (Al_2O_3, ZrO_2 i glinokrzemian sferyczny o frakcjach C_{90}, C_{150} i C_{212}). Każdy z tych materiałów został poddany trzem modyfikacjom z wykorzystaniem azotku krzemu z wodorotlenkiem sodu (Si_3N_4+NaOH), 3-aminopropylotrietoksysilan (APTES), Tetraetoksysilan (TEOS). Na podstawie przeprowadzonych badań składu chemicznego, fazowego, mikrostruktury, a także badania termograwimetryczne powierzchni wytypowano jeden rodzaj glinokrzemianu o frakcji 150μm, po modyfikacji z azotku krzemu z wodorotlenkiem sodu (Si_3N_4+NaOH). Drugą częścią przeprowadzonych badań była weryfikacja wytworzonego kompozytu. W tym celu zostały wykonane badania składu chemicznego, morfologii powierzchni, porowatości, zwilżalności jak i również badania wytrzymałościowe. Dokonano również oceny biologicznej wykonując badanie cytotoksyczności.

Wyniki wymienionych badań wykazały korzystny wpływ zastosowania wypełniacza w postaci glinokrzemianu sferycznego w cementach kostnych o osnowie polimerowej.